Synthesis and characterization of ruthenocene-containing complexes with biomedical applications

A dissertation submitted in accordance with the requirements for the degree

Magister Scientiae

in the

Department of Chemistry

Faculty of Natural and Agricultural Sciences

at the

University of the Free State

by

Christiaan Coenraad Joubert

Supervisor

Prof. J.C. Swarts

Acknowledgements

I would hereby like to thank my supervisor, Prof. J.C. Swarts for his excellent guidance throughout the duration of my project, his support in both scientific and personal matters and the time devoted to my studies.

I would like to thank Elizabeth (Lizette) Erasmus for XPS measurements.

I would like to thank the National Research Foundation for funding.

Thank you to all the members of the Physical Chemistry Group, and the various people I have worked with during my studies. Thanks for so many fun times, all the friends I made, had lunch with and partied with throughout the duration of my project.

A big "thank you" to my family for their unwavering support and guidance.

Abstract

Polysuccinimide was modified by reactions with aminopropyl morpholine and ethylenediamine to give a water-soluble biodegradable polymeric drug carrier. Ruthenocene has been functionalized in sixteen different reactions to ultimately give four ruthenocene-containing carboxylic acids of the form $Rc(CH_2)_nCOOH$ (n = 0 – 3). These were covalently anchored to the amino-terminated side chains of the polyaspartamide carrier polymer utilizing the coupling agent *O*-benzotriazolyl-*N,N,N'N'*–tetramethyluronium hexafluorophosphate. These four new ruthenocene-polymer conjugates represent the first water-soluble ruthenocene peptide macromolecular conjugates ever made. XPS, ^1H NMR spectroscopy and elemental analysis aided the characterisation of the new ruthenocene-containing polymers.

A cyclic voltammetry study of all the ruthenocene-containing carboxylic acids in CH_2Cl_2/0.1 M $[NBu_4][B(C_6F_5)_4]$ were carried out. Despite the use of this non-coordinating solvent/electrolyte system, none of the ruthenocene-containing carboxylic acids exhibited a chemical reversible Rc/Rc^+ redox couple. The formal oxidation potentials of the free carboxylic acids were $E^{o'}$ = 776, 484, 494 and 516 mV vs. FcH/FcH^+ for the acids containing zero, one, two and three CH_2 spacer units between the ruthenocenyl and COOH functional groups respectively. One CH_2 group was enough to eliminate any communication between these two functional groups. Electrochemistry in aqueous media was conducted on the ruthenocene-containing polymers. The oxidation potential of the polymer bound ruthenocene moiety ranged between $397 \leq Ep_a \leq 631$ mV, with the latter, highest, oxidation potential belonging to the compound having no separator CH_2 groups between the ruthenocenyl and CONH functional groups.

***Keywords**:* Polyaspartamide, ruthenocene, electrochemistry, polymeric drug carriers, water-soluble.

Opsomming

Polisuksienimied is deur reakies met aminopropiel morfolien en etileendiamien gewysig om ‘n wateroplosbare bio-afbreekbare polimeriese geneesmiddeldraer te lewer. Rutenoseen is in sestien verskillende reaksies gefunktionaliseer om uiteindelik vier rutenoseen-bevattende karboksielsure van die vorm $Rc(CH_2)_nCOOH$ (n = 0 – 3) te gee. Dit is kovalent aan die amino-getermineerde sykettings van die poliaspartamied draerpolimeer geanker deur van die koppelings reagens *O*-bensotriasoliel-*N,N,N’N’*–tetrametieluronium heksafluorofosfaat gebruik te maak. Hierdie vier nuwe rutenoseen-polimeer konjugate verteenwoordig die eerste wateroplosbare rutenoseenpeptied makromolekulêre konjugate wat nog ooit gemaak is. Die karaterisering van die nuwe rutenoseen-bevatende polimere is deur XFS, ^{1}H KMR spektroskopie en elementanaliese ondersteun.

‘n Sikliese voltammetrie studie van al die rutenoseen-bevattende karboksielsure is uitgevoer in CH_2Cl_2/0.1 M $[NBu_4][B(C_6F_5)_4]$. Ten spyte van die gebruik van hierdie nie-koördinerende oplosmiddel/elektroliet systeem, het nie een van die rutenoseen-bevatende karboksielsure 'n elektrochemiese omkeerbare Rc/Rc^+ redokskoppel vertoon nie. Die formele oksidasiepotensiale van die vry karboksielsure is $E^{o'}$ = 776, 484, 494 and 516 mV vs. FcH/FcH^+ vir sure met nul, een, twee en drie CH_2 skakeleenhede tussen die rutenoseniel en COOH funtionele groepe onderskeidelik. Een CH_2 groep was genoeg om enige beduidende kommunikasie tussen hierdie twee funksionele groepe uit te skakel. Elektrochemie is uitgevoer op die rutenoseen-bevattende polimere in water. Die oksidasiepotensiaal van die polimeergebinde rutenoseeneenheid het in die gebied $397 \leq Ep_a \leq 631$ mV gewissel, waar die hoogste oksidasiepotensiaal tot die verbinding met geen spasieerende CH_2 groepe tussen die rutenoseniel en CONH funksionele groepe behoort.

Kernwoorde: poliaspartamied, rutenoseen, elektrochemie, polimeriese geneesmiddeldraer, wateroplosbaar.

Table of contents

Chapter 3

Results and Discussion 33

Chapter 4

Experimental 63

List of structures

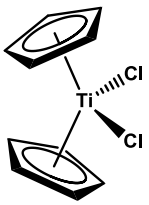

1

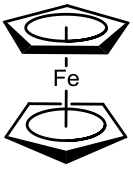

2

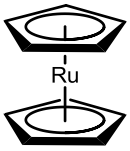

3

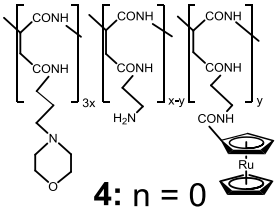

4: n = 0

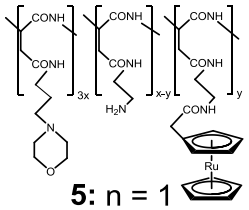

5: n = 1

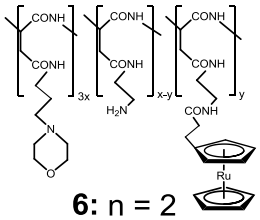

6: n = 2

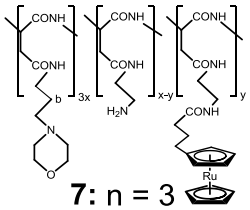

7: n = 3

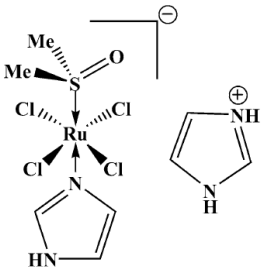

8

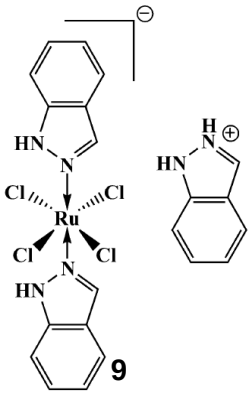

9

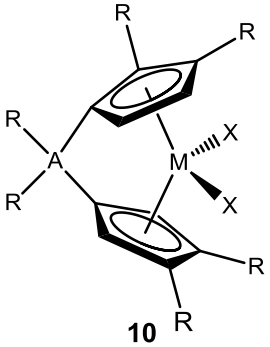

10

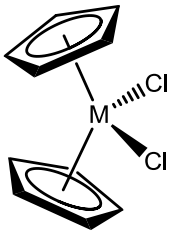

11

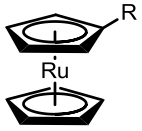

12

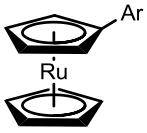

13

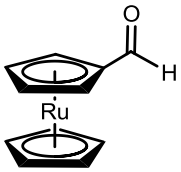

14

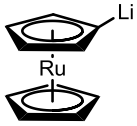

15

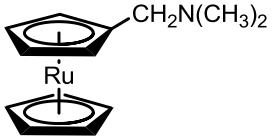

16

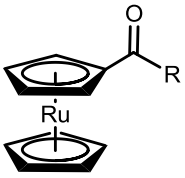

17

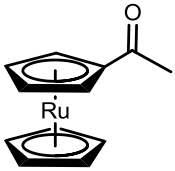

18

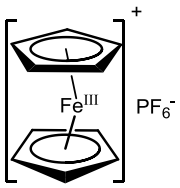

19

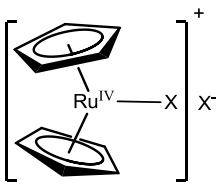

20

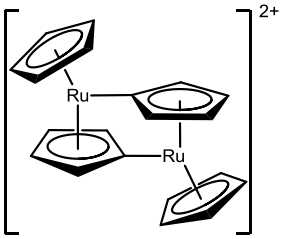

21

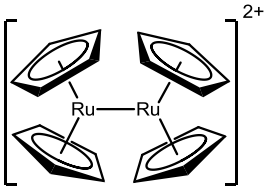

22

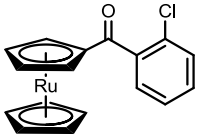

23

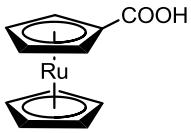

24a

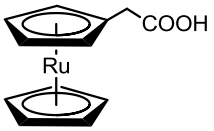

24b

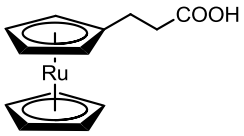

24c

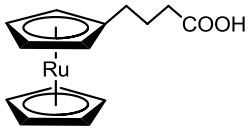

24d

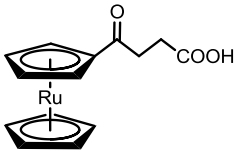

25

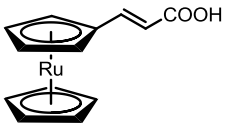

26

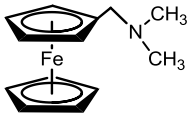

27

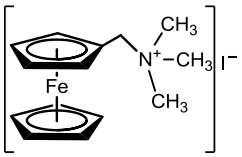

28

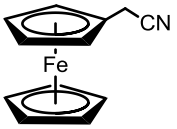

29

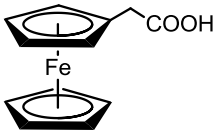

30b

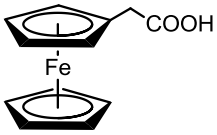

30b

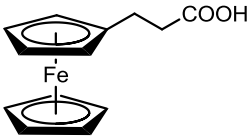

30c

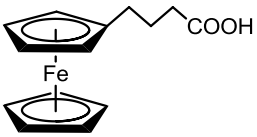

30d

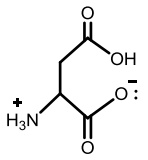

31

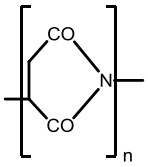

32

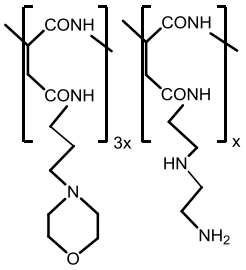

33

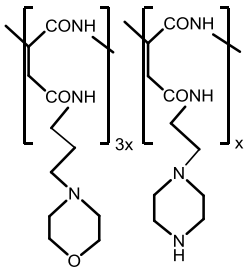

34

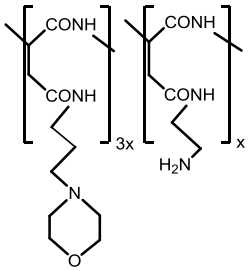

35

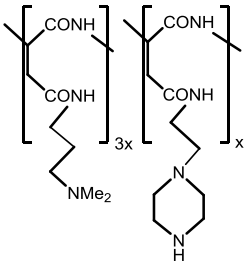

36

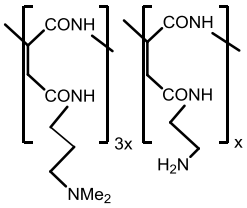

37

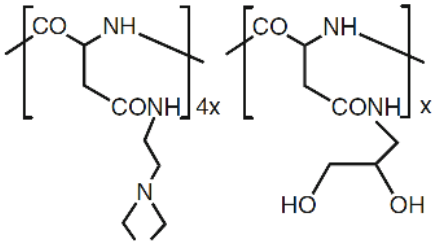

38

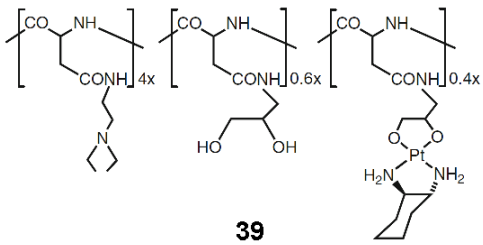

39

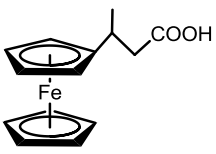

40

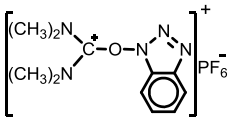

41

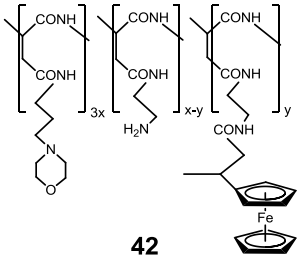

42

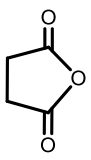

43

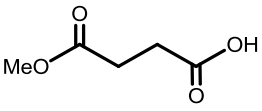

44

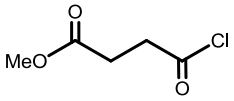

45

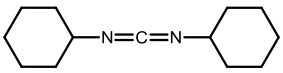

46

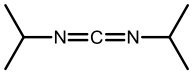

47

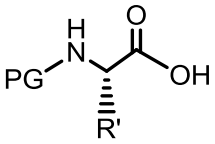

48

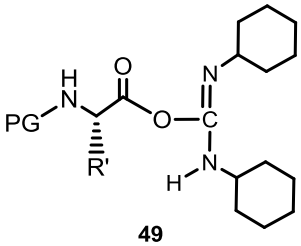

49

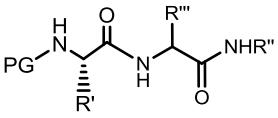

51

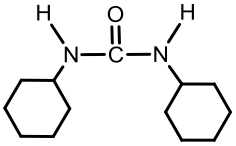

52

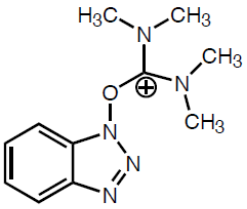

53

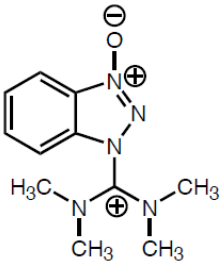

54

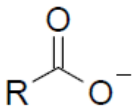

55

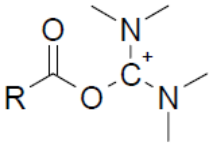

56

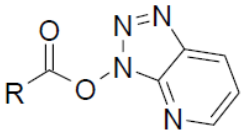

57

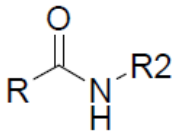

58

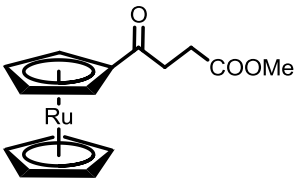

59

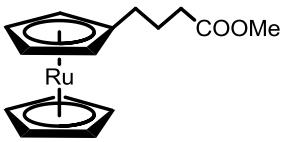

60

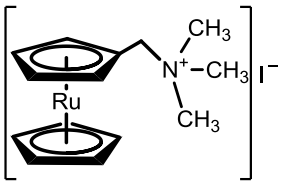

61

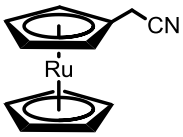

62

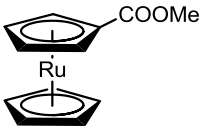

63

List of abbreviations

ArN_2^+	aryl diazonium salt
Bu	butyl
t-BuLi	tertiary-butyllithium
CO	carbon monoxide
Cp	cyclopentadienyl, (C_5H_5)
CV	cyclic voltammetry
DACH-Pt	*trans*-1,2-diaminocyclohexanediaquaplatinum(II) dinitrate
DCC	dicyclohexylcarbodiimide
DIC	diisopropylcarbodiimide
DMF	dimethylformamide
DMSO	dimethyl sulfoxide
DNA	deoxyribonucleic acid
E_{pa}	peak anodic potential
E_{pc}	peak cathodic potential
Fc	ferrocenyl, $Fe^{II}(\eta^5\text{-}C_5H_5)(\eta^5\text{-}C_5H_4)$
Fc^+	ferrocenium, $[Fe^{III}(\eta^5\text{-}C_5H_5)_2]^+$
FcH	ferrocene, $Fe^{II}(\eta^5\text{-}C_5H_5)_2$
^{1}H NMR	proton nuclear magnetic resonance
HBTU	*O*-benzotriazolyl-*N,N,N′,N′*-tetramethyluronium hexafluorophosphate
i_{pa}	peak anodic current
i_{pc}	peak cathodic current
IR	infrared spectroscopy
PF_6	hexafluorophosphate
PG	protecting group
Rc	ruthenocenyl, $Ru^{II}(\eta^5\text{-}C_5H_5)(\eta^5\text{-}C_5H_4)$
Rc^+	ruthenocenium, $[Ru^{III}(\eta^5\text{-}C_5H_5)_2]^+$
RcH	Ruthenocene, $Ru^{II}(\eta^5\text{-}C_5H_5)_2$
XPS	X-ray photoelectron spectroscopy

1 Introduction and aims of study

1.1 Introduction

Cancer is the leading cause of death in developed countries and the second leading cause in developing countries.[1] Platinum-containing complexes like cisplatin and its derivatives oxaliplatin and carboplatin have been actively used as anti-cancer drugs. Cisplatin is a very effective anticancer drug and has been the flagship metal-containing molecule for chemotherapy for over 30 years. However, most if not all anticancer drugs have side-effects that limit their effective use in chemotherapy substantially. These include acute systemic toxicity, which limits the dose size that can be administered to a patient and the induction of drug resistance. Other major drug shortcomings include their capabilities to induce allergic reactions, insufficient aqueous solubility, inaccessibility to diseased sites, premature drug metabolism and lack of selectivity.[2] The latter disadvantage probably represents the most serious limitation of all chemotherapeutic drugs; the inability of the drug to selectively react only with diseased sites in the body while largely remaining unreactive towards healthy tissue. A consequence of this lack of selective action in cancer therapy is that it simultaneously causes severe or sometimes unacceptable damage to healthy tissue.[3] This sad state of affairs necessitates the development of antitumor drug delivery systems with improved selectivity to specifically target tumour cells. If antitumor agents could be selectively administered to cancerous cells it would significantly increase its therapeutic efficiency and reduce its side effects. To this extent the use of macromolecular drug carriers for targeting tumours can considerably improve selective cancer eradication in chemotherapy especially if the drug is inactive while it is anchored to the macromolecular carrier.[4] Biocompatible synthetic polymers can act as solubilizing agents for anti-cancer agents and they can be chemically modified to incorporate site-specific targeting groups that guide drugs to cancer cells for site-specific drug release. Such polymer-drug conjugates can increase the effectiveness of an anticancer drug compared to their low molecular weight analogues.[5] Water-soluble polymeric drug carriers offer the following advantages in chemotherapy:[5,6]

i) Improved solubility of hydrophobic drugs to facilitate unhindered drug distribution in the human central circulatory system (the blood).

ii) Cell entry by adsorptive pinocytosis, a cell entry mode only available to large molecules.

iii) Passive diseased site targeting by the enhanced permeability and drug retention effect.

iv) Improved control over drug serum concentrations, (i.e. restricting the drug concentrating between the minimum toxic and minimum effective levels).

v) Slow drug release after accumulation in the target tissue from the polymer-drug conjugate (the enhanced depot effect).

vi) Prolonged polymer-protected drug concentrations expressed as half lives in body serum.

Conjugates of macromolecules with organometallic complexes have received only limited attention for biological application including their use in chemotherapy. Ferrocene-conjugates are to the author's knowledge the only investigated metallocene-macromolecular conjugate for which antineoplastic properties have been reported.[7]

When intravenously administered, the polymeric drug carrier with a drug anchored to it acts as transport vehicle designed to travel principally intact through the central circulation system to the diseased area. Once internalised into diseased cells, enzymatic chopping of the polymeric carrier backbone will release the bioactive agent for action on the target tissue.[5] By anchoring the antineoplastic ferrocene derivative 3-ferrocenylbutanoic acid onto a water soluble poly-aspartamide drug carrier, an 8 fold increase in antineoplastic activity was observed.[8]

While many metallocenes-derivatives, such as titanocene dichloride,[9] have shown highly promising antineoplastic activity, the water-insoluble sandwich metallocenes ferrocene and ruthenocene display very low or no cytotoxicity at all. In fact, despite its similar structure to ferrocene, ruthenocene anticancer activity remains largely unexplored. Chibale's research on the antimalarial properties of ruthenocene derivatives is the only meaningful biological study available.[10,11] The lack of biological studies on ruthenocene compared to ferrocene can be

attributed to the greater chemical challenges in the syntheses of substituted ruthenocenes compared to ferrocenes.

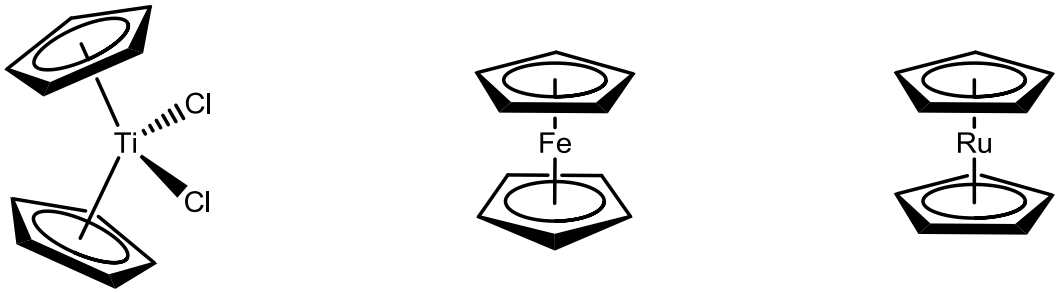

1 2 3

Figure 1.1: Structure of titanocene dichloride, ferrocene and ruthenocene**.**

Also, despite the promising results of ferrocene-containing polyaspartamide conjugates,[8,12] no communication of ruthenocene-polymer-drug conjugates have been published to date.

For ferrocenene derivatives anticancer activity is often inversely related to the formal reduction potential.[13,14] Due to ruthenium's position in group 8 directly below iron, if oxidation is also the necessary precursor step for the cytotoxic phenomena to be observed in ruthenocene derivatives, one would expect enhanced cytotoxicity for ruthenocene with lower reduction potentials.[15] This stresses the importance of electrochemical studies in the design of new potentially bio-active ruthenocene-containing compounds.

1.2 Aims of study

With the above background, the following goals were set for this study.

1) The synthesis of a series of potentially antineoplastic ruthenocene-containing carboxylic acids of the form $Rc(CH_2)_nCOOH$ (n = 0 – 3), where Rc = $Ru^{II}(\eta^5\text{-}C_5H_5)(\eta^5\text{-}C_5H_4)$, the ruthenocenyl group.

2) The synthesis of a polyaspartamide derivative as water-soluble, biodegradable polymeric drug carrier bearing side chains with anchoring sites for anchoring of ruthenocene-containing carboxylic acids

3) The anchoring of ruthenocene-containing carboxylic acids described in goal 1 to the side chains of the polymer described in goal 2, to from ruthenocenyl-polymer conjugates. These ruthenocene-containing polymers would have the nominal structure below.

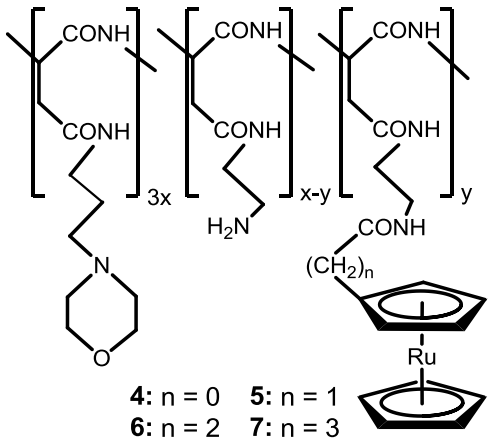

4) Study the electrochemical behaviour of ruthenocene, its carboxylic acid derivatives and the polymer-bound ruthenocene derivatives by means of cyclic voltammetry, square wave and linear sweep electrochemical studies.

---

1 A. Jemal, F. Bray, M.M. Center, J. Ferlay, E. Ward, D. Forman, *A Cancer Journal for Clinicians*, 69, **61** (2011)

2 R. Satchi-Fainaro, R. Duncan, C.M. Barnes, *Adv. Polym. Sci.* 1, **193** (2006)

3 Y. Luo and G.D. Prestwich, *Current Cancer Drug Targets*, 209, **2**, (2002)

4 M.R. Dreher, W. Liu, C.R. Michelich, M.W. Dewhirst, F. Yuan, A. Chilkoti, *J. Natl. Cancer Inst.* 335, **98** (2006)

5 L.L. Komane, E.H. Mukaya, E.W. Neuse, C.E.J. van Rensburg, *J. Inorg. Organomet. Polym.* 111, **18** (2008)

6 Y. Luo, G.D. Prestwich, *Cur. Cancer Drug Tar.*, 209, **2**(2002)

7 A.I. Mufula, E.W. Neuse, J. *Inorg. Organomet. Polym*., doi 10.1007/s10904-011-9497-3 (2011)

8 J.C. Swarts, D.M. Swarts, D.M. Maree, E.W. Neuse, C. La Madeleine, J.E. Van Lier, *Anticancer Res*., 2033, **21** (2001)

9 R.J. Knox and P.C. McGowan. *International patent WO 2004/005305*.

10 M.A.L. Blackie, K. Chibale, *Metal-Based Drugs*, doi:10.1155/2008/495123 (2008)

11 P. Beagley, M.A.L. Blackie, K. Chibale, C. Clarkson, J.R. Moss, P.J. Smith, *J. Chem. Soc., Dalton Trans.*, 4426, **23** (2002)

12 E.W. Neuse, *J. Inorg. Organomet. Polym.*, 3, **15** (2005)

13 J.C. Swarts, T.G. Vosloo, S.J. Cronje, W.C. du Plessis, C.E.J. van Rensburg, E. Kreft, J.E. van Lier, *Anticancer Res.*, 2781, **28** (2008)

14 E. Fourie, E. Erasmus, J.C. Swarts, A. Jakob, H. Lang, G.K. Joone, C.E.J. van Rensburg, *Anticancer Res.*, 825, **31** (2011)

15 P. Pigeon, S. Top, A.Vessières, M. Huché, E. A. Hillard, E. Salomon, G. Jaouen, *J. Med. Chem.* 2814, **48** (2005)

2 Literature survey

2.1 Introduction

This chapter provides a literature survey of selected aspects relevant to the goals set for this study. Recent developments in metallocene anticancer agents will be discussed, including their shortcomings and progress to demonstrate the need for the development of new types of anticancer drugs. Specific reference will be made with regard to ruthenocene to motivate the strategy to anchor ruthenocene to a drug delivery system as has been proven beneficial in the case of ferrocene.[16] Finally, a background will be provided on the synthesis, general chemistry and electrochemical behaviour of ruthenocene, its derivatives and polymer-drug conjugates.

2.2 Organometallic antitumor agents

Organometallic compounds are metal complexes that contain at least one direct covalent carbon-metal bond. Developments in organometallic chemistry have mostly been directed towards their usefulness in the catalytic synthesis of a number of commercially valuable chemical products. Some of the successful industrial processes of this type of reaction include the Monsanto process which involves the carbonylation of methanol to acetic acid, the Wacker process which is used for the conversion of ethylene to acetaldehyde and the hydroformylation of olefins to aldehydes.[17] The most common classes of organometallic compounds that are being developed are metallocenes, half-sandwich compounds, CO-, carbene- and π-ligand complexes. Many of these complex classes have now also found application in medicinal chemistry.[18] They offer unprecedented versatility as pharmaceuticals because of their structural variety, the kinetics of ligand substitution when coordinative bonds with biomolecules are pertinent, the combination of rigidity around the metal and flexibility in the ligands, the variety of available interactions (π-stacking, hydrogen-bonding, coordinative bond formation and spatial recognition) and their redox

properties.[19] Thus organometallic complexes have been developed as anticancer agents, radiopharmaceuticals for diagnosis and therapy, and biosensor probes.

2.2.1 Ruthenium antitumor agents

Ruthenium is a unique metal in the platinum group of transition metals. It has a partially filled 4*d* subshell which allows it to form complexes that are useful in a wide variety of applications including electronics,[20] catalysis, biosensors[21], photochemistry and anticancer drugs[22].

Cancer is a large class of malignant diseases caused by accelerated and uncontrolled proliferation of cells. Defective cellular apoptosis (programmed cell death) is a major cause in the development and progression of cancer.[23] Apoptosis is the process by which cells 'commit suicide' in a controlled manner. Destroyed cells spill out onto surrounding cells and cause damage that are quickly removed. Despite the widespread use of platinum-based anticancer compounds such as cisplatin in chemotherapy over the past 30 years, new metal-based antineoplastic drugs needs to be developed. All chemotherapeutic drugs including platinum-based drugs impose clinical limitations by the incidence of acute systemic toxicity and drug resistance. The rationale behind the development of almost all metal-based drugs, including platinum-containing drugs, is to synthesise compounds which induce apoptosis by targeting DNA. It is now known that ruthenium anticancer drugs do not mimic platinum drugs by direct interaction with DNA. The different mechanism of ruthenium from that of cisplatin is advantageous in that it helps to overcome platinum drug resistance in tumour cells.[24] The non-cross-resistance is partly due to the ability of ruthenium complexes to mimic iron in its binding to biological molecules, such as transferrin, thereby exploiting the mechanisms for non-toxic transport of iron.[25] Transferrin is iron-binding blood plasma glycoproteins with the natural function of transporting iron to cells. Due to ruthenium's similarity to iron this transport mechanism is biologically available to transport especially coordinated ruthenium complexes to cancer cells which leads to these ruthenium complexes accumulating in neoplastic regions rather than normal tissue.[26] Transferrin-ruthenium complexes are actively moving to cancerous tissue which contains high external transferrin receptor densities. Once the transferrin-ruthenium drug conjugate is bound to the transferrin receptors on the outside of the cancer cells, the ruthenium complex is released from the transferrin carrier and then immediately internalized by the tumour.[27] This delivery

mechanism is very unique and the polymer drug delivery system synthesized in this study borrows a little from this natural occurring process.

Ruthenium-based drugs are often less toxic compared to platinum drugs. Ruthenium will remain in its relatively inactive Ru^{3+} oxidation state while it is transported to the tumour site. This is simply because of activation by reduction while the Ru^{3+} drug circulates in the blood having high pH(~8) and free oxygen content is less feasible than in cancer cells.[28] The Kreb's cycle lowers the pH around the tumour to create a suitable environment to reduce Ru^{3+} to Ru^{2+}.[29] With all these properties ruthenium is predicted to produce drugs that are distinct from existing platinum-based drugs.

NAMI-A and KP1019 are two ruthenium drugs that have already entered clinical trials.

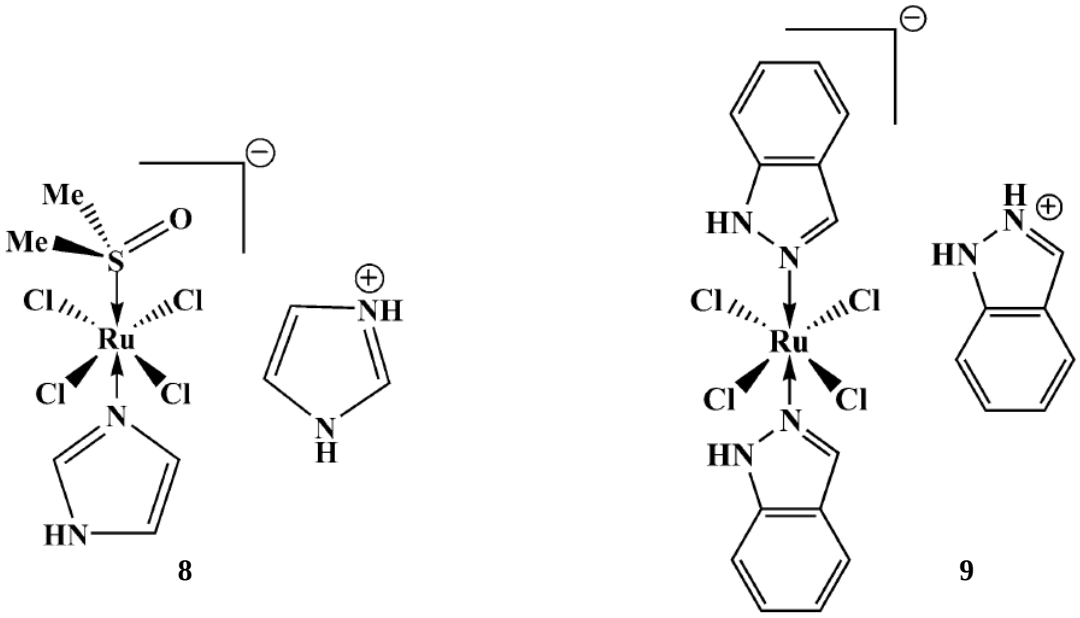

Figure 2.1: Chemical structure of NAMI-A and KP1019

NAMI-A is a Ru(III) complex molecule with imidazole and DMSO coordinated to the ruthenium, Figure 2.1 (left). NAMI-A elicited antitumor and antimetastatic activities in preclinical studies. KP1019 is a stable Ru(III) complex which contain two indazole heterocycles coordinated to ruthenium centre via nitrogen atoms, Figure 2.1 (right). KP1019 promoted apoptosis in a number of cancer cell lines as well as in a range of tumour models by direct cytotoxic activity.[27]

2.3 Metallocenes

Metallocenes are compounds which exist in a "sandwich" structure, in which a metal is sandwiched between two cyclopentadienyl ($C_5H_5^-$, Cp) rings and covalently bound to all ten cyclopentadienyl carbon atoms. Unsubstituted metallocenes normally contain the formula fragment $M(C_5H_5)_2$ where M includes almost all the transition metals.

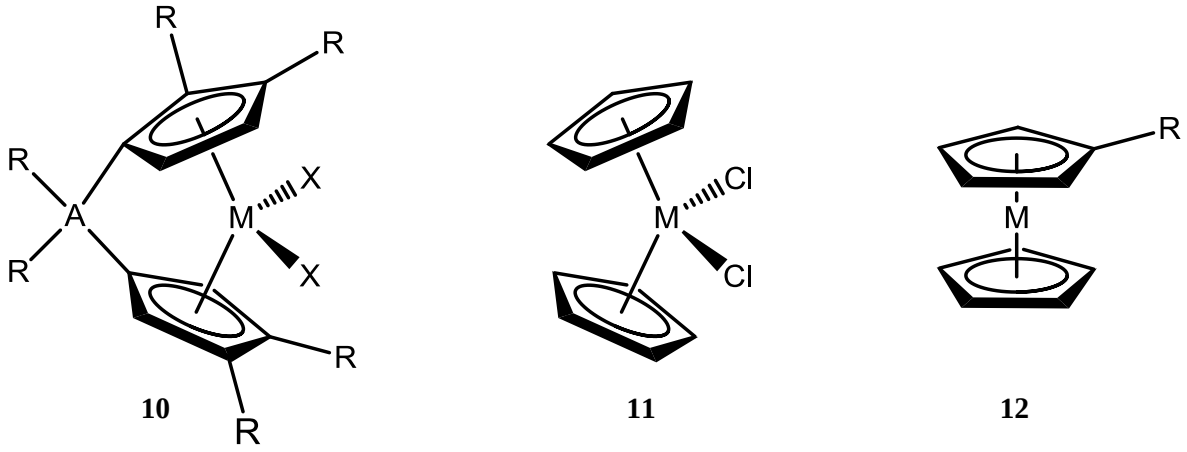

10 **11** **12**

M = transition metal
A = optional bridging atoms
R = H, alkyl or other hydrocarbon groups
X = halogen or alkyl groups

Group 4 cationic metallocene dichlorides
M = Ti, Zr, Hf

mono-substituted group 8 metallocenes
M = Fe, Ru, Os

Figure 2.2 Different types of metallocenes. The positions R, M, A and X represent sites where metallocenes may be chemically modified.

Many different types and variants of metallocenes are possible by variation of the central metal atom, changing the non-cyclopentadienyl ligands and cyclopentadienyl ring substitutions. These changes lead to variations in the compounds' electronic properties, as well as in the steric and coordination environment of the metal. One of the defining characteristics of metallocenes, such as ferrocene and ruthenocene, is their aptitude to undergo electrophilic aromatic substitution reactions.[30] Friedel-Crafts acylations are one of the most important reactions in this class; it also provided evidence of aromaticity for these metallocenes.[31]

Group 4 cationic metallocenes are mostly known as Ziegler-Natta class 2 catalysts. In general they have the composition Cp_2MCl_2 (M = Ti, Zr, Hf), such as titanocene dichloride, and are highly efficient at catalysing polymerisation of α-olefins. Variation of the substituents attached to the cyclopentadienyl rings leads to changes in catalyst selectivity and activity.[32]

The two Cp rings can be linked with bridges, like -CH_2-CH_2- or -Si(Ph_2)-, such compounds are known as ansa-metallocenes.

The metallocenes of group 8 are stable compounds with the metal in its formal 2+ oxidation state to have 18 valance electrons. Ferrocene, ruthenocene and osmocene all exhibit substitution reactions that are characteristic of aromatic systems. The electrophilic reactivity of these metallocenes decreases in the order: ferrocene > ruthenocene > osmocene.[33] Ferrocenes have been extensively researched and numerous good reviews have been written on them.[34,35,36,37,38] They have been applied in the fields of catalysts, pharmaceuticals and electrochemistry amongst others. The general chemistry of ruthenocenes and osmocenes has been researched much less, mostly because they are much less reactive and much more expensive. Research during this study was focussed on mono-substituted derivatives of ruthenocene.

2.3.1 Ruthenocene

Ruthenocene undergoes many reactions characteristic of aromatic compounds, enabling the preparation of substituted derivatives. Ruthenocene is closely related to the isoelectronic ferrocene; consequently most substitution reactions for ferrocene can be adapted to prepare the similar ruthenocene derivative. Ruthenocene is a system that is less "superaromatic" than ferrocene.[39] Thus, deuterium exchange in acid medium proceeds in ruthenocene much slower than in ferrocene.[40] The general organic chemistry of the mono-substitution of ruthenocene relevant to this study is shown in Scheme 2.1

Acetyl ruthenocene, **18,** can be prepared by the Friedel-Crafts acylation of ruthenocene with acetic anhydride or acetyl chloride in the presence of aluminium chloride as a catalyst. When a mixture of ruthenocene and ferrocene is subjected to competitive acylation by the Friedel-Crafts method ferrocene is acylated predominantly.[40] Friedel-Crafts acylation of acid chlorides to metallocenes gives a method of attaching a wide variety of different substituents to the ruthenocenoyl group, **17**.

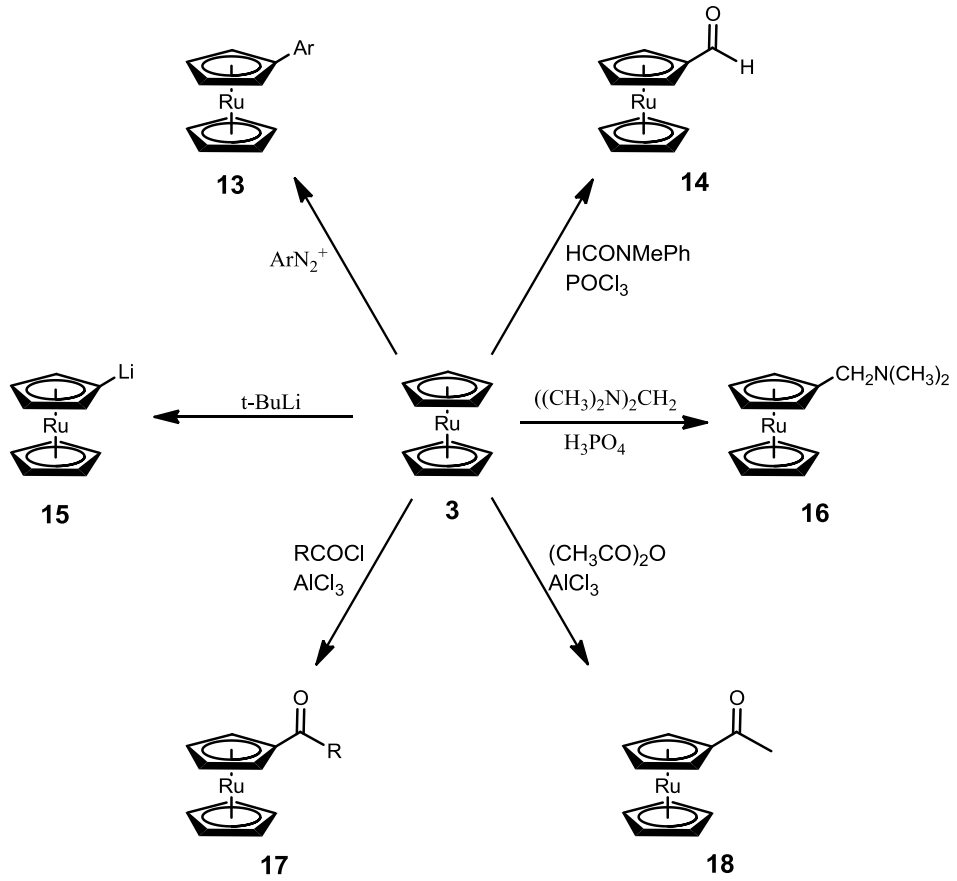

Scheme 2.1 Synthesis of a variety of reactive monosubstituted ruthenocene derivatives. (ArN_2^+ = aryl diazonium salt, *t*-BuLi = tertiary-butyllithium)

Ruthenocene aldehyde, **14**, is prepared by reacting ruthenocene with *N*-methylformanilide (N-MeFA) in the presence of phosphorous oxychloride.[41] To synthesize the aryl or alkyl-substituted ruthenocene derivatives, **13,** ruthenocene is reacted with the appropriate diazonium salt.[42] The mono-lithiation of ruthenocene to give **15** is performed by the same method as for ferrocene, in which the metallocenes are reacted with *t*-butyllithium.[43] It has long been established that ruthenocene is more reactive towards lithiation than ferrocene.[33] This higher reactivity can be assigned to the much less negative charge on the cyclopentadienyl rings of ruthenocene than on those of ferrocene and thus a higher acidity of the ruthenocene system.[43] *N,N*-dimethylaminomethyl ruthenocene, **16**, can be prepared by the Mannich reaction of ruthenocene with *N,N,N',N'*-tetramethyldiaminomethane in glacial acetic acid at in the presence of phosphoric acid.[42] All these ruthenocene compounds are useful precursors to larger ruthenocene-containing molecules.

A very interesting reaction of ruthenocene is the electrochemical preparation of a bis-(ruthenocenium) dication, **22** $[(RuCp_2)_2][B(C_6F_5)_4]_2$ which arises from the one-electron oxidation of ruthenocene in dichloromethane containing either $[NBu_4][B(C_6F_5)_4]$ or $[NBu_4][B(C_6H_3(CF_3)_2)_4]$.

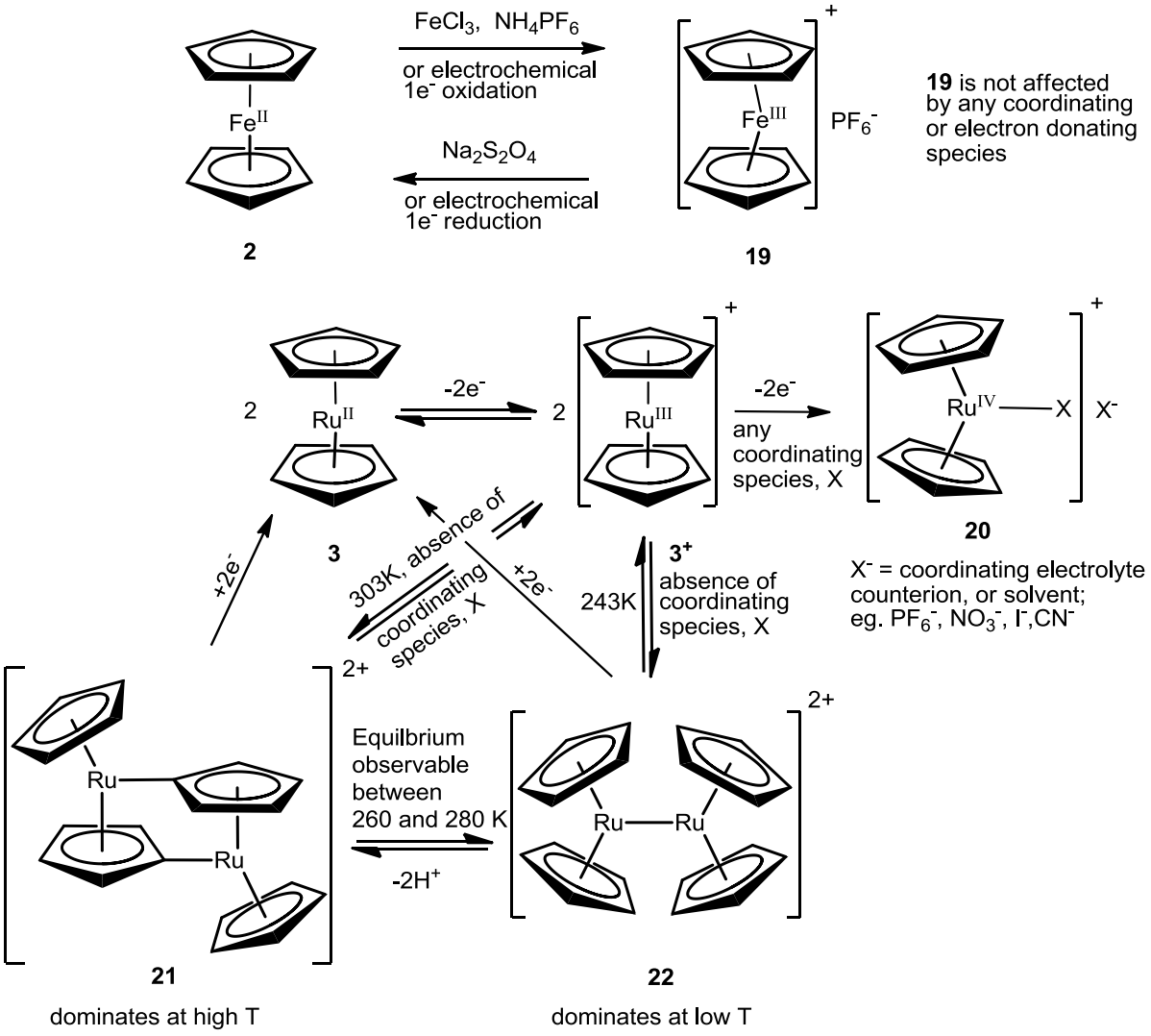

Scheme 2.2 The electrochemical oxidation chemistry of ferrocene is much more simple than the oxidation of ruthenocene. Oxidation, in the absence of coordination species, leads to several species in equilibrium with each other.

Precipitation of $[(RuCp_2)_2][B(C_6F_5)_4]_2$ occurs during anodic electrolysis of ruthenocene at 243 K when the supporting electrolyte is $[B(C_6F_5)_4]^-$, allowing its isolation.[44] The monomeric $[RuCp_2]^+$ cation, $\mathbf{3}^+$**,** exists if the counter anion is $[B(C_6F_5)_4]^-$ or $[B(C_6H_3(CF_3)_2)_4]$. In the presence of all other anions, $\mathbf{3}^+$, converts to the Ru(IV) species, see Scheme 2.2. $[RuCp_2]^+$ cation, $\mathbf{3}^+$**,** is in fast equilibrium with the dimeric species $[(RuCp2)2]^{2+}$, **22,** at low temperature (243 K).[45] At higher temperature another dinuclear ruthenium equilibrium

species, **21** dominates. In the case of ferrocene, the preparation of ferrocenium salts involve the one-electron oxidation of ferrocene by an oxidizing agent eg. $FeCl_3$ followed by the addition of a counter-ion like $[PF_6]^-$ to yield $[FeCp_2][PF_6]$, **19**.[46] In contrast, for ruthenocene, the rapid reaction between $\mathbf{3}^+$, and almost any anion, generates a Ru^{4+} complex such as $[Ru(PF_6)Cp_2][PF_6]$, **20,** in the case where the anion is $[PF_6]^-$.[44, 47] Analogous complexes of the type $[RuCp_2X]^+$, where X = halide, have been isolated.[47, 48]

2.3.2 Synthesis of ruthenocene carboxylic acids.

This part gives a background on the preparation of the series of ruthenocene-containing carboxylic acids $Rc(CH_2)_nCOOH$ (n = 0 – 4, **24a - 24d**), which relates to goal 1. The anchoring of the ruthenocene-containing drug to the polymeric drug carrier by an amide bond implies the availability of a ruthenocene-containing carboxylic acid. Reference will also be made to the already known synthetic procedures of ferrocene-containing acids **24a - 24d**[42, 49,50]

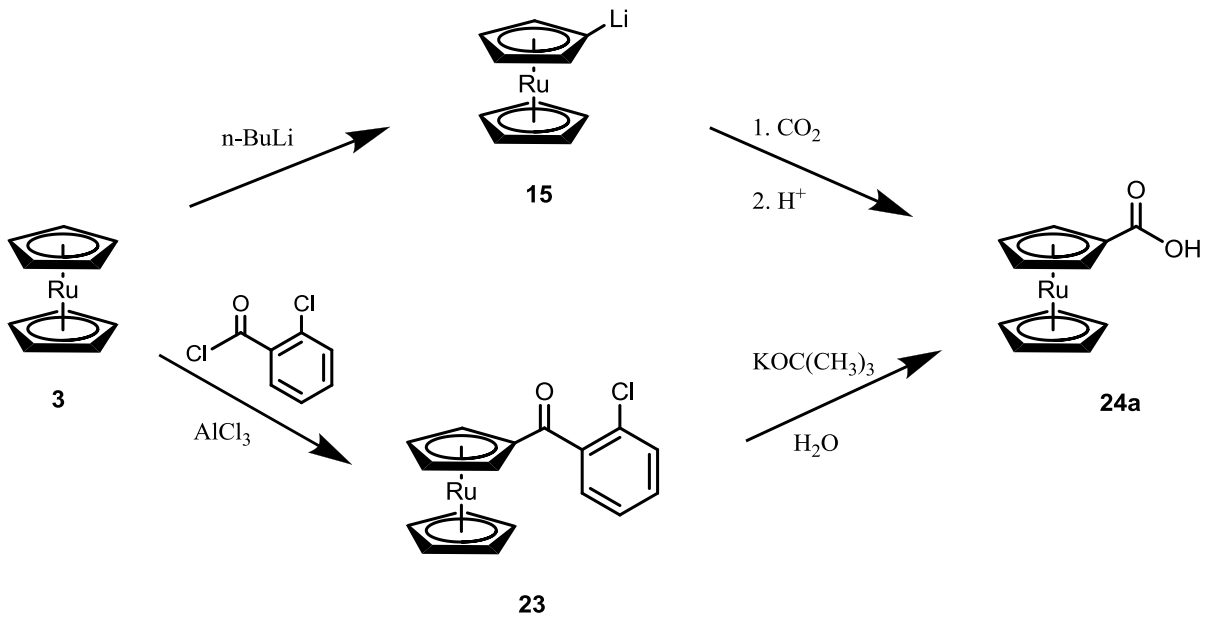

Scheme 2.3 Two different routes for the synthesis of ruthenocenecarboxylic acid, 24a.

Ruthenocene carboxylic acid, **24a,** has been prepared via two different pathways. Reaction of ruthenocene with *n*-BuLi results in a lithioruthenocene, which when treated with carbon dioxide followed by HCl, yields ruthenocene carboxylic acid.[33] In an alternative synthesis ruthenocene, **3**, is first reacted with 2-chlorobenzoylchloride to yield 2-chlorobenzoylruthenocene, **23**. This product is then reacted with potassium *tert*-butoxide in the presence of water to yield **24a**.[51]

Ferrocene-containing carboxylic acids of the form $Fc(CH_2)_nCOOH$ (n = 0, **30a**, n = 1, **30b**, n = 2, **30c**, and n = 3, **30d**) have been prepared by multi-step organic synthesis, Scheme 2.4. This study will adapt these procedures to also be applicable to ruthenocene acids despite the lower reactivity of ruthenocene.

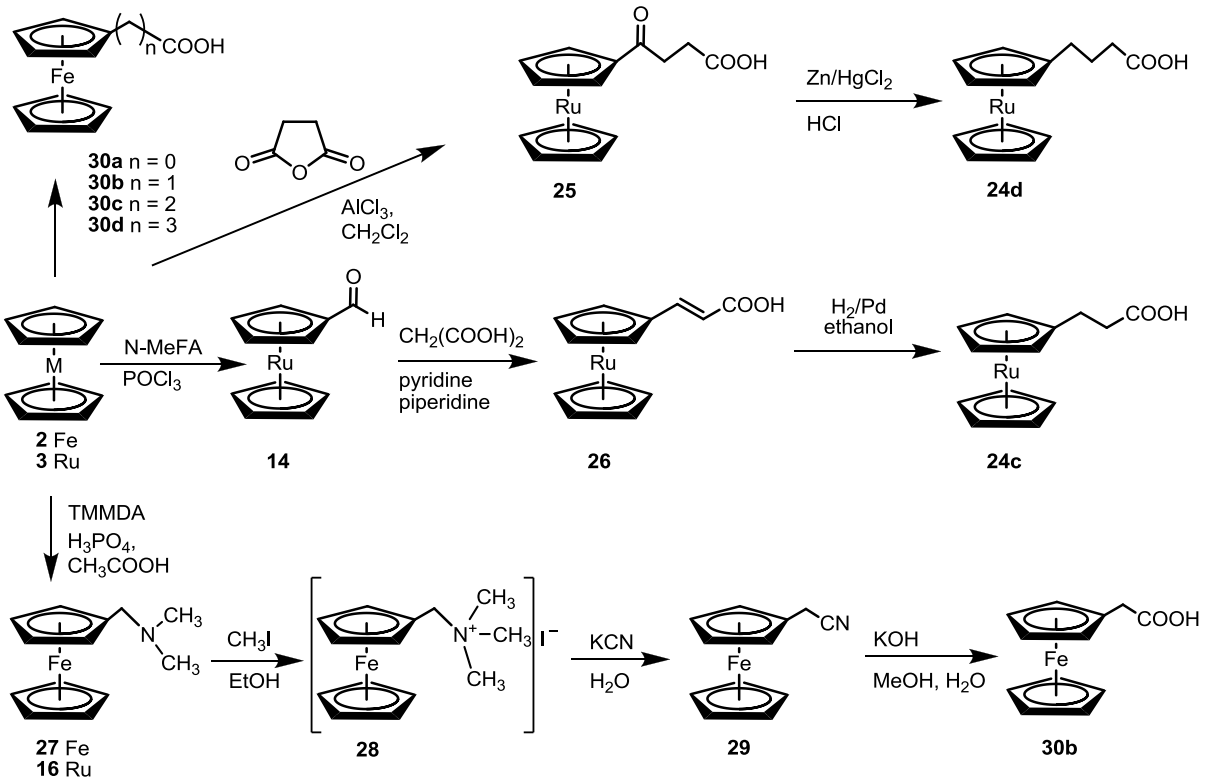

Scheme 2.4 Synthesis of ferrocene and ruthenocene-containing carboxylic acids.

Ferrocenyl acetic acid, **30b**, may be prepared from *N*,*N*-dimethylaminomethylferrocene, **27**. Treatment of **27** with methyl iodide gives *N*,*N*,*N*-trimethylaminomethylferrocenyl iodide, **28**, followed by cyanation gives ferrocenylacetonitrile, **29**. Hydrolyses of the nitrile, **29,** gives the acid, **30b**.[52] As far as the ruthenocene analogues in this multistep synthesis are concerned, only *N*,*N*-dimethylaminomethylruthenocene, **16**, is known.[42, 53] 3-Ruthenocenylpropanoic acid, **24c**, has been prepared by Kamiyama *et al*., from ruthenocenylcarboxaldehyde, **14**, and malonic acid, followed by the hydrogenation of **26**.[49] 4-Ruthenocenylbutanoic acid, **24d,** is prepared by the Friedel-Crafts acylation of ruthenocene, **3**, with succinic anhydride to liberate **25**, which is reduced by the Clemmenson reduction to liberate **24d**.[42] However attempts to repeat this reaction in this study produced unacceptably low yields.

2.4 Polymeric drug carriers

A major challenge in cancer chemotherapy is the selective delivery of small molecule anticancer agents to tumour cells. Polymer-drug carriers stand out as a uniquely promising tool to achieve this and will be discussed in this section with reference to goals 2 and 3. The problems associated with small-molecule chemotherapeutic drugs are discussed followed by a discussion of the general strategy towards the syntheses of water-soluble polymeric drug carriers and polymeric-drug conjugates. Methods of drug release from the polymeric carrier and drug uptake are discussed and finally, selected examples of relevant existing polymer-drug conjugates and their properties are given.

2.4.1 Limitations of conventional small-molecule chemotherapeutic drugs

Lack of water solubility and numerous detrimental side effects of anticancer drugs limit their effective use in chemotherapy substantially. These side-effects include the induction of drug resistance and acute systemic toxicity, which limits the dose size that can be administered to a patient. Other major drug shortcomings include their tendency to induce allergic reactions, inaccessibility to diseased sites, premature drug metabolism and lack of selectivity.[54] The latter disadvantage probably represents the most serious limitation of all chemotherapeutic drugs; the inability of the drug to selectively react only with diseased sites in the body while largely remaining unreactive towards healthy tissue. A consequence of this lack of selective action in cancer therapy is that it simultaneously causes severe or sometimes unacceptable damage to healthy tissue. The inability of chemotherapeutic agents to gain access to the infected site at an appropriate dosage reduces their therapeutic effectiveness. Furthermore, the metastatic nature of tumour cells requires that total tumour cell destruction be achieved early in treatment, before drug resistance is developed, or a mutation in the cancer cell line renders the drug completely ineffective. To combat these negative aspects associated with most if not all chemotherapeutic drugs, new antineoplastic materials are increasingly being synthesised and evaluated,[55, 56] combination therapy has been investigated in the hope of finding synergistic effects,[57] completely new ways of fighting cancer, such as photodynamic cancer therapy,[58] is being investigated, and new methods of delivering an active drug to a cancerous growth are being developed.[59, 60]

2.4.2 Properties of polymeric drug carriers

To overcome the pharmacological hurdles in the way of disease treatment, vehicles capable of carrying the cytotoxic agent in a highly concentrated form exclusively to the diseased site

will be beneficial. This will allow the efficient killing of diseased cells while largely leaving the surrounding healthy cells unharmed. To achieve this goal biocompatible polymer drug carriers, carrying a substantial amount of drugs are developed. Biocompatible synthetic polymers can take advantage of the rather unique pharmacokinetic behaviour of macromolecular compounds in the mammalian organism. They may increase the therapeutic index of the drug by facilitating endocytotic cell entry of the conjugate and making more drug molecules available at the diseased sites while reducing unwanted systemic drug exposure.[60] By localizing the drug at the desired site of action, macromolecular therapeutics have improved drug efficacy and enhanced patient safety due to the lower doses.[16] Since small molecule drugs and macromolecular drugs enter cells by different pathways, multi-drug resistance can be minimized. Other advantages of macromolecular drug carriers in chemotherapy are itemised in Chapter 1.

2.4.3 Synthetic strategies for polymeric drug delivery devices

An ideal macromolecular drug would consist of four parts as a bioconjugate system: [61]

1) a macromolecular carrier,
2) a biodegradable spacer unit,
3) an antitumor drug and
4) a targeting agent.

Synthetic polymers allow for design-specific structural tailoring. A general strategy to synthesise water-soluble polymeric drug carriers and covalently anchor a potential drug to it is shown in Scheme 2.5 (scheme adapted from references 55 and 63). The process also includes functionalization of the drug to allow anchoring to the polymeric drug carrier *via* a biodegradable bond. These polymers are to contain a biodegradable, linear main chain composed of sub units bearing water-solubilizing groups and other sub units equipped with functional groups suitable for reversible drug binding (anchoring), and still other sub units capable of harboring a homing device. A homing device would represent some molecular entity permitting selective targeting to the diseased tissue.[63]

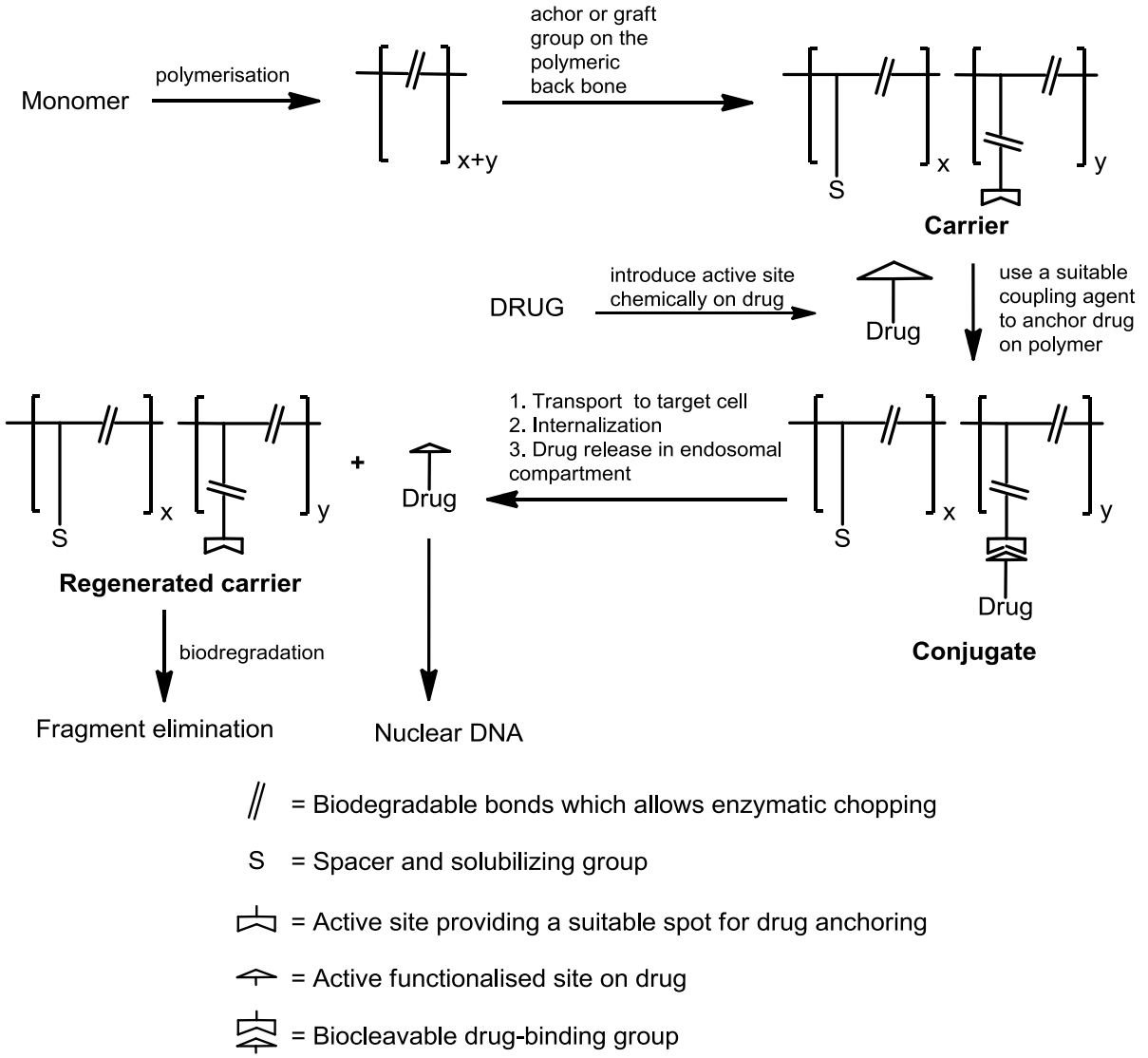

Scheme 2.5 Drug binding and drug release

Upon bioreversible binding of the drug molecule to the carrier, the resulting polymer-drug conjugate, acting as a pro-drug, will transport the drug component to and into the target cell, where the payload of drug must be separated from the carrier and delivered as a free drug in the cancer cell interior. The controlled release of the drug inside the cancer cell should in principle serve to activate it and allow the drug to destroy or damage the DNA of cancer cells in a way that is sufficient to cause cancer cell death. The biocleavable drug binding group shown in Scheme 2.5 may be a peptide (*i.e.* amide), sugar or nucleotide bond. In order to meet the need for biodegradation, a precondition for smooth elimination of the fragmented polymer chain in the ‘‘spent’’ state after release of the drug component, biofissionable groups, *e.g.* ester, amide, or urethane links, must be incorporated into the polymer backbone. Derivatives of aspartic acid are biocompatible (*i.e.* non-toxic) and especially suitable as

polymeric drug carriers.[62] Since cancer cells have a higher demand for energy and building blocks of tissue, *i.e.* amino acids, they in principle must show a faster uptake of polyaspartamide derivatives than normal cells.[55] In order to meet the important requirement of water solubility, a solubilizing agent prone to aquation was grafted onto the polymeric backbone. This solubilizing unit also serves to keep active sites on the polymer sufficiently far apart to prevent unwanted side reactions such as crosslinking.

The drug-anchoring functionality on the polymer back bone should be capable of reacting with any reactive group on the drug molecule. Preferred anchoring sites on the polymer include the carboxylic acid group which can react with nucleophilic (amino or hydroxyl) sites on the drug. Alternatively, they can be primary or secondary amine functionalities to react with drug-containing carboxylic or aldehyde groups.[63] Lastly, the carrier's molecular mass should exceed 20,000–25,000 so as to retard kidney clearance, yet should stay below 100,000 to avoid toxic effects as sometimes observed with large macromolecules.[63]

2.4.4 Cell uptake and drug release

Uptake and internalization of polymers such as **39** (description, page 20, scheme 2.8) by cells probably occurs by endocytosis, in particular fluid phase pinocytosis as described by Duncan[64,65] and shown in Figure 2.3. Here cells pinch off and internalise small fluid-filled plasma membrane vesicles of about 250 Å in diameter. These vesicles are similar to phagocytic vacuoles, and they fuse with primary lysosomes to form secondary lysosomes. Release of the drug from the dissolved polymeric drug carriers inside the newly formed secondary lysosomes occur by enzymatic hydrolysis of biodegradable amide (peptide) bonds due to the action of more than 50 hydrolytic enzymes that are generated in the Golgi apparatus.[66]

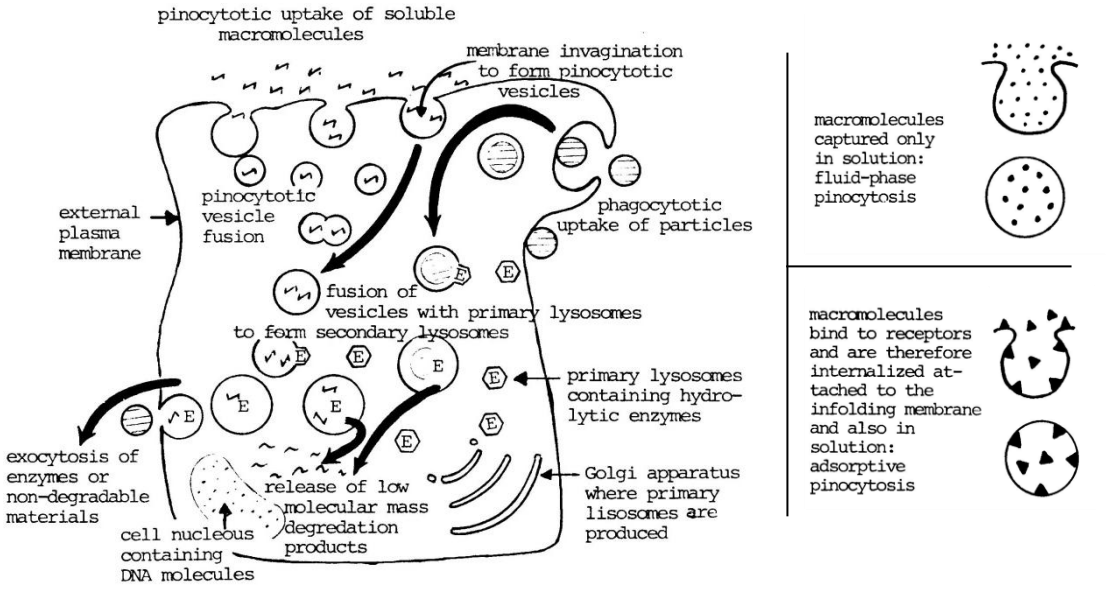

Figure 2.3 Cellular pinocytic uptake of soluble macromolecules (Adapted from references 64 and 50)

Biodegradable bonds other than the peptide bond may also be used to achieve release of the drug from the polymer as well as digestion of the polymer itself to small-molecule degradation products. These would include bonds that can be cleaved by redox reactions or acid hydrolysis. These bonds should be stable at physiological pH (~7.4) but cleavable inside the acidic pH (~5.5) maintained within the lysosome. After polymer degradation, the low molecular mass products, which now include the released drug itself, allows targeted access of the drug to the nuclear DNA.[55] Non-biodegradable macromolecules would accumulate within secondary lysosomes for release by exocytosis. If a polymeric drug carrier can be exclusively targeted to a cancer cell it follows that the released drug will exclusively destroy cancer cells and not any normal healthy tissue.

2.4.5 Selected examples of polymer-antitumor drug conjugates

Water-soluble derivatives of poly(L-α-amino acid) acids have properties that mimic proteins, making them attractive choices for polymeric drug carriers. These properties include increasing solubility and stability of drug attachments, disease targeting capabilities, drug encapsulation possibilities, the prospect of bypassing multidrug resistance factors, low toxicity, minimal stimulation of the immune system, and biodegradability.[67] Derivatives of poly(aspartic acid) are central to this study.

Aspartic acid, **31** has been thermally polymerised to polysuccinimide, **32,** of molecular mass 57 000 within 2 hours at 180 °C under reduced pressure.[62]

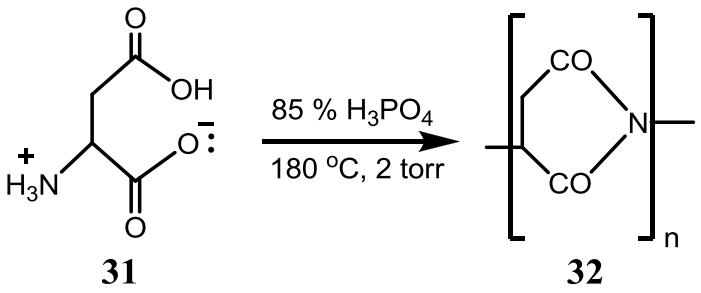

Scheme 2.6 The polymerisation of aspartic acid, 31 to polysuccinimide, 32

Neuse and Perlwitz[68] prepared several derivatives of polyaspartamides by aminolytic ring opening addition of primary amines. The synthesis of polyaspartamides start out from polysuccinimide, the amide rings of which are opened by nucleophilic reaction with amines in aprotic medium, generally N,N-dimethylformamide, as shown in Scheme 2.7.[62,69] The functionalization with substituents R´ and R´´ were chosen in order to obtain desirable properties built into the polymeric carrier.

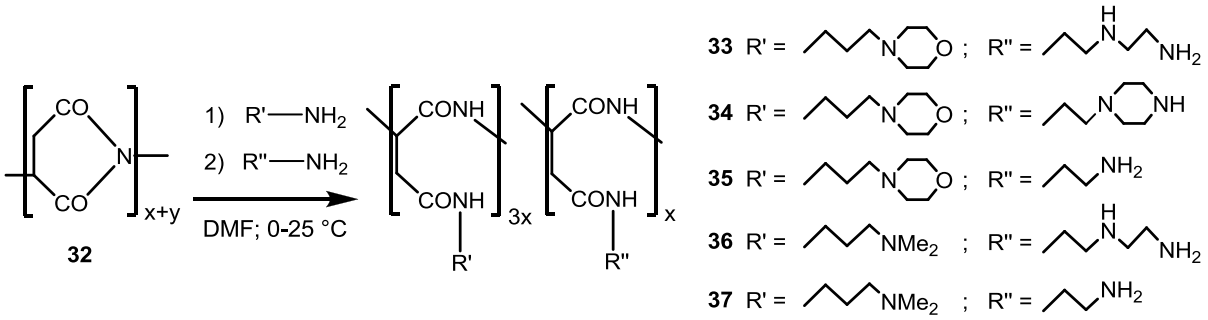

Scheme 2.7 Potential polymeric drug carriers with amino groups which lend themselves to coupling.

The group R´ is chosen mainly to enhance the water solubility of the carrier polymer, but also serves as a spacer unit to keep active sites on the polymer sufficiently far apart to prevent unwanted side reactions including crosslinking. R´´ have a terminal reactive functional group which can act as a suitable binding site for drug attachment. The groups should be separated from the main chain by short (5 - 15 constituent-atoms) side chains or spacers to diminish the steric inaccessibility caused by the polymeric backbone. Amino groups lend themselves to coupling reactions with carboxyl groups under mild conditions. Such coupling can often be carried out in aqueous or mixed aqueous-organic solvents with the aid of techniques developed in amino acid chemistry by biochemist. This functionalization represents a highly versatile method for the preparation of water-soluble, non-toxic and non-immunogenic

polyamides possessing specific side groups, including those capable of binding medicinal agents.

Neuse *et al.* successfully exploited this reaction for the development of highly bioactive anticancer drug conjugates, especially platinum compounds.[67,69,70] One example of such a conjugation originating from polysuccinimide, involved the successive addition of 3-aminopropane-1,2-diol as the hydroxyl donor, followed by a second amine as the solubilizing and target-homing component and finally metal attachment *via* chelation with *trans*-1,2-diaminocyclohexanediaquaplatinum(II) dinitrate.

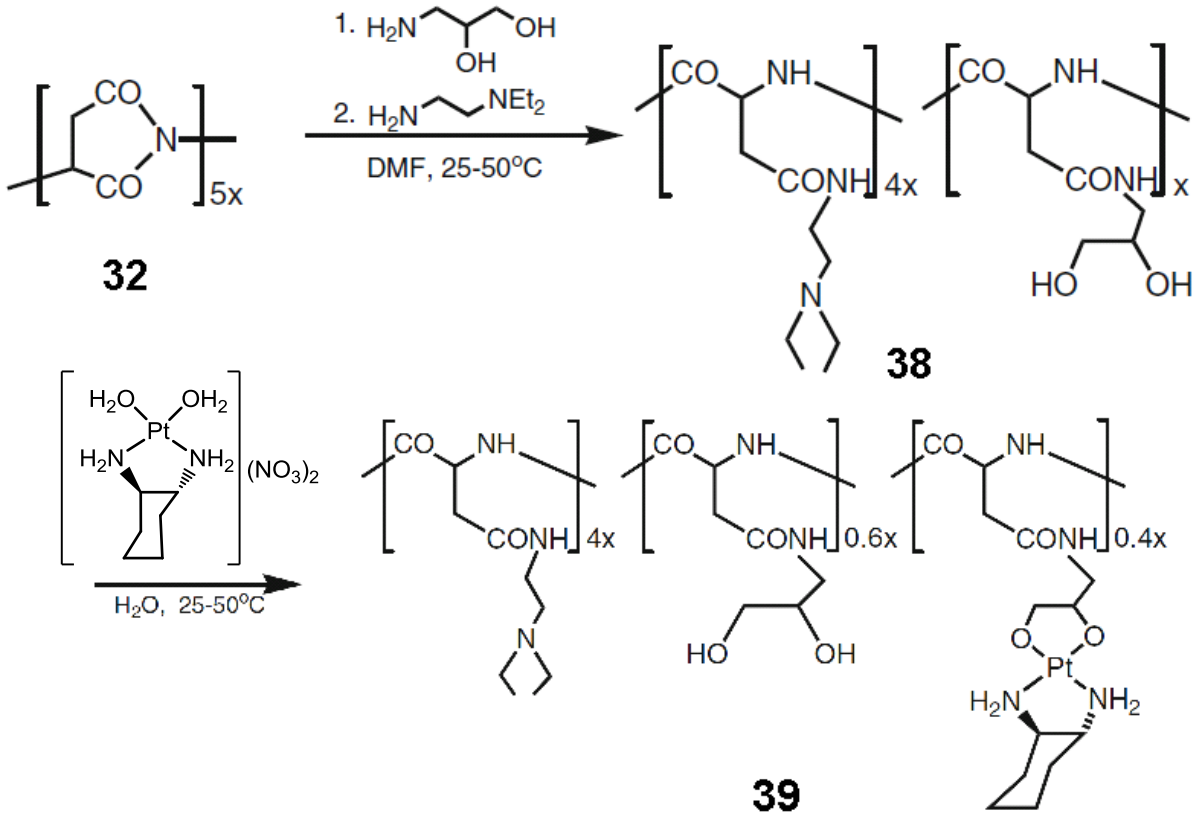

Scheme 2.8 The synthetic route to prepare the platinum-containing copolyaspartamide 39 from polysuccinimide, 32.

Such platinum-containing polymers in which the metal is carrier-bound will deliver the free bioactive Pt complex hydrolytically for its cytotoxic action.

Derivatives of ferrocene have been anchored onto functionalised polysuccinimide derivatives by Swarts *et al.* The antineoplastic ferrocenyl group **40** was anchored onto the polymeric drug carrier **35** to obtain the carrier-drug conjugate **42**.[76]

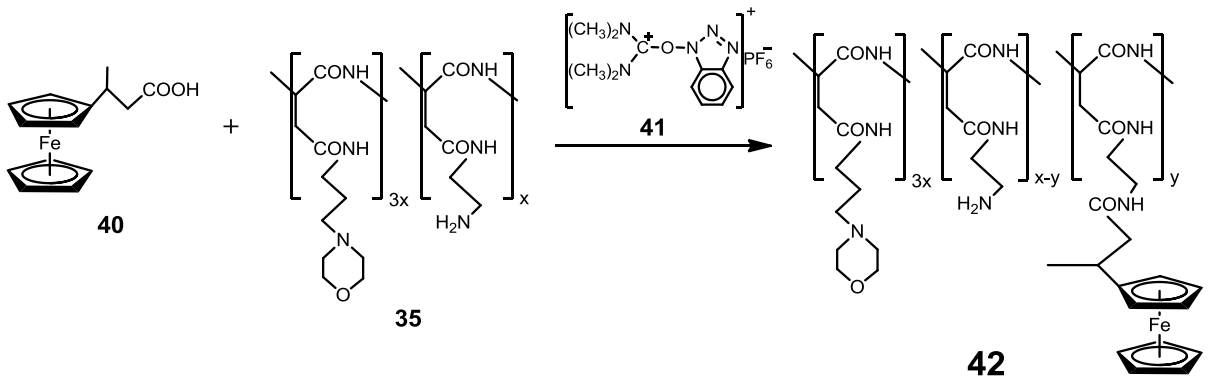

Scheme 2.9 Anchoring of the antineoplastic ferrocenyl group to a polyaspartamide derivative

The carboxylic acid-amine coupling agent O-benzotriazolyl-*N,N,N`,N`*-tetramethyluronium hexafluorophosphate**, 41,** has induced degrees of coupling approaching 90 % (that is y = 0.9x in Scheme 2.9) within 1 hour at room temperature. In a study where the cytotoxicity of the free drug **40**, was compared with that of the polymer-drug conjugate **42**, the polymer-based drug displayed an increase of almost one order of a magnitude, from a LD 90 value of 500 µg/ml for **40** to 80µg/ml *drug content* utilising polymer device **42**.[16]

2.5 Electrochemical studies

Several good reviews give good background on the theory and techniques pertaining to electroanalytical chemistry.[71,72,73] In this section only some of the most important parameters and definitions utilized in chapter 3 will be highlighted. In addition, some aspects of the not well understood electrochemistry of ruthenocene will be explored.

2.5.1 Voltammetry

Voltammetry comprises a group of electroanalytical techniques in which information about an analyte is derived from the measurement of current as a function of applied potential. The three most used types of voltammetry, and the only ones relating to this study, are cyclic voltammetry, square wave voltammetry and linear sweep voltammetry. Cyclic voltammetry is the most versatile electroanalytical technique and gives a direct method of measuring the formal reduction potential of an electrochemical active species. The most important parameters pertaining to cyclic voltammetry are the peak anodic potential (E_{pa}), peak cathodic potential (E_{pc}) and the magnitudes of the peak anodic current (i_{pa}) and peak cathodic current (i_{pc}), see Figure 2.4.

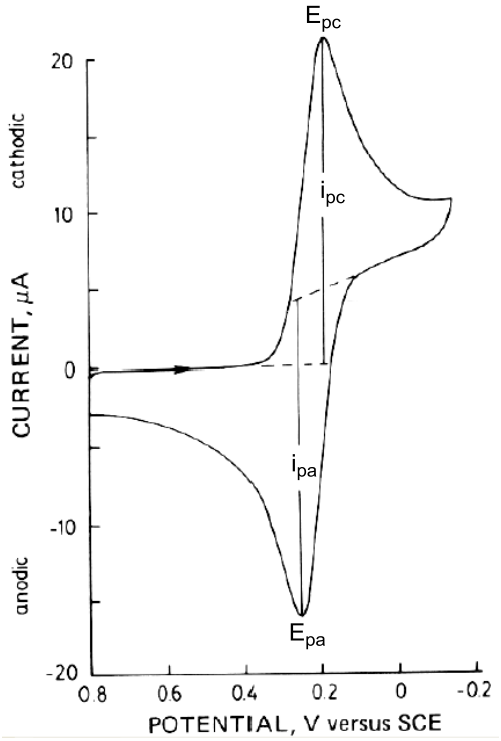

Figure 2.4 Cyclic voltammogram of 6 mM $K_3Fe(CN)_3$ in 1 M KNO_3. Scan initiated at 0.8 V versus SCE in negative direction at 5 mV/s. (Diagram adapted from ref. 71)

For an electrochemical reversible redox couple the formal reduction potential is midway between the two peak potentials, $E^{o'} = (E_{pa} + E_{pc})/2$ and the difference in peak potentials (ΔE_p) should theoretically be 59 mV at 25 °C for a one electron process. The ratio between i_{pa} and i_{pc} for an electrochemical reversible redox couple should approach unity.[71, 72]

2.5.2 Ferrocene

Ferrocene and the ferrocenium ion comprise an almost ideally reversible redox pair that has become the internal standard for non-aqueous reference potentials.[74] The high rate of electron transfer and electrochemical reversibility of the ferrocenyl moiety, invariably leads to $\Delta E_p = E_{pa} - E_{pc}$ close to 59 mV and i_{pc}/i_{pa} ratios close to 1 during cyclic voltammetry studies. Related to this study the formal reduction potential of the ferrocene-containing carboxylic acid series, with the same structure as **24a - 24d**, have been documented by Blom *et al.*[75] and the formal reduction potential of a ferrocene-containing polymer conjugates, similar to polymers **4 - 7**, by Swarts *et al.*[76]

2.5.3 Ruthenocene

Due to ruthenium's position in group 8 below iron, the ionization potential of ruthenocene, **3,** is considerably higher than that of ferrocene, **2**.[77]

Despite the extensive use of ferrocene as a model redox system for non-aqueous studies, the electrochemistry of ruthenocene and osmocene have been far less studied and remain less well understood. Compared to the simplicity of the ferrocenium/ferrocenyl couple (Fc^+/Fc), that of ruthenocenyl electrochemistry is far more complex.[44] In coordinating solvent/electrolyte systems the oxidation of ruthenocene proceeds by a one-step irreversible $2e^-$ process.[78] Electrochemical studies in the weakly coordination solvent dichloromethane and a weakly nucleophilic supporting electrolyte with either $[B(C_6F_5)_4]^-$ or $[B(C_6H_3(CF_3)_2)_4]^-$ as the counter anion has shown that the oxidation of ruthenocene is an inherent one electron, quasi-Nernstian process giving the unstable 17-electron ruthenocenium cation, $[RuCp_2]^+$, $\mathbf{3}^+$.[79] This cation equilibrates with a metal-metal bonded dimer $[Ru_2Cp_4]^{2+}$, $\mathbf{22}^{2+}$, which is increasingly preferred at low temperatures.[45] When the supporting electrolyte anion is $[B(C_6F_5)_4]^-$, the dimer precipitates at 243 K, giving the light-yellow $[(RuCp_2)_2][B(C_6F_5)_4]_2$. At higher temperatures, dimer $\mathbf{21}^{2+}$ is increasingly favoured.

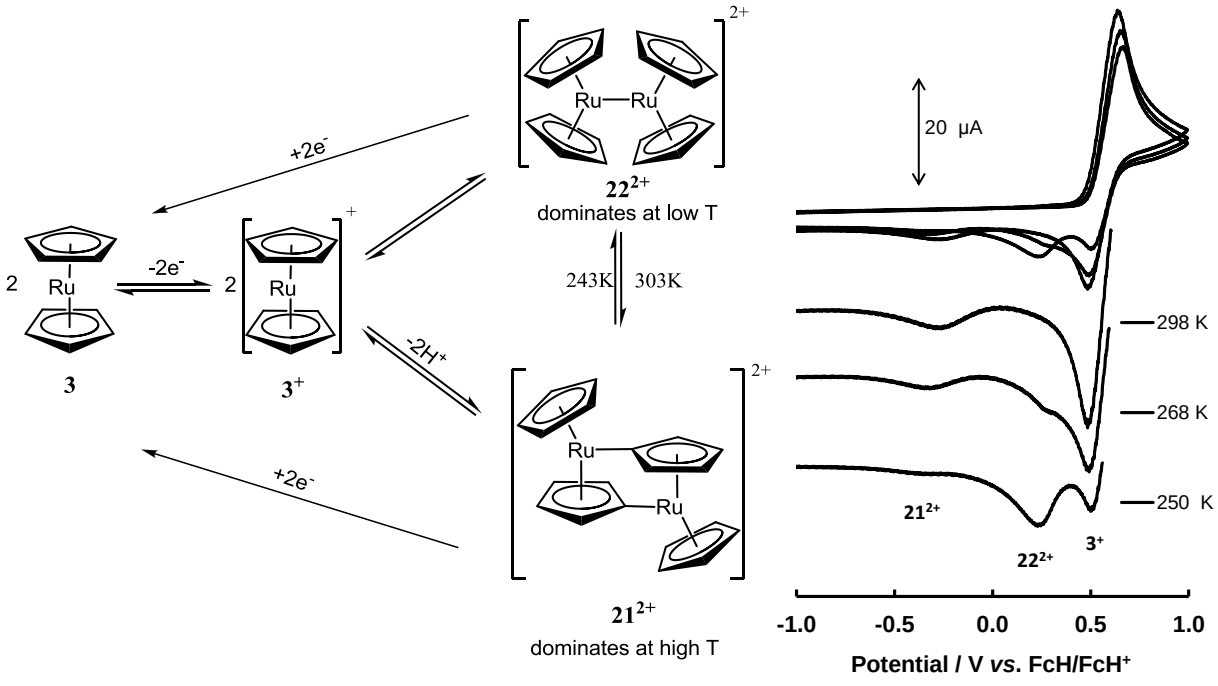

Scheme 2.10 Electrochemical behaviour of ruthenocene.. *Right:* **CV's of 2mM CD_2Cl_2 solutions of ruthenocene in the presence of 0.2 M $[NBu_4][B\{C_6H_3(CF_3)_2\}_4]$ at 25 °C, -5 °C and -23 °C at a scan rate of 300 mV/s (CV's from reference 45)**

The equilibrium position between $\mathbf{21}^{2+}$ and $\mathbf{22}^{2+}$ is highly dependent on the temperature. At all temperatures traces of $\mathbf{3}^{+}$ in equilibrium with $\mathbf{(3\text{-}H)}^{+}$ are present, as indicated by a variable temperature NMR study.[45]

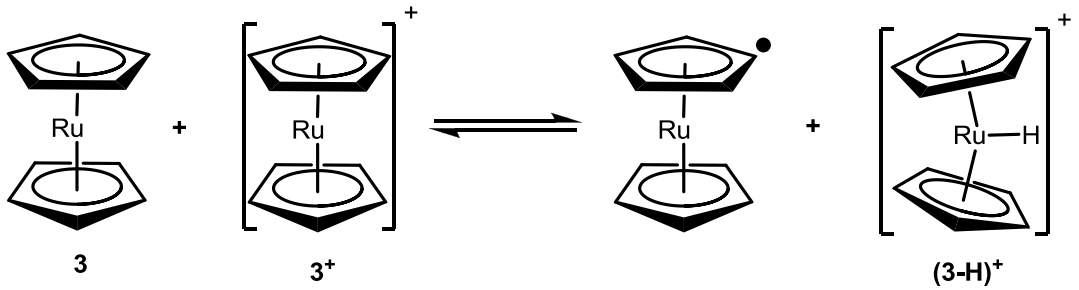

Scheme 2.11 The formation of a ruthenocene hydride, $\mathbf{(3\text{-}H)}^{+}$

2.6 General synthetic procedures

2.6.1 Carboxylic acid derivatives

Carboxylic acid derivatives are a family of closely related functional groups, including acyl chlorides, acid anhydrides, esters and amides. They can all be prepared from the parent carboxylic acid and convert back to the carboxylic acid on hydrolysis. The order of reactivity of carboxylic acid derivatives are as follows: acyl chloride > anhydride > ester = carboxylic acid > amide. In general only acyl chlorides and acid anhydrides are reactive enough to undergo Friedel-Craft acylation with aromatic compounds. Acid chlorides are much more reactive than acid anhydrides towards acylation. The electronegative chlorine atom pulls the binding electrons toward it in the carbon-chloro bond, making the carbonyl carbon very electrophilic.

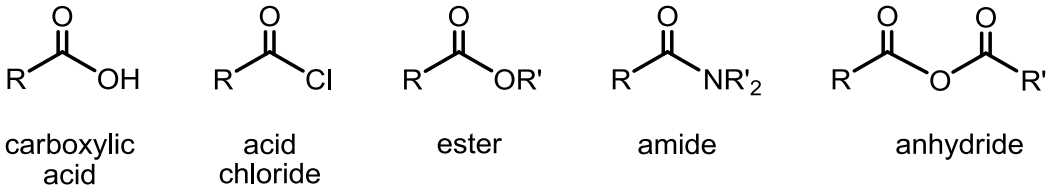

Figure 2.5 Carboxylic acid derivatives

A method to convert succinic anhydride to an acid chloride for increased reactivity towards Friedel-Crafts acylation was described by Cason.[80] In the first step the succinic anhydride ring is opened with methanol to create a mixed carboxylic acid/methyl ester, **44**. This methyl ester serves as a protecting group which is easily removed under basic conditions but stable

enough to allow conversion of the carboxylic acid portion of the molecule to an acid chloride without formation of the diacid chloride.

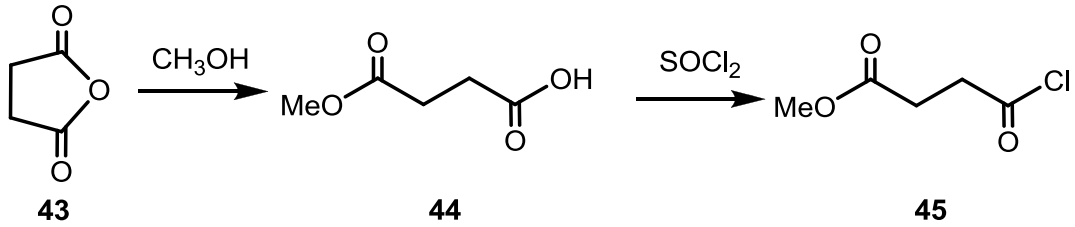

43 **44** **45**

Scheme 2.12 Conversion of succinic anhydride to a mixed acid chloride methyl ester derivative, 45.

2.6.2 Amide synthesis

Amide bonds are the most stable of the carbonyl derivatives due to the high resonance stabilization between the nitrogen-carbon and oxygen-carbon bonds. Amides can be prepared in various ways, for this study only the preparation of amide bonds by the reaction between carboxylic acids and amines will be discussed. This reaction is well known in the production of peptides, in which multiple amino acids are linked via amide bonds. In biological circles, amide bonds are also known as peptide bonds. Formation of the peptide linkage between amino acid segments is one of the most important reactions in biochemistry.[81]

Amides can be prepared from an amine and a carboxylic acid together at elevated temperatures in the absence of a catalyst.

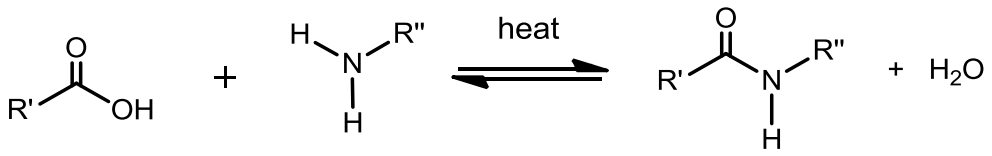

Scheme 2.13 Preparation of an amide via the reaction of a carboxylic acid with an amine

However to ensure specific coupling between the required carboxyl and amino groups under mild conditions the use of coupling agents is required. The coupling reagent activates the carboxylic acid for amide bond formation.

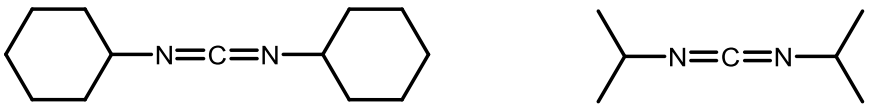

46 47

Figure 2.6 Dicyclohexylcarbodiimide (DCC), 46 and *N,N'*-Diisopropylcarbodiimide (DIC), 47 are two amide-inducing coupling agents.

Dicyclohexylcarbodiimide (DCC) and diisopropylcarbodiimide (DIC) are commonly used catalysts to prepare amides, acid anhydrides and esters from carboxylic acids.[81, 82]

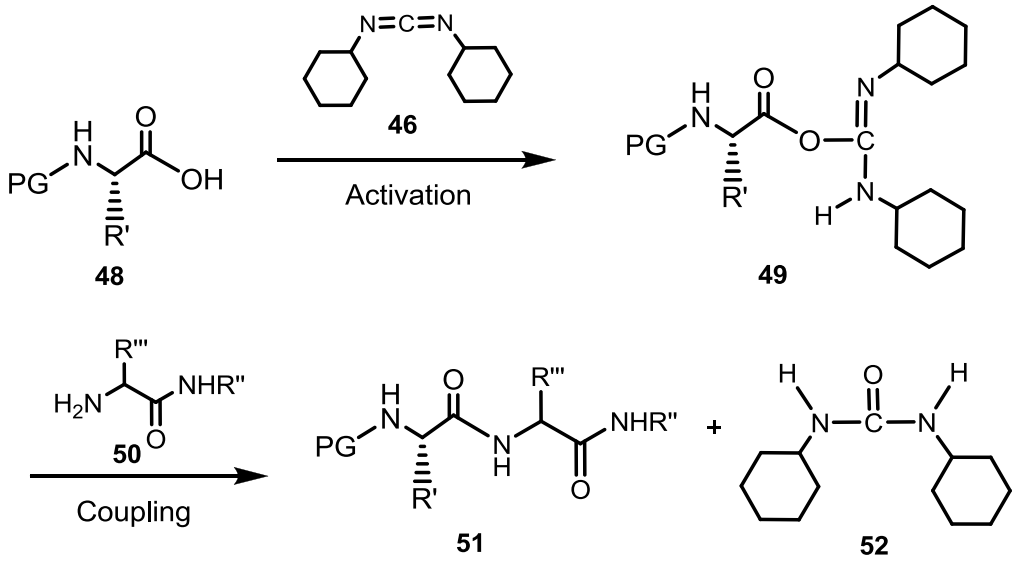

Scheme 2.14 Simplified general mechanism of amide bond formation.

In the activation step an intermediate, **49,** is produced by the reaction of a carboxylic acid, **48**, with DCC, **46.** This intermediate then undergoes aminolysis to form an amide, **51,** and dicyclohexylurea, **52.** [83]. These coupling reagents can also transform primary amides to nitriles, which is useful in organic synthesis but is an unwanted side reaction in peptide synthesis.[81]

Gross [84, 85] introduced *O*-Benzotriazolyl-*N,N,N',N'*-tetramethyluronium hexafluorophosphate (HBTU), **53,** a useful peptide coupling reagents in aqueous reactions. The high efficiency of this uronium salt has been evaluated and proven by model reaction tests and the successful synthesis of various amides.[86] Originally the uronium isomer, **53**, was thought to be the active species. However, upon solving of the X-ray structure of HBTU, the guanidinium species, **54,** was found to be predominant.

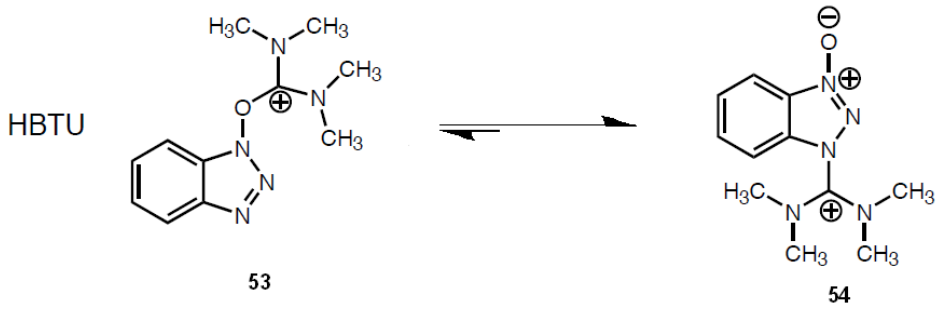

Scheme 2.15 Equilibrium between the uronium species, 53, and guanidinium species, 54.

The HBTU based amide coupling is in principle the same as for DCC and also facilitated in two steps, activation and coupling (Scheme 2.16).

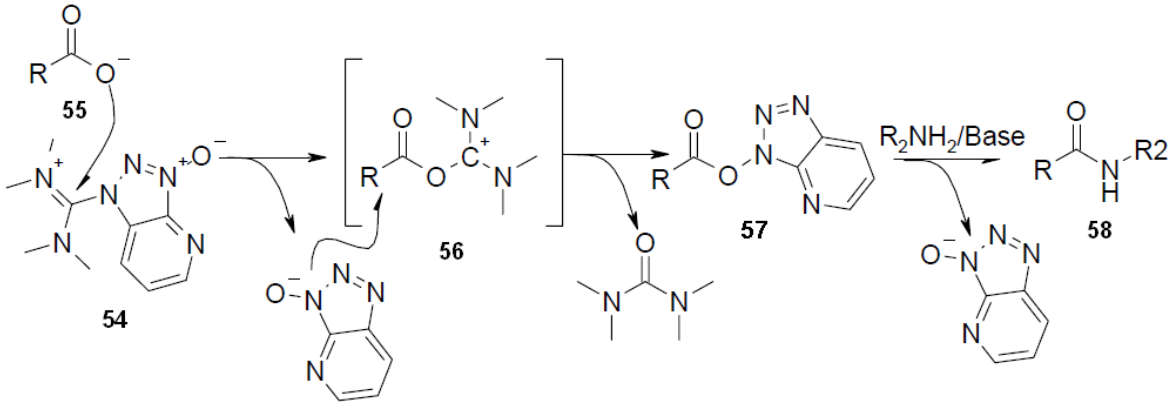

Scheme 2.16 Mechanism of the HBTU-mediated amide coupling[60, 86]

In the activation step the uronium/guanidinium species, **54,** reacts with the deprotonated carboxylic acid group, **55,** forming an activated ester, **56**, which may convert to activated ester, **57**. In the coupling step the activated ester reacts with the amino group to form the amide, **58**.[86, 87]

2.7 X-ray photoelectron spectroscopy

X-ray photoelectron spectroscopy (XPS) is a quantitative spectroscopic technique that can be used to determine empirical formula, the elemental composition, electronic state and chemical state of the elements within a material from binding energies.[88] XPS spectra are obtained by irradiating a material with an X-ray beam while at the same time measuring the kinetic energy and number of core electrons that escape from the top 1 to 10 nm of the

material being analysed. Because the energy of the incident X-ray wavelength is known, the electron binding energy of each of the emitted electrons can be determined from equation 3.1;

Equation 3.1 $EB = h\nu - (KE + \varphi)$,

where *EB* is the binding energy of the electron, $h\nu$ is the energy of the X-ray photons being used, *KE* is the kinetic energy of the electron as measured by the instrument and φ is the work function of the specific spectrometer. A typical XPS survey spectrum gives the number of emitted photoelectrons against their binding energy (BE). Each element provides us with at least one photoemission peak, with a distinct binding energy. In addition to the expected photoelectron peaks, an XPS wide scan spectrum also exhibit peaks due to Auger electrons. These originate because the atom from which the photoelectron has left is a highly excited ion, with a hole in one of its inner shells. This ion then undergoes a series of internal relaxation events to emit energetic electrons from an excited atom, known as the Auger effect. An emitted Auger electron will have a kinetic energy (KE) of;

Equation 3.2 $KE = E_K - (E_{L1} + E_{L2})$,

where E_K, E_{L1}, E_{L2} are respectively the core level, first outer shell, and second outer shell electron energies.

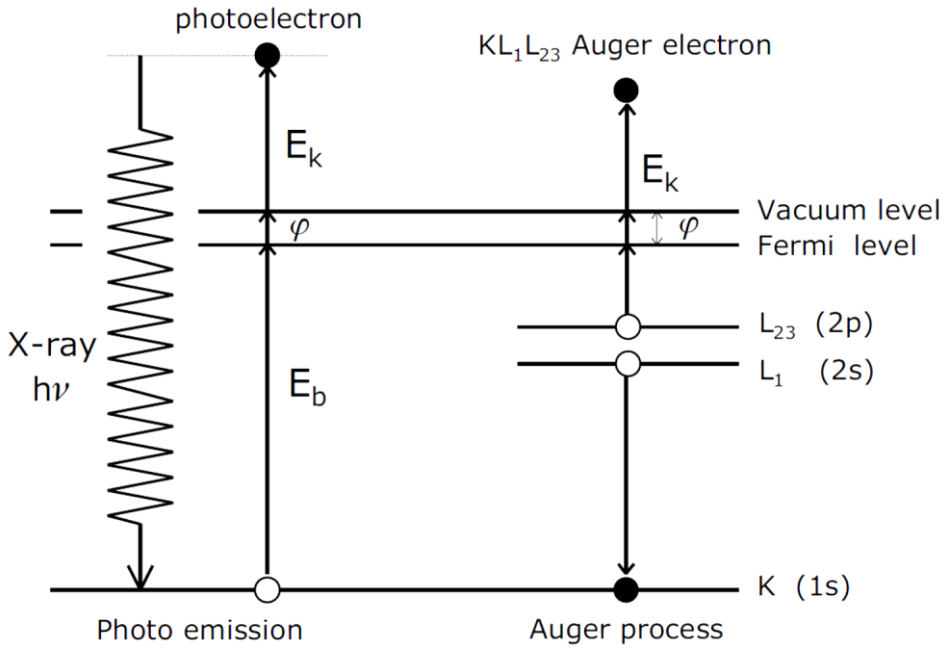

Figure 2.7: Photoemission and the Auger process. On the left an incident X-ray photon is absorbed and a photoelectron emitted. From the kinetic energy the binding energy of the photo electron is calculated. The atom becomes an unstable ion with a hole in one of the core levels. On the right side the excited ion relaxes by filling the core hole with an electron from a higher shell. The energy released by this transition is taken up by another electron, the Auger electron, which leaves the sample with an element specific kinetic energy. (Reference 88)

XPS have become a practical and straightforward characterization technique for probing surfaces. However, in this study XPS was solely used to provide information on the empirical formula of the analysed compounds. XPS quantitative measurements are ± 10% accurate, which is far less than the accuracy required for empirical formula measurements from elemental analysis. However, XPS can confirm the existence of many more elements than ^{1}NMR (eg. ruthenium), and give information on their electronic state, all from one measurement. Even wet chemistry elemental analysis requires a dedicated sample and experimental routine for each metal or element other than C, H and N to be determined.

---

[16] J.C. Swarts, D.M. Swarts, D.M. Maree, E.W. Neuse, C. La Madeleine, J.E. van Lier, *Anticancer Res.* 2033, **21** (2001)

[17] L.B. Hunt, *Platinum Metals Rev*., 76, **28** (1984).

[18] G. Gasser, I. Ott, N. Metzler-Nolte, *J. Med. Chem*., 3, **54** (2011).

[19] A.M. Pizarro, A. Habtemariam, P.J. Sadler, *Top Organomet. Chem*., 21, **32** (2010).

[20] F. Juarez, D. Monceau, D. Tetard, B. Pieraggi, C. Vahlas, *Surface Coatings Tech.*, 44, **163** (2003) .

[21] M. Wenzel, E. Nipper, W. Klose, *Radiochem. Radiopharm.*, 367, **18** (1977).

[22] I. Kostova, *Curr. Med. Chem.*, 1085, **13** (2006).

[23] S. Kasibhatla, B. Tseng, *Mol. Cancer Ther*., 573, **2** (2003).

[24] V. Brabec, O. Nováková, *Drug Resistance Updates*, 111, **9** (2006).

[25] P. Som, Z.H. Oster, K. Matsui, G. Guglielmi, B.R. Persson, M.L. Pellettieri, S.C. Srivastava, P. Richards, H.L. Atkins, A.B. Brill, *Eur. J. Nucl. Med.*, 491, **8** (1983).

[26] G. Sava, S. Zorzet, T. Giraldi, G. Mestroni, G. Zassinovich, *Eur. J. Cancer Clin. Oncol*., 841, **20** (1984).

[27] E.S. Antonarakis, A. Emadi, *Cancer Chemother. Pharmacol.*, 1, **66** (2010).

[28] A. Bergamoa, G. Sava, *Dalton Trans.*, 7817, **40** (2011).

[29] R.A. Gatenb, R.J. Gillies, *Nature Reviews*, 891, **4** (2004).

[30] D. Carmichael, P. Le Floch, X. F. Le Goff, O. Piechaczyk, N. Seeboth, *Chem. Eur. J.*, 14486, **16** (2010).

[31] R.B. Woodward, M. Rosenblum, M.C. Whiting, *J. Am. Chem. Soc.*, 3458, **74** (1952).

[32] P.C. Möhring, N.J. Coville, *J. Organomet. Chem.*, l, **479** (1994).

[33] M.D. Rausch, E.O. Fischer, H. Grubert. *J. Am. Chem. Soc*., 76, **82** (1960).

[34] A. Federman-Neto, A.C. Pelegrino, V.A. Darin, *ChemInform* **35**, (Issue 43) doi:10.1002/chin.200443242 (2004).

[35] M.F.R. Fouda, M.M. Abd-Elzaher, R.A. Abdelsamaia, A.A. Labib, *Appl. Organometal. Chem.*, 613, **21** (2007).

[36] R.H. Fish, G. Jaouen, *Organometallics*, 2166, **22** (2003).

[37] C.S. Allardyce, A. Dorcier, C. Scolaro, P. Dyson, *Appl. Organometal.Chem.* 1, **19** (2005).

[38] D.R. van Staveren, N. Metzler-Nolte. *Chem. Rev*., 5931, **104** (2004).

[39] A.N. Nesmeyanov, A.A. Lubovich, S.P. Gubin, *Russ. Chem. Bull*., 1761, **21** (1972).

[40] E.O. Fischer, M. von Foerster, C.G. Kreiter, K.E. Schwarzhans, *J. Organomet. Chem*., 113, **7** (1967).

[41] D.E. Bublitz, W.E. McEwen, J. Kleinberg, *J. Am. Chem. Soc*., 1845, **84** (1962).

[42] O. Hofer, K. Schloegel, *J. Organomet. Chem.*, 443, **13** (1968).

[43] R. Sanders, U.T. Mueller-Westerhoff, *J. Organomet. Chem.*, 219, **512** (1996).

[44] S. Trupia, A. Nafady, W.E. Geiger, *Inorg. Chem*., 5480, **42** (2003).

[45] J.C. Swarts, A. Nafady, J.H. Roudebush, S. Trupia, W.E. Geiger. *Inorg. Chem*., 2156, 48 (2009).

[46] N.G. Connelly, W.E. Geiger, *Chem. Rev*., 877, **96** (1996).

[47] K. Kirchner, H. W. Dodgen, S. Wherland, J. P. Hunt, *Inorg. Chem.*, 2381, **29**, (1990).

[48] Y.S Sohn, A.W. Schlueter, D.N. Hendrickson, H.B. Gray, *Inorg. Chem.*, 301, **13**, (1974).

[49] S. Kamiyama, T.M. Suzuki, T. Kimura, A. Kasahara, *Bull. Chem. Soc. Jpn.*, 909, **51** (1978).

[50] D. Lednicer, J.K. Lidsay, C.R. Hauser, *J. Org. Chem.*, 653, **23** (1958).

[51] K.C. Kemp, E. Fourie, J. Conradie, J.C. Swarts, *Organomet.*, 353, **27** (2008).

[52] P.J. Graham, R.V. Lindsey, G.W. Parshall, M.L. Peterso, G.M. Whitman, *J. Am. Chem. Soc*., 653, **23** (1958).

[53] P. Beagley, M.A.L. Blackie, K. Chibale, C. Clarkson, J.R. Moss, P.J. Smith, *J. Chem. Soc., Dalton Trans.*, 4426, **23** (2002).

[54] R. Satchi-Fainaro, R. Duncan, C.M. Barnes, *Adv. Polym. Sci.* 1, **193** (2006).

[55] J.C. Swarts, *Macromol. Symp.*, 123, **186** (2002).

[56] P. Köpf-Maier, H. Köpf, *Chem. Rev.*, 1137, **87** (1987).

[57] G.R. Gale, L.M. Atkins, S.J. Meischen, A.B. Smith, E.Walker, *Cancer Treat. Rep.*, 445, **61** (1977).

[58] W.M. Sharman, C.M. Allen, J.E. van Lier, *Drug Discovery Today*, 217, **44** (1997).

[59] G. Caldwell, E.W. Neuse, C.E.J. van Rensburg, *J. Inorg. Organomet. Polym.*, 217, **7** (1997).

[60] A.I. Mufula, E.W. Neuse, *J. Inorg. Organomet. Pol*., doi 10.1007/s10904-011-9497-3 (2011).

[61] Y. Luo, G.D. Prestwich, *Curr. Cancer Drug Tar*., 209, **2** (2002)

[62] P. Neri, G. Antoni, F. Benvenuti, F. Cocola, G. Gazzei, *J. Inorg. Organomet. Polym.*,217, **7** (1992).

[63] E.W. Neuse, *J. Inorg. Organomet. Polym.*, 3, **15** (2005).

[64] R. Duncan, J.Kopecek, *Adv. Polymer Sci*., 51, **57** (1984).

[65] M.D. Maree, E.W. Neuse, E. Erasmus, J.C. Swarts, *Metal-Based drugs*, doi:10.1155/2008/217573 (2008).

[66] A.J. Barrett, A.M. Gotto, *Lysosomal Enzymes in Lysosome, a Laboratory Handbook*; ed. J.T. Dingle, Elsevier, Amsterdam, 1977 p. 19.

[67] L.L. Komane, E.H. Mukaya, E.W. Neuse, C.E.J. van Rensburg, *J. Inorg. Organomet. Polym.*, 111, **18** (2008).

[68] E.W. Neuse, A.G. Perlwitz, *Polyamides as drug carriers: Water soluble Polymers*; eds. S.W. Shalaby, C.L. McCormick, G.B. Butler, *American Chemical Society*, Washington DC, 1991, ch 25, pp 395-404

[69] D.D. N'Da, E.W. Neuse, *J. Inorg. Organomet. Polym.*, 468, **20** (2010).

[70] D.D. N'Da, E.W. Neuse, M. Nell, C.E.J. van Rensburg, *S. Afr. J. Chem*., 33, **59** (2003).

[71] P.T. Kissiger, W.R. Heineman. *J. Chem. Educ*., 290, **60** (1983).

[72] G.A. Mobbot, *J. Chem. Educ*., 697, **60** (1983).

[73] H.J. Gericke, N.I. Barnard, E. Erasmus, J.C. Swarts, M.J. Cook, M.A.S. Aquino, *Inorg. Chim. Acta*, 2222, **363**, (2010).

[74] R.R. Gagne, C.A. Koval, G.C. Lisensky, *Inorg. Chem.*, 2854, **19** (1980).

[75] N.F. Blom, E.W. Neuse, H.G. Thomas, *Transition Met. Chem*., 301, **12** (1987).

[76] J.C. Swarts, G.J. Lamprecht, E.W. Neuse, *J. Inorg. Organomet. Polym*., 143, **4** (1994).

[77] P. Pigeon, S. Top, A. Vessières, M. Huché, E.A. Hillard, E. Salomon, G. Jaouen, *J. Med. Chem.*, 2814, **48** (2005).

[78] T. Kuwana, D.E. Bublitz, G. Hoh, *J. Am. Chem. Soc*., 5811, **82** (1960).

[79] M.G. Hill, W.M. Lamanna, K.R. Mann, *Inorg. Chem.*, 4687, **30** (1991).

[80] J. Cason, *Org. Synth. Coll. Vol*, 169, **3** (1955).

[81] K.V.S.R.G. Prasad, K. Bharathi, B.B. Haseena, *Int. J. Pharm. Sci. Rev. Res*., 108, **8** (2011).

[82] M.H. Kim, D.V. Patel, *Tetrahedron Lett.*, 5603, **35** (1994).

[83] M. Goodman, *Methods of Org. Chem. (Houben-Weyl) add. and suppl. vol. to the 4th ed., Vol. E 22a*, pp. 425–888 (2002).

[84] V. Dourtoglou, J.C. Ziegler, B.Gross, *Synthesis*, 572 (1984).

[85] V. Dourtoglou, J.C. Ziegler, B.Gross, *Tetrahedron Lett.*, 1269 (1978).

[86] P. Li, J.C. Xu, *J. Peptide Res.*, 129, **58** (2001).

[87] P. Öhrngren, M.Sc Study, *Synthesis of a Hepatitis C Virus NS3 Serine Protease Inhibitor with a Novel Peptidomimetic Scaffold*, Uppsala University, Sweden (2004).

[88] I. Chorkendorff, J.W. Niemantsverdriet, *Concepts of Modern Catalysis and Kinetics*, WILEY-VCH, Weinheim, 2003, pp 135-139.

3 Results and Discussion

3.1 Introduction

The results of this research are discussed with respect to the synthesis and characterisation of a series of ruthenocene-containing carboxylic acids. This is followed by a description of the synthesis of a polyaspartamide drug carrier and covalent anchoring of ruthenocene-containing carboxylic acids to this polymer. Finally a discussion of the electrochemistry of all the ruthenocene-containing carboxylic acids and polymers is given as per goal 4. The synthetic component of this research topic stems from goals 1 – 3 in Chapter 1. The characterisation presented covers proton nuclear magnetic resonance (^{1}H NMR), Infrared spectroscopy (IR), X-ray photoelectron spectroscopy (XPS) and electrochemistry (goal 4).

3.2 Synthesis

3.2.1 The synthesis of ruthenocene-containing carboxylic acids

The first ruthenocene-containing carboxylic acid synthesized was ruthenocene carboxylic acid, **24a.** This acid contains no separator unit between the carboxylic and ruthenocenyl group. It was obtained in a two-step synthetic sequence. First, in a Friedel-Crafts acylation reaction ruthenocene, **3**, was added to 2-chlorobenzoylchloride to yield 2-chlorobenzoylruthenocene, **23** as yellow crystals in 64 % yield. The compound **23** was characterized by ^{1}H NMR spectroscopy (spectrum 1: see appendix at the back of the thesis). Treatment of **23** with potassium *tert*-butoxide in the presence of water yielded, after acidification, ruthenocenoic acid, **24a,** as a light yellow powder. The infrared transmission peaks for the carbonyl groups of the ketone, **23** and the acid, **24a** were observed at 1644 cm^{-1} and 1659 cm^{-1} respectively (spectrum 27 and 28: see appendix). The appearance of a large OH peak for **24b** between 2500 cm^{-1} and 3000 cm^{-1} confirmed the conversion from ruthenocene, **3,** to the carboxylic acid.

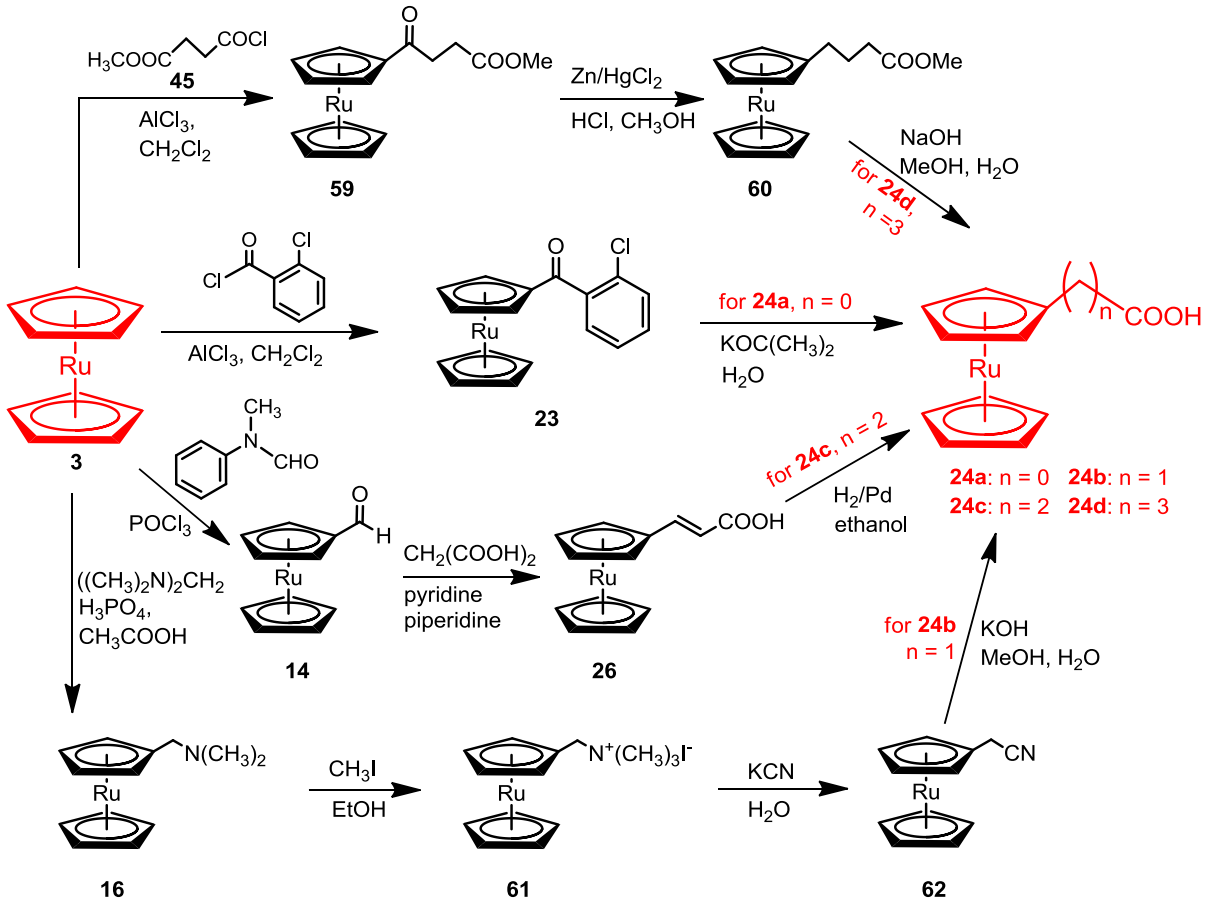

Scheme 2.17 Synthesis of ruthenocene carboxylic acids.

2-Ruthenocenylethanoic acid, **24b**, was prepared in a four step synthesis from ruthenocene, **3.** In the first step *N,N*-dimethylaminomethylruthenocene, **16** was prepared (**Scheme 2.17**) as described by Hofer.[89] This reaction involved the treatment of ruthenocene, **3** with *N,N,N',N'*-tetramethyldiaminomethane in acetic acid containing H_3PO_4 to give **16** in 56 % yield after the work-up as a light yellow liquid which turned brown overnight in air. Consequently the tertiary amine was immediately reacted with methyl iodate to produce the stable quaternary ammonium salt *N,N,N*-trimethylaminomethylruthenocene iodide, **61,** in 72 % yield within 30 min. ^{1}H NMR (spectrum 3 and 4) showed the change from six to nine methyl proton resonances when going from **16** to **61**. The peak at δ 3.09 ppm and δ 4.57 ppm for **16** and **61** respectively, indicated the 2 protons of the methylene group**.** The quaternary amine **61** was treated with potassium cyanide to afford ruthenocenylacetonitrile, **62,** by a similar method as described for ferrocene by Lednicer.[90] An infrared transmission peak observed at 2252 cm^{-1} (Spectrum 31) is typical of the stretching absorption frequency of a nitrile group. The basic hydrolysis of **62** gave 2-ruthenocenylethanoic acid, **24b**, in 51 % yield. Infrared transmission

peaks at 1706 cm^{-1} (symmetrical) and 1691 cm^{-1} (antisymmetrical) for the C=O group and 2908 cm^{-1} (broad) for the O-H group shows the replacement of the nitrile with a carboxylic acid was successful.

Ruthenocene carboxaldehyde, **14**, was used as the first precursor in the synthesis of 3-ruthenocenylpropanoic acid, **24c**. Ruthenocenylcarboxaldehyde, **14**, was prepared by reacting ruthenocene, **3**, with N-methylformanilide, in the presence of phosphorus oxychloride. The aldehyde **14** was obtained as bright yellow crystals in 74 % yield. ^{1}H NMR spectrum 7 (see appendix) shows the aldehyde proton resonates at δ 9.72 ppm. The second synthetic step involves the Michael addition of malonic acid to **14,** in the presence of piperidine as catalyst, to yield 3-ruthenocenylpropenoic acid, **26,** in 90 % yield. Hydrogenation of **26** with hydrogen at 10 bar, catalysed by palladium on activated charcoal gave 3-ruthenocenylpropanoic acid, **24c**. Surprisingly ^{1}H NMR (Spectrum 9) only shows a singlet for the four protons of the two methylene groups. However treatment of **24c,** with sodium hydroxide, gave the sodium salt of **24c**. The protons for the two methylene groups of the salt were resolved and resonate at δ 2.27 ppm and δ 2.38 ppm respectively.

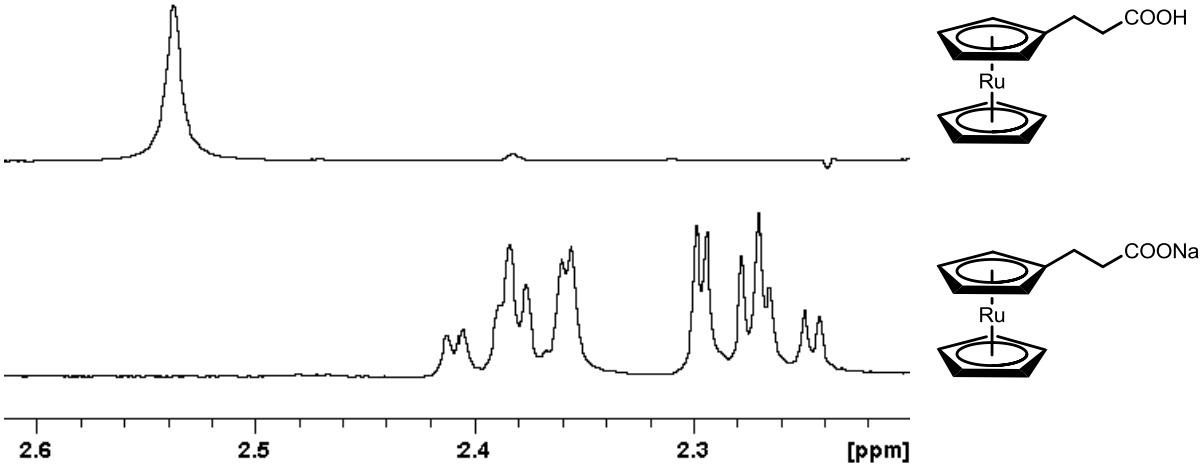

Figure 2.8 A portion of the ^{1}H NMR spectrum of $RcCH_2CH_2COOH$ showing the 4 methylene peaks resonate as a singlet (top). Resolved methylene peaks were observed for the salt $RcCH_2CH_2COO^-Na^+$ (bottom). The full spectrum for 24c can be found in the appendix. (Spectrum 9).

4-Ruthenocenylbutanoic acid, **24d,** was previously prepared by Hofer *et al.*[89] in a two-step synthesis (Scheme 2.4, page 13). The first reaction involved the Friedel-Crafts acylation of ruthenocene, **3**, with succinic anhydride, to liberate 3-ruthenocenoylpropanoic acid **25.** This was followed by the Clemmensen reduction of **25** to yield **24d.** However this described

synthesis of **25** could not be repeated by the author in yields exceeding 22 %. Furthermore the Clemmensen reduction of **25** gave **24d** in a low yield of 2.5 %. This was in contrast to the claimed yields obtained in the synthesis of 3-ferrocenoylpropanoic acid (95 %) and 4-ferrocenylbutanoic acid (91 %) with the same method and materials in the labs of the author. To achieve a higher yield in the Friedel-Crafts acylation of ruthenocene, succinic anhydride was replaced with 3-(carbomethoxy)propionyl chloride, **45** (Scheme 2.17). The reaction with the acid chloride **45** gave methyl 3-ruthenocenoyl propanoate, **59,** as a yellow powder in 74 % yield. The improvement of the yield expresses the much higher reactivity of an acid chloride towards Friedel-Crafts acylation than an anhydride. The Clemmensen reduction of **59** in a methanol-water-acetic acid mixture gave methyl 4-ruthenocenylbutanoate, **60,** in 74 % yield. Hydrolysis of **60** gave 4-ruthenocenylbutanoic acid, **24d,** as a white powder in 93 % yield.

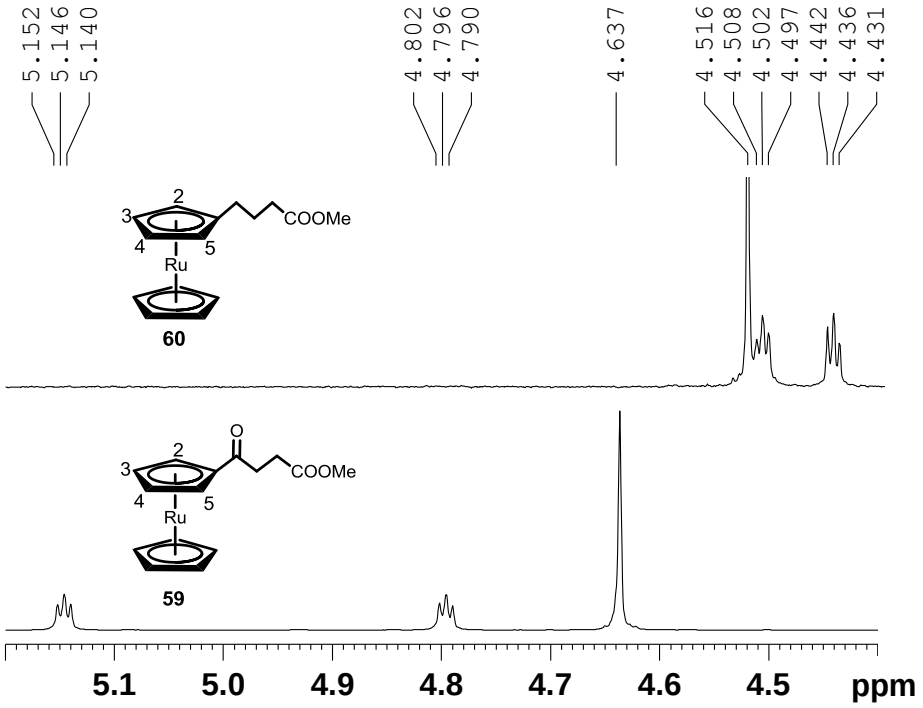

Figure 2.9 ^{1}H NMR of the ruthenocenyl fragment of $RcCH_2CH_2CH_2COOMe$, 60 and $RcCOCH_2CH_2COOMe$, 59.

In **Figure 2.9** one can clearly see the differences that electron-donating side groups ($CH_2CH_2CH_2COOMe$ in **60**) and electron-withdrawing substituents ($COCH_2CH_2COOMe$ in **59**) induce in the ^{1}H NMR spectrum of the ruthenocenyl group. The unsubstituted

cyclopentadienyl ring of **59** and **60** shows almost the same chemical shift: 4.64 and 4.52 ppm, respectively. It implies that shielding or deshielding effects of the substituents (here due to electron-donating or electron-withdrawing properties of substituents on the cyclopentadienyl ring) is not transmitted effectively through the Ru^{II} core to the non-substituted cyclopentadienyl ring. The electron-donating or electron-withdrawing effect of substituents on the resonating positions of the protons on the substituted cyclopentadienyl ring is, however, significant. In the case of **60,** containing the electron-donating side group $CH_2CH_2CH_2COOMe$, the protons on the substituted cyclopentadienyl ring are actually resonating upfield of the unsubstituted cyclopentadienyl ring. The resonation positions of the 3, 4 protons (**Figure 2.9**) of **59** are 4.80 ppm, while for **60** they are at 4.50 ppm. The observed electron-donating or withdrawing effect on the protons directly adjacent to the substituent (2, 5 protons) is much larger than that of the protons furthest away from the substituent (3, 4 protons). The resonating position of the 2, 5 protons of **59** is 5.15 ppm, while for **60** the corresponding signal is observed at 4.44 ppm. This is a 0.7 ppm upfield shift and is solely the consequence of the electron-donating or withdrawing properties of the substituent.

The synthesis of 3-(carbomethoxy)propionyl chloride, **45,** was performed according to literature procedures.[91] In the first step the succinic anhydride ring was opened with methanol to create a mixed carboxylic acid/methyl ester, **44**. Thereafter **44** was converted to the mono acid chloride **45**.

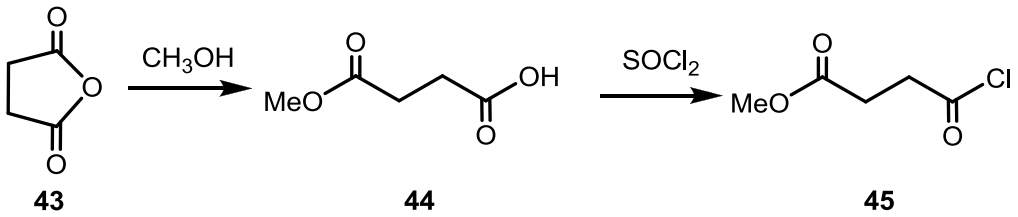

43 **44** **45**

Figure 2.10 The highlights of the reaction sequences involved in the synthesis of 3-(carbomethoxy)propionyl chloride, 45 according to the method of Cason, (Reference 91).

During the synthesis of 4-ruthenocenylbutanoic acid, **24d** infrared spectroscopy was used as a cheap and efficient way to test for the completeness of the reaction. Infrared frequencies for the functional groups for the series of compounds are assigned in **Figure 2.11** for comparison.

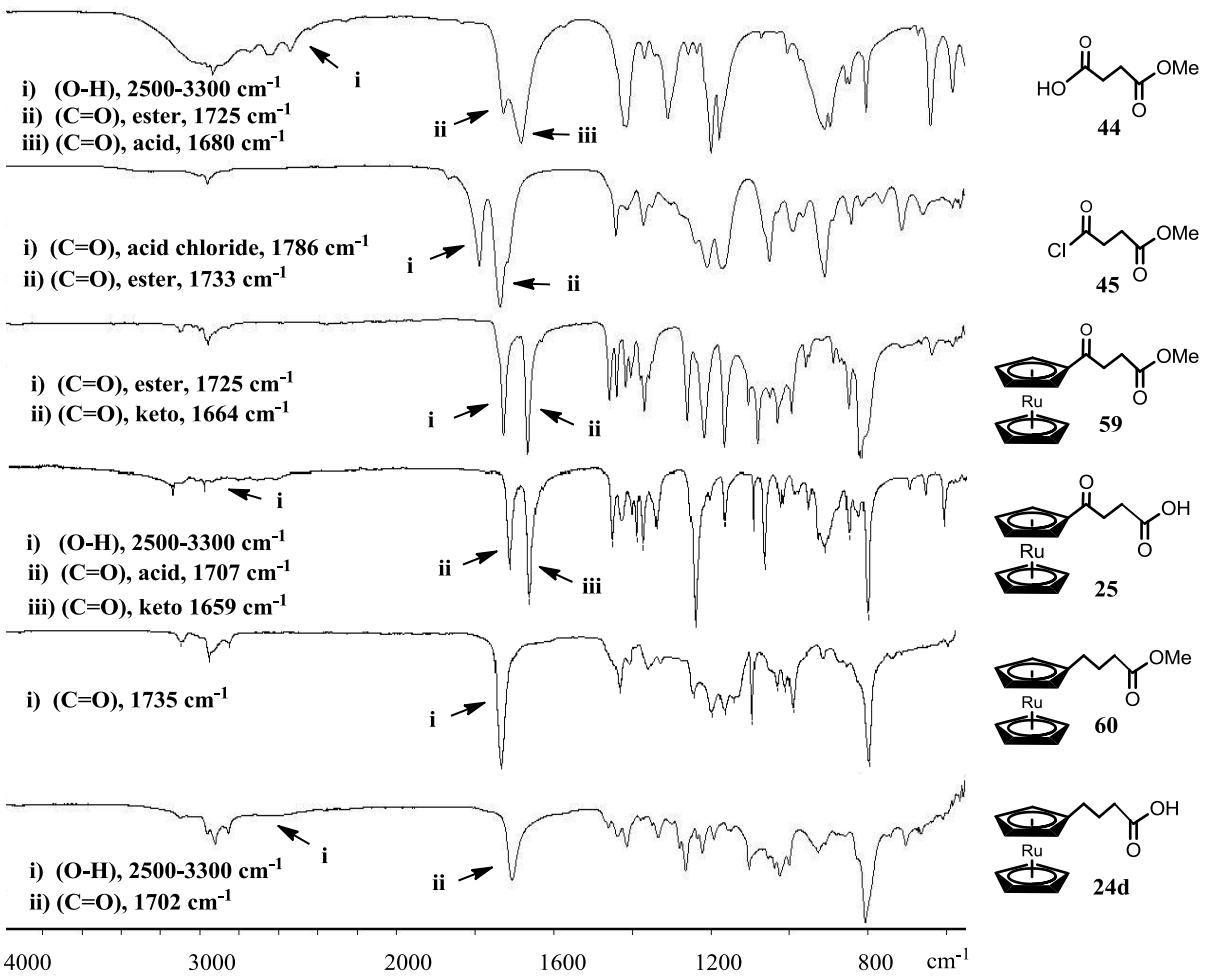

Figure 2.11 The infrared spectra with structures and assignment of dominant peaks.

All methyl esters for compounds in this series (**45, 59** and **60**) produce peaks between 1724 cm^{-1} and 1733 cm^{-1}. The carbonyl group in carboxylic acid containing compounds (**44, 25** and **24d)** shows peaks ranging between 1680 cm^{-1} and 1707 cm^{-1}. The acid chloride carbonyl group in **45** elicits a peak with the highest wavenumber of any carbonyl group in this series at 1786 cm^{-1}. Infrared frequencies for the ruthenocenoyl-keto group in compounds **25** and **59** were 1659 cm^{-1} and 1664 cm^{-1}, respectively. The carboxylic acid group of compounds **24d, 25** and **44** produce a broad IR band (2500 – 3300 cm^{-1}). However, this broad band is very weak for all ruthenocene-containing carboxylic acids in this study, probably due to H-bonding effects.

3.2.2 Polymer synthesis

Having completed the synthesis of ruthenocene-containing carboxylic acids as stated in goal 1 (Chapter 1), the attention was focussed on the preparation of carrier polymers to which the

carboxylic acids could be anchored. On account of the properties of polymeric drug carriers discussed in Chapter 2, paragraph 2.2.3, it was decided to concentrate on modifications of polysuccinimide, **2** for anchoring of ruthenocene-containing carboxylic acids.

3.2.2.1 Preparation of the polysuccinimide

DL-Aspartic acid, **31** was thermally polymerised to polysuccinimide, **32,** within 2 hours at 180 °C under reduced pressure, according to known procedures, [92] to produce a white solid in 97 % yield.

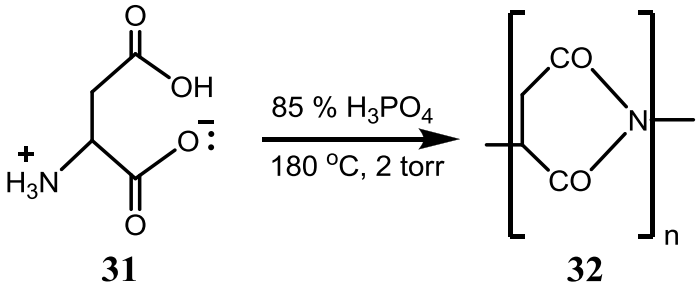

Scheme 2.18 The polymerisation of DL-aspartic acid, 31 into polysuccinimide, 32.

Preparation of **32** by this method is reported to give a polymer of molecular mass 57 000, having inherent viscosity η_{inh} = 300 ml·g^{-1} according to reference 93. Polysuccinimide, **32,** is insoluble in water and most organic solvents, except *N,N*-dimethylformamide (DMF) and dimethyl sulfoxide (DMSO). The ^{1}H NMR spectrum of **32** in DMSO-d_6 shows signals at 5.24 ppm (1H, CH), 3.18 ppm (1H, CH_2) and 2.68 ppm (1H, CH_2).

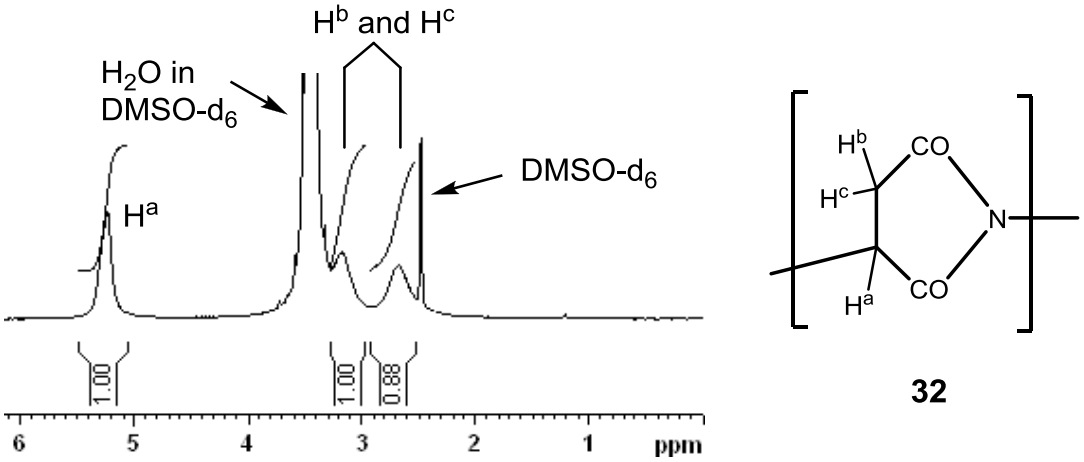

Figure 2.12 ^{1}H NMR spectrum of polysuccinimide, 32, in DMSO-d_6.

The absence of a resonating signal in the ^{1}H NMR (Spectrum 16, **Figure 2.12**) of **32** at approximately 4.80 ppm reveals that there are no noticeable uncyclized aspartic acid units in

the polymer backbone of **32**. This is also confirmed by the absence of N-H stretch infrared absorptions (Spectrum 42) in the region between 3200 and 3700 cm^{-1}. N-H stretch absorptions are generally observed with primary and secondary amines and amides including aspartic acid but not with tertiary amines and amides. A large peak is observed at 1709 cm^{-1} for the C=O stretching frequency of **32** in the IR spectrum.

3.2.2.2 Functionalization of polysuccinimide

Polysuccinimide, **32**, underwent ring opening by consecutive addition of the amines N-(3-aminopropyl)morpholine and ethylene diamine at appropriate reaction time, to produce poly-*α,β-DL*-[*N*-(3-(morpholin-4-yl)propyl)aspartamide-co-*N*-(2-aminoethyl)aspartamide, **35**. [94] This reaction is shown in **Scheme 2.19**.

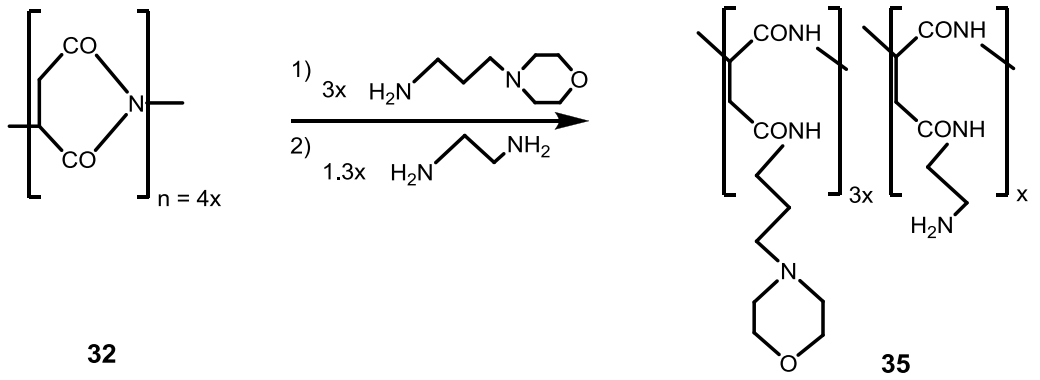

Scheme 2.19 The ring opening reaction of polysuccinimide, 32 to produce an amine-functionalized polyaspartamide.

The morpholino group enhances the water solubility of **32.** It also serves as a spacer unit to keep the reactive amino sites of the polymer sufficiently far apart [95] to prevent (or at least limit) cross amidation reactions which lowers the relative molecular mass of the polymer substantially. The aminoethyl group has reactive side-chain terminal NH_2 groups as a binding site for the ruthenocene-containing carboxylic acids under mild conditions. This binding site is separated from the main chain by 5 atoms to diminish the steric inaccessibility caused by the polymeric backbone. The target is to produce **35** with one amine active site for every three morpholino groups.

The synthesis starts with the addition of *N*-(3-aminopropyl)morpholine, in the ratio morpholine moles:polysuccinimide repeating units = 3:4, to polysuccinimide disolved in DMF, with very careful weighing of the starting materials. This is stirred for 25 minutes at 0 °C to prevent heat build-up during initial stages of the reaction, followed by stirring for a

further 5 hours at room temperature to effect complete anchoring of the morpholino groups. The resulting intermediate is then treated with ethylene diamine in 1.3 times molar excess at 0 °C and stirred at this temperature for 20 min, before continuing stirring for another 5 hours at room temperature. The excess of ethylene diamine would favour complete mono-substitution above crosslinking. The resulting product, now water-soluble, is subjected to aqueous dialyses in 12 000 molecular mass cut-off membrane tubing for removal of most of the constituent material with molecular masses below 12 000. The carrier polymer **35,** having viscosity[96] η_{inh} = 8 ml.g^{-1} is collected in the solid state after freeze-drying as a fluffy, highly hygroscopic white material in 52 % yield.

The absence of a peak in the ^{1}H NMR Spectra 17, 18 and 19 in the vicinity of 5.24 ppm indicated that there are no observable unopened polysuccinimide units in the polymer backbone of **35**. The actual ratio between the morpholino and amino groups varied between 3:1 (the value aimed for) and approximately 3:2. As the author became more experienced in accurately weighing the small quantities of starting material liquids, the ratio of morpholine:amine side-chains closely approached 3:1.

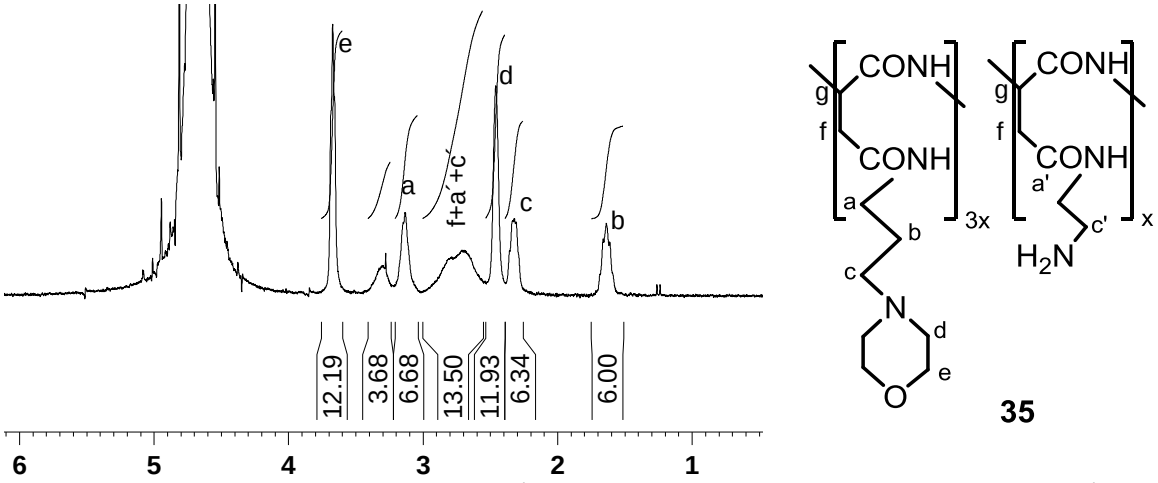

Figure 2.13 Proton assignment on the ^{1}H NMR spectrum of polymer 35 in D_2O. ^{1}NMR δ_H /ppm: 1.64 (m, 6H, b-CH_2); 2.32 (m, 6H, c-CH_2); 2.46 (s, 12H, d-CH_2); 2.55–3.00 (m, 12H, f-CH_2+a´-CH_2, c´-CH_2); 3.14 (m, 6H, a-CH_2); 3.67 (s, 12H, e-CH_2)

From the ^{1}H NMR (**Figure 2.13**, Spectrum 17) of **35,** in D_2O, all the protons can be discerned, except the four protons on the tertiary carbon on the polymer backbone. These four protons lie directly underneath HOD solvent signal at 4.6 ppm. The peaks for ruthenocene also lie in the region of 4.6 ppm. Therefore, the sample has also been subjected to a ^{1}H NMR analysis in DMSO-d_6 (Spectrum 18, **Figure 2.14**). In DMSO-d_6 the H_2O peak are shifted upfield, to

reveal the resonates of the protons on the tertiary carbon, at 4.47 ppm. These protons actually integrate for 4.6 rather than the expected 4, consistent with a morpholine:amine ratio closer to 3:2.

The protons on the tertiary carbon are important in this study as the protons on the ruthenocenyl group anchored to the polymer resonates overlap with this peak. To obtain the degree of coupling the integration value of 4.6 has been subtracted from the overlapping peaks.

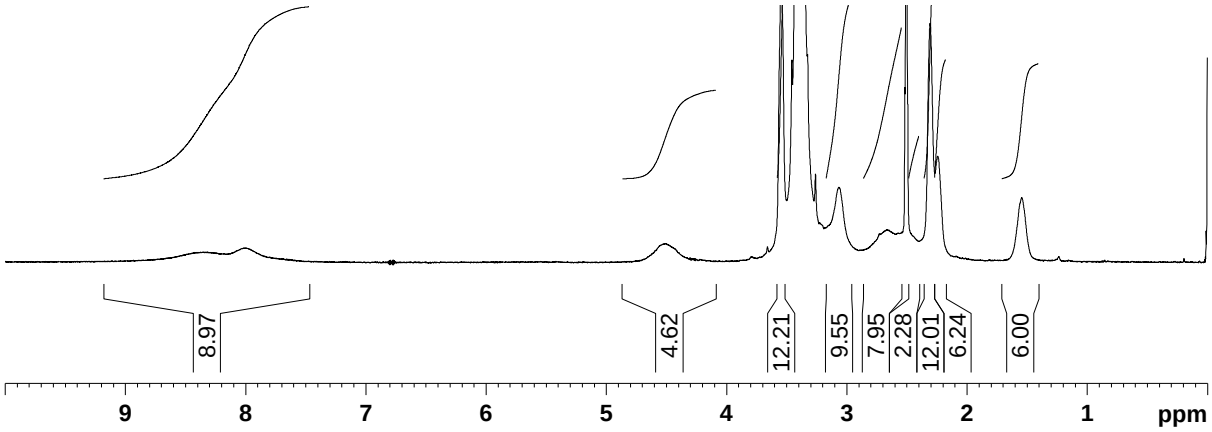

Figure 2.14 The ^{1}H NMR spectrum of polymer 35 in DMSO-d_6 reveals the signal for the protons on the tertiary carbon at 4.50 ppm (integration value 4.62). The peak for the amide protons, which are absent in D_2O, is observed between 7.38 and 8.94 ppm.

The ^{1}H NMR spectrum of **35** in DMSO-d_6 shows a broad signal between 7.38 – 8.94 ppm for the amide protons. Following the addition of 5 % D_2O to the DMSO-d_6 solvent, this broad signal is quenched by the replacement of all the amide protons with deuterium. This ^{1}H NMR peak is also absent when D_2O is the solvent.

The various infrared bands between 2700 and 3700 cm^{-1} are assigned to the primary amine (NH_2) and the secondary amide (CONH) groups of **35** which are created by the ring opening reactions, see spectrum 43.

3.2.2.3 Anchoring of ruthenocenylcarboxylic acid derivatives to the carrier polymer 35

In order to address goal 3, Chapter 1, ruthenocene-containing carboxylic acids, **24a – 24d,** were anchored to the side chains of polymer **35,** to obtain the carrier-drug conjugates **4 – 7**.

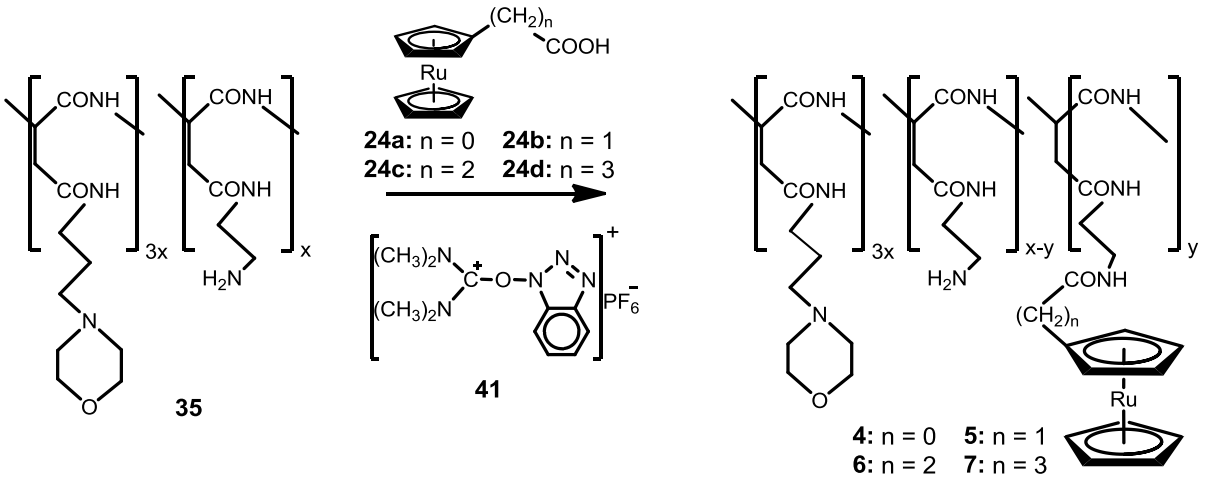

Figure 2.15 Anchoring of ruthenocene-containing groups, 24a – 24d to polyaspartamide derivative, 35.

The carboxylic acid amine coupling to form a biodegradable amide bond was performed in a H_2O:DMF (1:1) mixture in 2 hours at room temperature in the presence of triethylamine. *O*-benzotriazolyl-*N*,*N*,*N*`,*N*`-tetramethyluronium hexafluorophosphate (HBTU)**, 41,** was used as coupling agent, and induced coupling degrees ranging between 70 % (that is y = 0.7x in **Figure 2.15**) and 98 % (y = 0.98x). The same conditions were employed for the coupling of all four acids, **24a – 24d.** Subsequently each polymer was subjected to aqueous dialysis in 12 000 molecular mass cut-off membrane tubing, freeze-dried and stored in an air-tight container. Polymers were obtained in high yields with increased coupling efficiency for carboxylic acids as the separator between the ruthenocenyl group and carboxylic acid functional group increases, see **Table 2.1**, page 46.

The successful anchoring of the ruthenocenyl groups to the carrier polymer has been quantified from the ^{1}H NMR spectra of polymers **4 – 7** in D_2O and DMSO-d_6. Apart from the proton resonances of the ruthenocenyl group and those of the protons on the tertiary carbon of the backbone, which overlaps with the HOD solvent signals, all the peaks for the protons on the ruthenocene-containing polymers could be discerned in D_2O as solvent (**Figure 2.16**). However, in DMSO-d_6 as ^{1}H NMR solvent, the ruthenocenyl and aspartic acid peaks could be discerned (**Figure 2.17**).

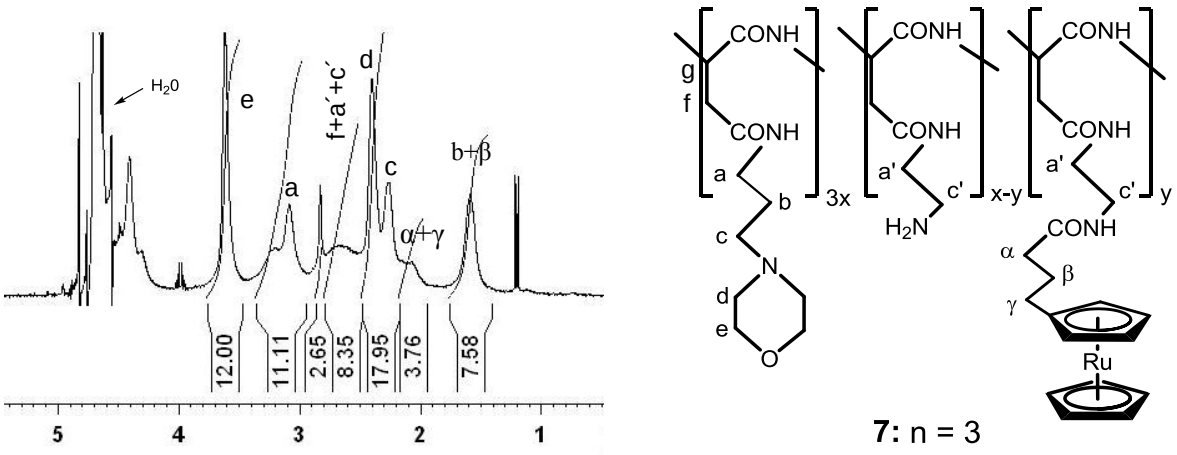

Figure 2.16 The proton assignment on the ^{1}H NMR spectrum of polymer 7 in D_2O. δ_H /ppm: 1.40–1.76 (m, 8H, b-CH_2 + β-CH_2); 2.17-2.46 (m, 18H, c-CH_2 + d-CH_2); 2.46-2.78 (bs, 8H, asp-CH_2); 2.82 (s, 2H, α-CH_2); 2.95-3.36 (m, 10H, a-CH_2 + a´-CH_2 + c´-CH_2); 3.61 (s, 12H, e-CH_2),

The position of the proton resonances of the ruthenocenyl group anchored on polymers **4 – 7** is shown in **Figure 2.18**. These peaks have the same shift pattern, induced by the electron-donating or electron-withdrawing properties of the substituent on the ruthenocenyl group, as for the free carboxylic acids.

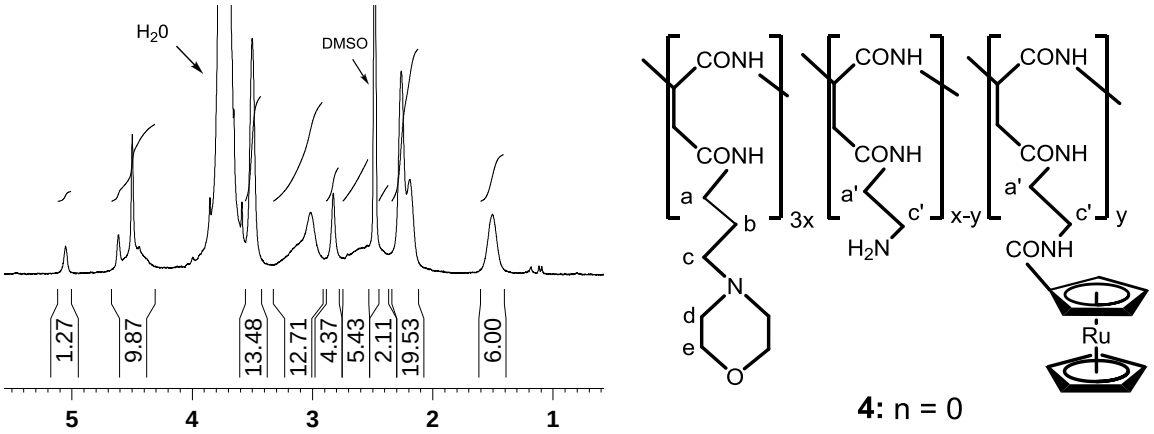

Figure 2.17 The ^{1}H NMR spectrum of polymer 4 in DMSO-d_6 reveals the peaks for the protons on the anchored ruthenocenyl group between 4.2 and 4.5 ppm.

The determination of the degree of ruthenocene coupling to carrier polymers is complicated by the position of the ^{1}H NMR resonances for the ruthenocenyl group. The degree of coupling is determined by the ratio of the ruthenocenyl peaks against that of the morpholino group anchored to the polymer backbone. However, the resonances for the protons on the aspartate tertiary carbon of the polymer backbone (4.3 – 4.7) overlap with those of the ruthenocenyl group.

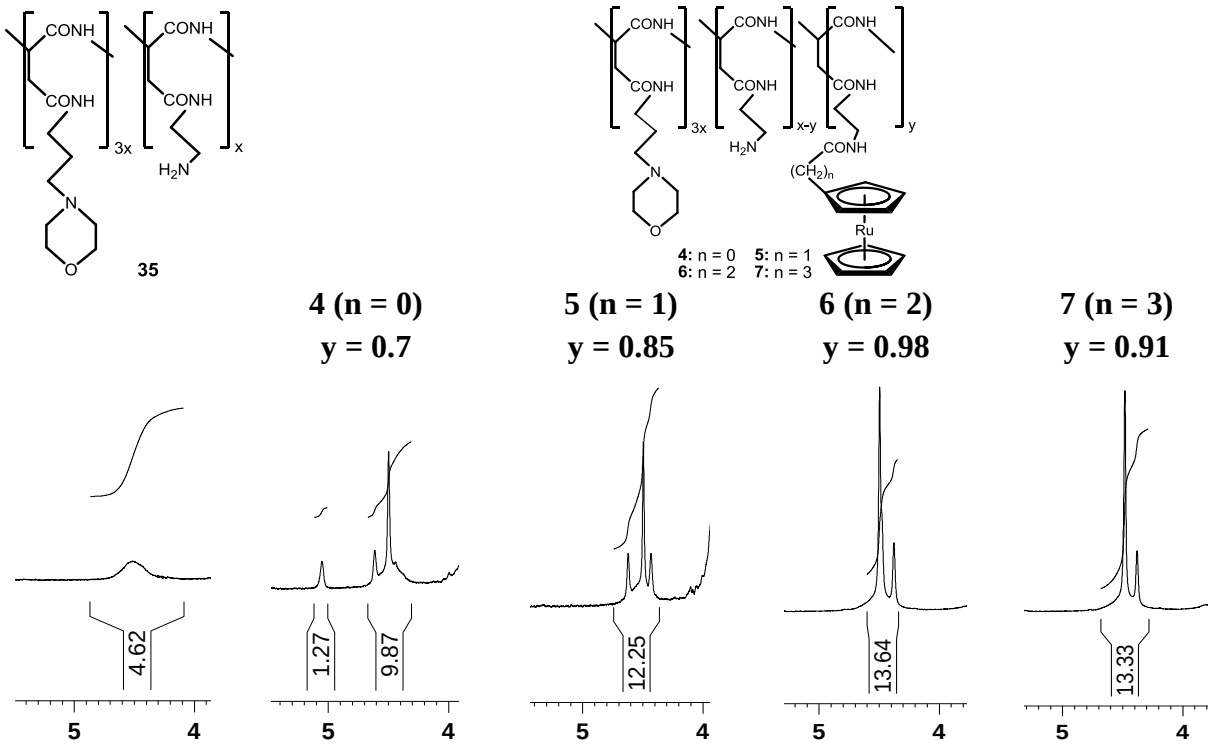

Figure 2.18 Part of the ^{1}H NMR spectrum in DMSO-d_6 of polymers 35, 4, 5, 6 and 7 showing the ruthenocenyl group on the polymers superimposed with the tertiary carbon proton peaks.

For polymer **4** the degree of coupling has been determined on the average, from the integration of two ^{1}H NMR signals (Spectrum 20, **Figure 2.18**). Integration of the two cyclopentadienyl (C_5H_4) protons at 5.05 ppm gave 1.27/2 = 0.64 (that is y = 0.64x in **Figure 2.15**). The remaining seven cyclopentadienyl proton peaks are superimposed with the four protons of the tertiary carbon in the polymer backbone, at 4.47 ppm, integrated for 9.87. By subtracting 4.6 from the combined integral, the coupling is calculated as (9.87 – 4.6)/7 = 0.75. The average of these two results gave (0.75 + 0.64)/2 = 0.70. Since 100% coupling to polymer **35** would require a value of 1.0 rather than the 0.70, it implies the degree of coupling for polymer **4** is 70 %. The degree of coupling for compound **5** is calculated by subtracting the integral for the protons of the carrier polymer from the combined integrate. The component of the integration in the 4.6 ppm region, that is contributed to the ruthenocenyl group, is given by (12.25 – 4.6)/9 = 0.85, which denote 85 % coupling. Once again the subtracted 4.6 integration value is the contribution of the four protons of the tertiary carbon in the polymer backbone. The coupling for **6** and **7** is calculated in the same manner and results are summarized in **Table 2.1**.

Table 2.1. Yields and degree of anchoring of the ruthenocenyl group to the carrier polymer

Polymer	Yield	Degree of Coupling
4	58 %	70 %
5	47 %	85 %
6	48 %	98 %
7	49 %	91 %

IR spectra 44 – 47 (see appendix) of the ruthenocenyl bearing polymers **4, 5, 6** and **7** show only minor differences in the fingerprint region compared to the spectrum of the free carrier polymer **35 (**spectrum 43).

3.3 XPS results.

X-ray Photoelectron Spectroscopy, (XPS) has been performed on compounds **6**, **24b** and **35** to gather information on the content of the samples. The atomic concentration of the atoms, derived from XPS survey scans compare, within the accuracy of XPS measurements, with the calculated composition obtained from ^{1}H NMR.

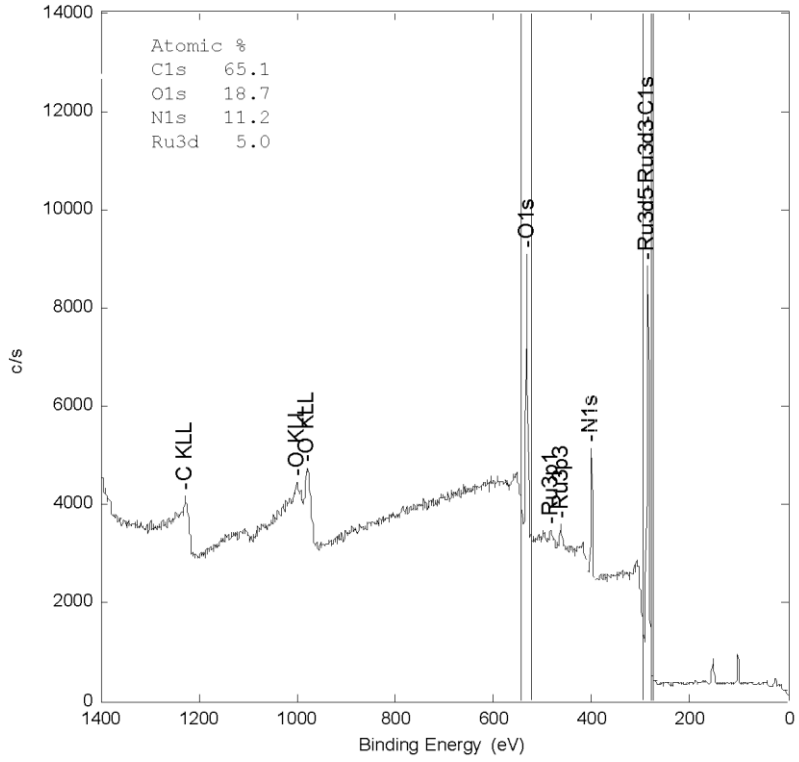

Figure 2.19 XPS survey scan of ruthenocene-containing polymer 6 showing the photoelectron and Auger peaks.

High resolution XPS scans (see **Figure 2.20**) have been taken for oxygen, carbon, nitrogen and ruthenium. The transitions of carbon 1s electrons are observed in the 290 – 282 eV range. The oxygen 1s band can be resolved into several bands between 533 and 531 eV. The nitrogen 1s transitions, attributed to the various amine and amide groups, are observed between 402 and 396 eV.

Table 2.2. The concentration of the atoms in the respective samples and binding energies for all elements derived from XPS measurements.

	C 1s			O 1s			N 1s			Ru 3d		
Compound	**[eV]**	**% calc**	**% exp**	**[eV]**	**% calc**	**% exp**	**[eV]**	**% calc**	**% exp**	**[eV]**	**% calc**	**% exp**
$RcCH_2COOH$, 24b	284.7	80.0	73.3	532.6	13.3	19.1				280.5	6.7	7.4
Carrier polymer, 35	284.7	64.6	67.8	531.7	18.4	20.1	399.3	16.9	11.4			
Ruthenocene-containing polymer, 6	284.6	68.7	65.1	531.4	15.0	18.7	399.3	15.0	11.2	280.0	1.3	5.0

A signal for ruthenium is observed for 2-ruthenocenylethanoic acid, **24b** and ruthenocene-containing polymer **6** at 484 ($3p_{1/2}$) and 462 ($3p_{3/2}$) eV. Ruthenium also gives a signal at 280 eV in the area of the C 1s transitions. (**Figure 2.20**)

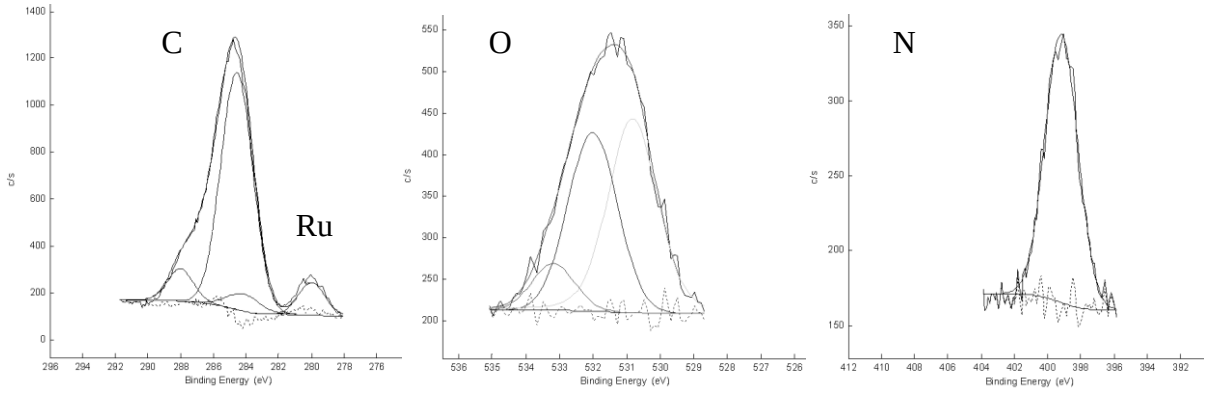

Figure 2.20 High resolution XPS scans of ruthenocene-containing polymer 6 for the transitions of C 1s (left), O 1s (middle) and N 1s electrons (right). An additional band is observed next to the C 1s transition at 280 eV for ruthenium.

XPS of **6** gives a qualitative proof of the anchoring of ruthenocene to the carrier-polymer but not with high enough accuracy to give information with regard to the degree of coupling.

3.4 Electrochemistry

Goal 4 (Chapter 1) of this study has been to investigate the electrochemical behaviour of ruthenocene, its carboxylic acid derivatives and the polymer-bound ruthenocene derivatives. The chemical behaviour of ruthenocene is similar to that of ferrocene in many ways. However, the electrochemical behaviour of ruthenocene in polar or protic solvents is very different from that of ferrocene and the oxidation potential of the ruthenocenyl-group is *ca.* 520 mV higher than its Fe analogues.

3.4.1 Cyclic voltammetry of ruthenocene-containing carboxylic acids

The carboxylic acids **24a – 24d** were dissolved in concentrations of 0.25 mM and the solutions contained 0.1 M $[NBu_4][B(C_6F_5)_4]$ as supporting electrolyte in dichloromethane. The three electrode system employed consisted of two Pt wires for the auxiliary and reference electrodes and a glassy carbon working electrode. The peak anodic (E_{pa}) and peak cathodic (E_{pc}) potentials (referenced against FcH/FcH^+) as well as the peak anodic (i_{pa}) and peak cathodic (i_{pc}) currents were determined by reading of the respective values from the cyclic voltammograms as shown in Figure 2.4 (page 22). The difference in peak potentials (ΔE_p) = $E_{pa} - E_{pc}$, formal reduction potential ($E^{o'}$) = $(E_{pa} + E_{pc})/2$ and ratio between i_{pa} and i_{pc} were then calculated, results are summarized in **Table 2.3**, page 51.

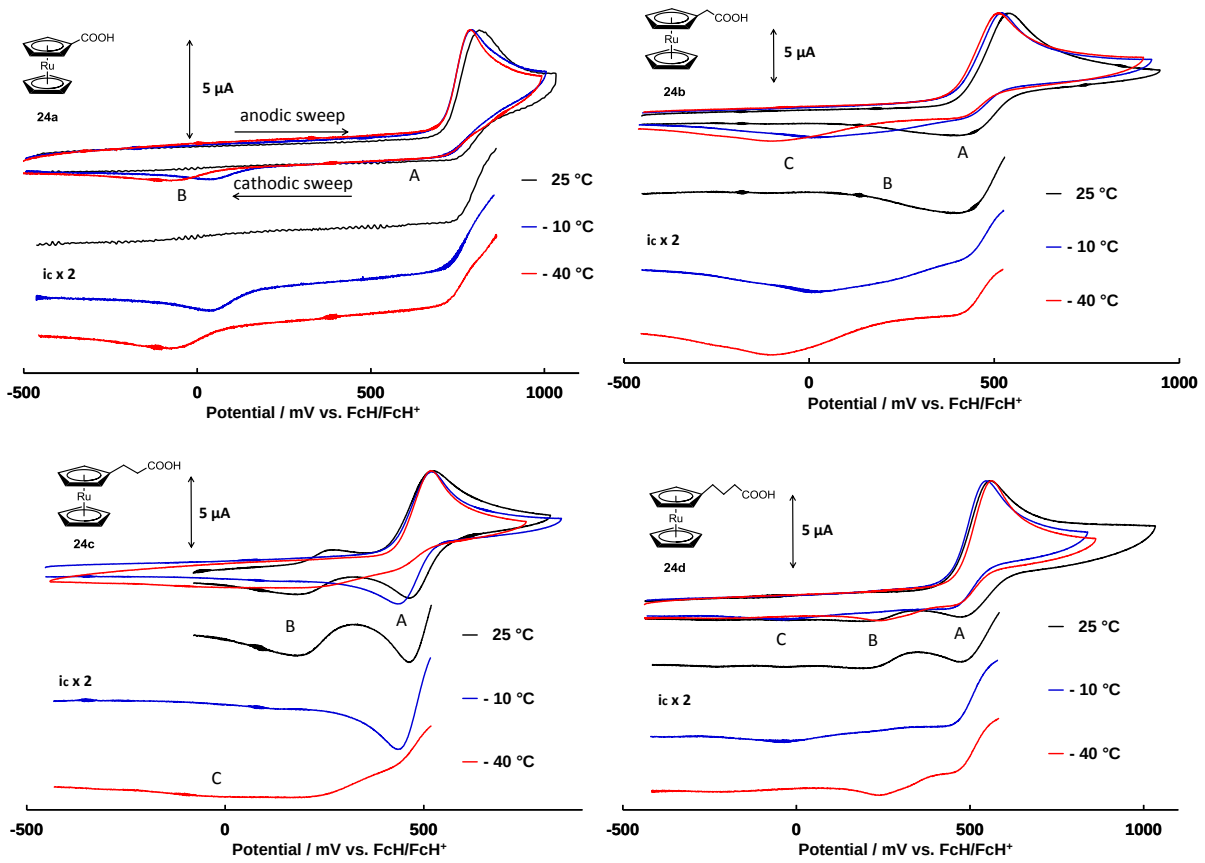

Figure 2.21 The cyclic voltammograms of 0.25 mM CH_2Cl_2 solutions of 24a – 24d in the presence of $[NBu_4][B(C_6F_5)_4]$ at 25, -10 and -40 °C at a scan rate of 100 mV·s^{-1}. The inset shows a double magnification of the cathodic waves.

From the CV's of **24a – 24d** at three different temperatures, **Figure 2.21**, the anodic scan shows only a single wave for the oxidation of Ru^{2+} to Ru^{3+}. The sequential cathodic scan of **24a, 24b, 24c** and **24d** at 25 °C shows a small reduction wave for Ru^{3+} back to Ru^{2+} at wave A with $\Delta E_p \leq 114$ mV and $484 \leq E^{o'} \leq 776$ mV at 25 °C and scan speed 100 mV·s^{-1}. The ruthenocenium cation is a 17 electron species. Such species are generally very unstable and would react or form an ion pair with any nucleophile to return to a stable 18-electron species. The reduction waves observed in a cathodic scan at more negative potentials than the reduction wave for Rc/Rc^+, wave B, can be due to a variety of side products from the oxidation of the ruthenocenyl group. Possible follow-up chemical reaction products of electrochemically generated Ru^{3+} include ruthenocenophanes,[97] metal-metal dimers,[100] metal-cyclopentadienyl dimers[99] and Ru^{4+} complexes.[98] The isolation and characterisation of the follow-up chemical reaction products and their assigment to the reduction waves observed in the cathodic scan require a variety of spectroscopic and other experiments which are outside the scope of this study.

The carboxylic acid group of RcCOOH, **24a** has a labile O-H bond and the oxygen atoms contains several free electron pairs. This opens various pathways to a chemical one-electron oxidation of Ru^{3+} species to Ru^{4+}. If this happens before the Ru^{3+} reduction can commence during the cathodic sweep at wave A, the size of reduction wave A will decrease just as it decreases upon the addition of PF_6, see **Figure 2.22**, adapted from reference 99.

In the weakly coordinating solvent like dichloromethane, and a weakly nucleophilic supporting electrolyte with either $[B(C_6F_5)_4]^-$ or $[B(C_6H_3(CF_3)_2)_4]^-$ as the counter anion the oxidation of substituted ruthenocene is an inherent one electron, quasi-Nernstian process giving the 17-electron ruthenocenium cation, $[RuCp_2]^+$, **3^+.** However, in coordinating solvent/electrolyte systems the oxidation of ruthenocene proceeds by a one-step irreversible $2e^-$ process. **Figure 2.22** shows the decrease of the reduction wave following the addition of the coordinating anion, PF_6^-, to an analyte solution.

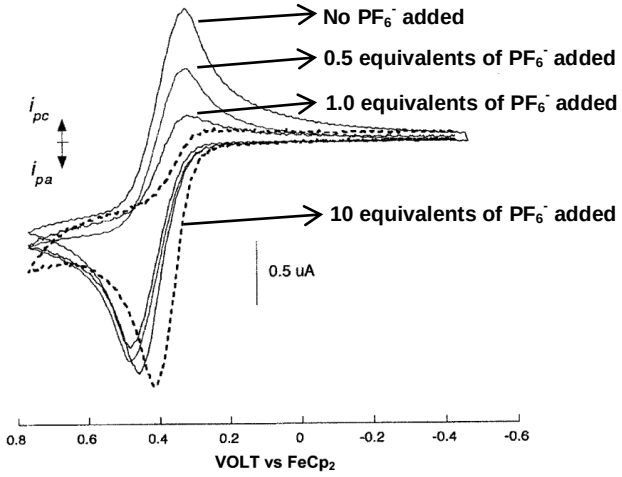

Figure 2.22 The CV scans showing the effect of successive additions of $[NBu_4][PF_6]$ to a solution of 2.2 mM ruthenocene in CH_2Cl_2/0.1 M $[NBu_4][B(C_6F_5)_4]$at 2 mm glassy carbon electrode, scan rate 200 $mV \cdot s^{-1}$, T = 25 °C. The three successive additions were of 0.5, 1, and 10 equivalents of $[PF_6]^-$ (Figure from reference 99). Note that the layout of the above CV's follows the non-IUPAC, American convention with i_{pc} upwards and i_{pa} downwards. Also the voltage axis runs from positive left to negative right rather than in the IUPAC convention used by the author.

Table 2.3. The cyclic voltammetry data (potentials vs. FcH/FcH^+), at a glassy carbon electrode, (surface area = 0.071 cm^2) of 0.25 mmol dm^{-3} solutions of 24a – 24d in dry dichloromethane containing 0.1 mol·dm^{-3} $[NBu_4][B(C_6F_5)_4]$ as supporting electrolyte at 25, -10 and -40 °C.

RcCOOH, 24a			wave A	Rc^0/Rc^+				2nd reduction wave B		3rd reduction wave C	
Temp	scan rate	E_{pa}/	E_{pc}/	$E^{o'}$/	ΔE/	i_{pa}/	i_{pc}/i_{pa}	E_{pc}/	i_{pc}/	E_{pc}/	i_{pc} /
K	$mV·s^{-1}$	mV	mV	mV	mV	μA		mV	μA	mV	μA
	100	815	737	776	78	4.51	0.25				
	200	820	735	778	86	5.94	0.25				
298	300	831	734	782	96	6.86	0.25				
	400	835	730	782	105	7.39	0.26				
	500	838	723	781	115	8.11	0.27				
Average				**780**			**0.26**				
	100	791	730	760	61	4.22	0.14	35	0.43		
	200	799	719	759	80	5.85	0.17	5	0.91		
263	300	803	715	759	88	7.03	0.17	-3	1.17		
	400	810	708	759	102	8.07	0.20	-13	1.35		
	500	815	708	762	107	8.81	0.20	-24	1.56		
Average				**760**			**0.18**				
	100	785	722	753	63	3.14	0.13	-81	0.29		
	200	798	717	757	81	4.39	0.16	-116	0.52		
233	300	808	712	760	96	5.29	0.14	-134	0.69		
	400	815	709	762	106	5.96	0.17	-147	0.81		
	500	821	703	762	119	6.59	0.18	-155	0.79		
Average				**759**			**0.16**				
$RcCH_2COOH$, 24b											
Temp	scan rate	E_{pa}/	E_{pc}/	$E^{o'}$/	ΔE/	i_{pa}/	i_{pc}/i_{pa}	E_{pc}/	i_{pc}/	E_{pc}/	i_{pc} /
K	$mV·s^{-1}$	mV	mV	mV	mV	μA		mV	μA	mV	μA
	100	541	427	484	114	8.43	0.38	323	0.91		
	200	553	419	486	134	9.02	0.40	304	1.60		
298	300	560	415	487	145	10.45	0.38	290	2.15		
	400	567	409	488	158	13.85	0.37	273	2.71		
	500	569	410	489	159	15.40	0.35	251	2.97		
Average				**487**			**0.38**				
	100	518	425	472	93	5.87	0.20	230	0.63	18	0.83
	200	525	419	472	107	8.49	0.25	194	1.45	-9	1.27
263	300	531	415	473	116	10.13	0.22	160	2.00	-26	1.45
	400	540	406	473	133	11.41	0.22	129	2.76	-37	1.61
	500	543	408	475	135	12.35	0.21	109	3.11	-57	1.89
Average				**473**			**0.22**				
	100	513	411	462	103	5.38	0.25	-103	1.39		
	200	522	406	464	116	7.16	0.21	-135	2.29		
233	300	531	399	465	132	8.10	0.21	-160	2.83		
	400	542	404	473	138	9.18	0.20	-176	3.38		
	500	545	400	473	144	9.88	0.20	-197	3.64		
Average				**467**			**0.21**				

$RcCH_2CH_2COOH$, 24c		wave A		Rc^0/Rc^+				2nd reduction wave B		3rd reduction wave C	
Temp	scan rate	E_{pa}/	E_{pc}/	$E^{o'}$/	ΔE/	i_{pa}/	i_{pc}/i_{pa}	E_{pc}/	i_{pc}/	E_{pc}/	i_{pc} /
K	$mV \cdot s^{-1}$	mV	mV	mV	mV	μA		mV	μA	mV	μA
	100	523	464	494	59	5.76	0.65	181	1.20		
	200	535	459	497	77	8.89	0.76	175	0.96		
298	300	545	457	501	88	9.82	0.85	170	1.20		
	400	551	455	503	96	10.97	0.89	158	1.47		
	500	557	452	504	105	12.50	0.89	157	1.36		
Average				**500**			**0.81**				
	100	521	436	478	85	5.37	0.72				
	200	532	421	477	111	7.67	0.63				
263	300	543	414	479	129	9.24	0.58				
	400	550	395	472	155	10.53	0.52				
	500	555	379	467	175	11.51	0.49				
Average				**475**			**0.59**				
	100	518	436	477	82	5.37	0.23	258	1.00	-24	0.29
	200	534	443	489	91	7.29	0.20	223	1.36	-42	0.74
233	300	546	435	490	112	8.53	0.20	193	1.83	-66	0.77
	400	555	432	494	123	9.67	0.20	185	2.10	-74	0.86
	500	566	438	502	128	10.58	0.19	175	2.30	-85	1.06
Average				**490**			**0.20**				

$RcCH_2CH_2CH_2COOH$,											
Temp	scan rate	E_{pa}/	E_{pc}/	$E^{o'}$/	ΔE/	i_{pa}/	i_{pc}/i_{pa}	E_{pc}/	i_{pc}/	E_{pc}/	i_{pc} /
K	$mV \cdot s^{-1}$	mV	mV	mV	mV	μA		mV	μA	mV	μA
	100	558	475	516	82	7.19	0.34	226	0.82		
	200	568	475	522	93	8.67	0.45	217	0.92		
298	300	571	473	522	98	9.68	0.50	206	1.27		
	400	575	464	520	111	11.51	0.51	186	1.36		
	500	578	463	521	115	13.06	0.52	192	1.48		
Average				**520**			**0.46**				
	100	547	444	496	103	6.90	0.34	221	0.20	-34	0.41
	200	555	442	499	113	8.72	0.34	218	0.54	-55	0.43
263	300	564	444	504	121	10.16	0.36	220	0.83	-80	0.52
	400	569	444	506	125	11.22	0.36	223	1.10	-90	0.58
	500	574	445	509	129	12.29	0.38	220	1.51	-102	0.73
Average				**503**			**0.36**				
	100	562	453	508	109	5.93	0.28	238	0.88		
	200	576	449	512	126	6.49	0.30	235	1.56		
233	300	584	444	514	140	7.94	0.30	229	2.10		
	400	592	437	515	155	9.18	0.31	228	2.36		
	500	598	445	521	153	9.50	0.32	225	2.86		
Average				**514**			**0.30**				

The decay of electrochemically generated oxidized ruthenocenium cations **24a**$^+$**, 24b**$^+$**, 24c**$^+$ and **24d**$^+$ is the fastest for **24a**$^+$ having no CH_2 spacer between the Rc^+ and COOH centres. This causes wave A to be virtually absent in the cathodic sweep of **24a.** For **24b**$^+$ through **24d**$^+$**,** the intensity of the reduction wave is fairly similar, implying that once the COOH group is separated from the ruthenocenyl group by one or more CH_2 spacer, the rate of Rc^+ (which contains Ru^{3+}) destruction is substantially slowed down.

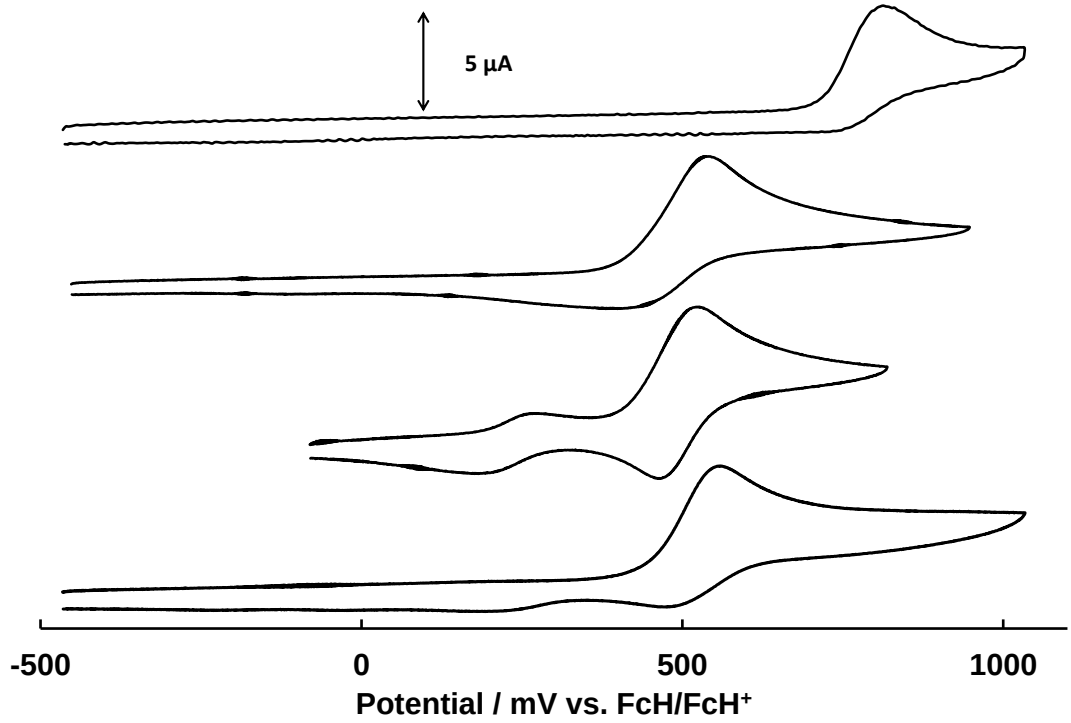

Figure 2.23 The cyclic voltammograms of 0.25 mM CH_2Cl_2 solutions of 24a – 24d in the presence of $[NBu_4][B(C_6F_5)_4]$ at 25 °C at a scan rate of 100 mV·s^{-1}.

To substantiate the conclusion that one CH_2 spacer unit effectively shields the Rc group from the influence of the electron withdrawing COOH group it is interesting to note that the peak anodic potential (E_{pa}) for **24b, 24c** and **24d** are very similar (E_{pa} = 541, 523 and 558 mV, respectively at 25 °C, ν = 100 mV·s^{-1}), see **Table 2.3**. In the case of **24a,** which does not contain any CH_2 separator groups a much larger E_{pa} value (815 mV, at 25 °C, ν = 100 mV·s^{-1}) is observed. This shows that one CH_2 separator group is enough to isolate (shield) the ruthenocenyl group from the electron-withdrawing carboxylic acid group.

In order to study the redox process of the ruthenocenyl group in the absence of a labile O-H bond (but still in the presence of O-atoms containing free electron pairs), ruthenocene acid,

24a, has been converted to its methyl ester, **63**. On the anodic CV scan of **63** a wave is observed at 843 mV for the oxidation of Ru^{2+} to Ru^{3+}. However, in the absence of the labile O-H bond of a COOH group the cathodic sweep of the methyl ester shows a much more pronounced wave A for the reduction of the Rc^{+} group back to Rc^{0} with $i_{pc}/i_{pa} = 0.54$, at $E_{pc} \approx$ 700 mV at 25 °C, see **Table 2.4**)

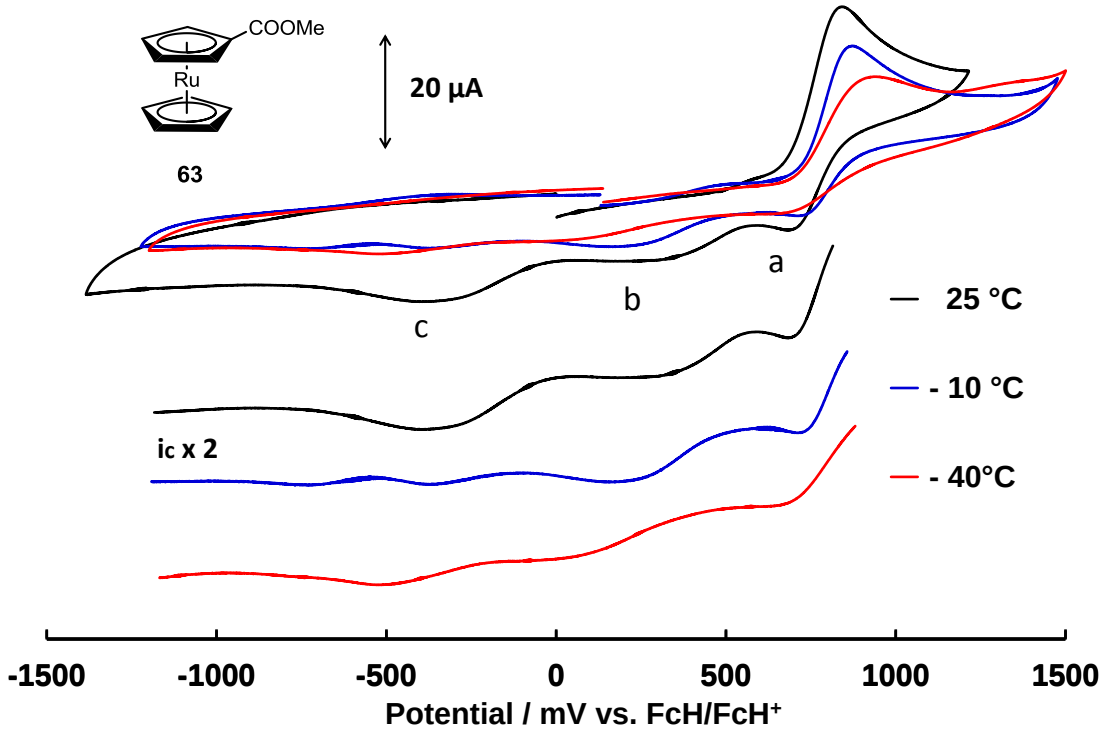

Figure 2.24 The cyclic voltammograms of 0.25 mM CH_2Cl_2 solutions of 63 in the presence of $[NBu_4][B(C_6F_5)_4]$ at 25, -10 and -40 °C at a scan rate of 100 mV·s^{-1}. The inset shows a double magnification of the cathodic waves.

Two broad cathodic product waves are also observed at lower potentials. (Ep_c = 253 mV and -396 mV at 298 K, ν = 100 mV·s^{-1}). The combined current for the three reduction waves, at 686, 253 and -396 mV approaches the current of the oxidation wave at 843 mV, thus $(i_{pc1} + i_{pc2} + i_{pc3})/i_{pa} = 0.96$. The electrochemical results of **63** are summarized in **Table 2.4**.

The addition of decamethylferrocene as internal standard to the solution of **63** alters the reduction wave in the cathodic scan, see **Figure 2.25**. A drift is observed in the reduction potentials associated with wave A during the cathodic scan with increasing scan speed. Such a drift is typical of an equilibrium being driven to one side in the time frame of the scan speeds utilized.[98]

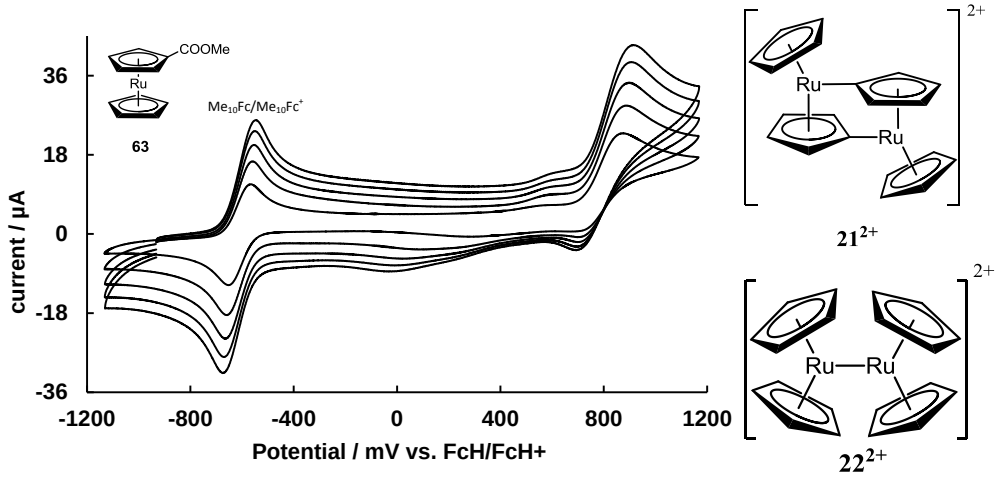

Figure 2.25 The cyclic voltammograms of 0.25 mM CH_2Cl_2 solutions of 63 in the presence of $[NBu_4][B(C_6F_5)_4]$ at -10 °C at a scan speeds of 100, 200, 300, 400 and 500 mV·s^{-1}. The structures (right) shows two equilibrium dimeric species which form following the oxidation of ruthenocene (Note: Not 63, but RcH) to ruthenocenium.

The nature of the species involved in the equilibrium associated with RcCOOMe, **63,** is not yet established, although it is pertinent to observe that the equilibrium species of unsubstituted ruthenocene involves two dimeric species shown in **Figure 2.25**.

Table 2.4. Cyclic voltammetry data (potentials versus FcH/FcH^+), at a glassy carbon electrode, (surface area = 0.071 cm^2) of 0.25 mmol dm^{-3} solutions of 63 in dry dichloromethane containing 0.1 mol dm^{-3} $[NBu_4][B(C_6F_5)_4]$ as supporting electrolyte at 25, -10 and -40 ^oC.

RcCOOMe, 36			wave A	Rc^0/Rc^+				2nd reduction wave B		3rd reduction wave C	
Temp.	scan rate	E_{pa}/	E_{pc}/	E^o/	ΔE/	i_{pa}/	i_{pc}/i_{pa}	E_{pc}/	i_{pc}/	E_{pc}/	i_{pc} /
K	mV·s^{-1}	mV	mV	mV	mV	µA		mV	µA	mV	µA
	100	843	686	764	157	27.33	0.47	253	6.73	-396	7.22
	200	851	693	772	158	37.84	0.51	249	10.23	-426	6.10
298	300	856	689	772	167	44.99	0.55	244	10.86	-480	6.80
	400	863	691	777	172	50.81	0.57	238	13.45	-487	6.17
	500	871	690	780	182	57.46	0.58	237	16.47	-490	5.89
Average				**773**			**0.54**				
	100	874	715	795	158	23.08	0.45	154	6.63	-368	2.15
	200	889	704	797	184	29.36	0.42	81	9.77	-414	3.05
263	300	899	701	800	198	32.94	0.43	34	12.28	-438	3.41
	400	907	693	800	213	37.38	0.44	5	13.94	-445	3.23
	500	912	699	806	213	40.02	0.46	10	14.16	-435	3.23

Average				**799**			**0.44**				
	100	941	701	821	240	16.85	0.25	34	5.06	-519	3.62
	200	961	676	819	286	20.35	0.26	-3	6.81	-586	6.15
233	300	980	653	816	327	24.90	0.24	-23	7.63	-620	7.20
	400	995	676	836	318	28.21	0.23	-14	8.48	-621	7.47
	500	1014	682	848	332	30.54	0.23	-19	10.27	-622	8.29
Average				**828**			**0.24**				

Ferrocene is by IUPAC convention the internal standard against which all redox potentials are reported. However, the redox wave of the FcH/FcH^+ couple overlaps with the reduction waves of the follow-up products of the oxidation of the ruthenocenyl group. Therefore decamethylferrocene, $Me_{10}Fc$, has been used as internal reference. Because of the electron-donating methyl groups on the Me_5Cp groups, decamethylferrocene is more easily reduced than ferrocene. In a CH_2Cl_2 solution of 0.25 mM ferrocene and 0.25 mM decamethylferrocene, containing 0.1 mM $[NBu_4][B(C_6F_5)_4]$ as electrolyte, the redox potential for the decamethylferrocenium/decamethylferrocene, $Me_{10}Fc/Me_{10}Fc^+$, couple is measured as -610 mV relative to the FcH/FcH^+ reference. The same concentrations of analyte and electrolyte have been applied in all cyclic voltammograms measured in organic solution and all potentials shifted to have decamethylferrocene at -610 mV.

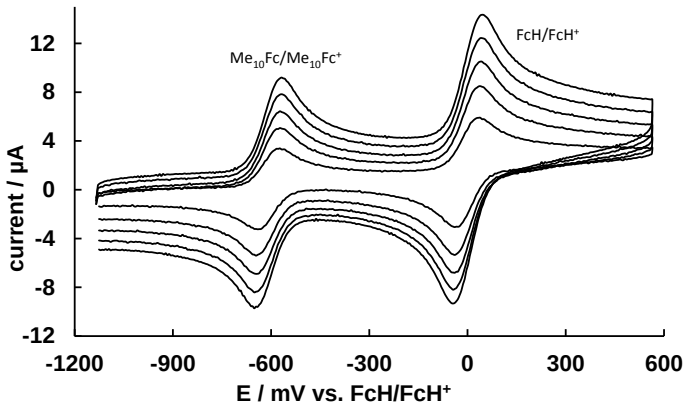

Figure 2.26 The cyclic voltammogram of 0.25 mM CH_2Cl_2 solution of $Me_{10}Fc$ and FcH in the presence of $[NBu_4][B(C_6F_5)_4]$ at 25 °C, at a scan rates of 100, 200, 300, 400 and 500 $mV \cdot s^{-1}$.

Neither ferrocene nor decamethylferrocene necessarily satisfy all the conditions of an internal reference, since both probably take part in the electrochemical process of the ruthenocenyl group. However, no drift is observed on the first oxidation wave of the ruthenocenyl group ($Ru^{2+} \rightarrow Ru^{3+}$) following the addition of either internal reference. The cathodic scan following the anodic scan to oxidize Ru^{2+} to Ru^{3+} shows a significant influence of the internal standard.

The decamethylferrocene has therefore only been used to determine the first oxidation potential, $E_{pa,}$ for the ruthenocene-containing group. The voltammograms not containing decamethylferrocene are then shifted to give the peak potentials against ferrocene.

Ferrocene and decamethylferrocene act as electron transfer agents and they influence the equilibrium between once-oxidized ruthenocenium species. The effect on the equilibrium is observed in the change in the reduction waves during a cathodic sweep following the addition of decamethylferrocene, see **Figure 2.27** and **Figure 2.28**. The change in potential in the reduction waves of **24a** with increasing scan speed is a tell-tale sign of an equilibrium, **Figure 2.27** (right). It is not clear how the ferrocene interferes with any components of any equilibrium that **24a – 24d** may be involved in. In the presence of decamethylferrrocene the system shows more Nernstian character (i.e. faster electrode kinetics). Since ferrocene is not known to form dimeric structures in the same way as ruthenocene does (see Chapter 2, page 23) the formation of ferrocenium-ruthenocenium dimers are unlikely.

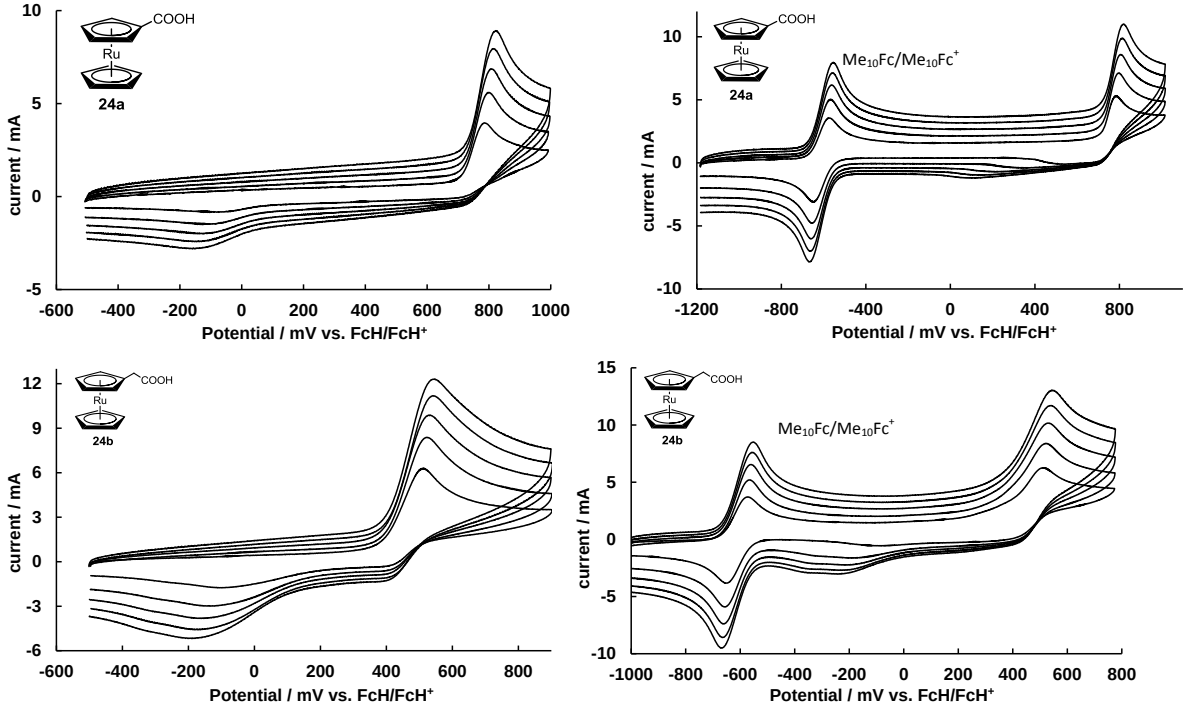

Figure 2.27 Cyclic voltammograms of 0.25 mM CH_2Cl_2 solution of 24a and 24b in the presence of $[NBu_4][B(C_6F_5)_4]$ at -40 °C shows the effect of the addition of an internal standard on the reduction waves in the cathodic sweep.

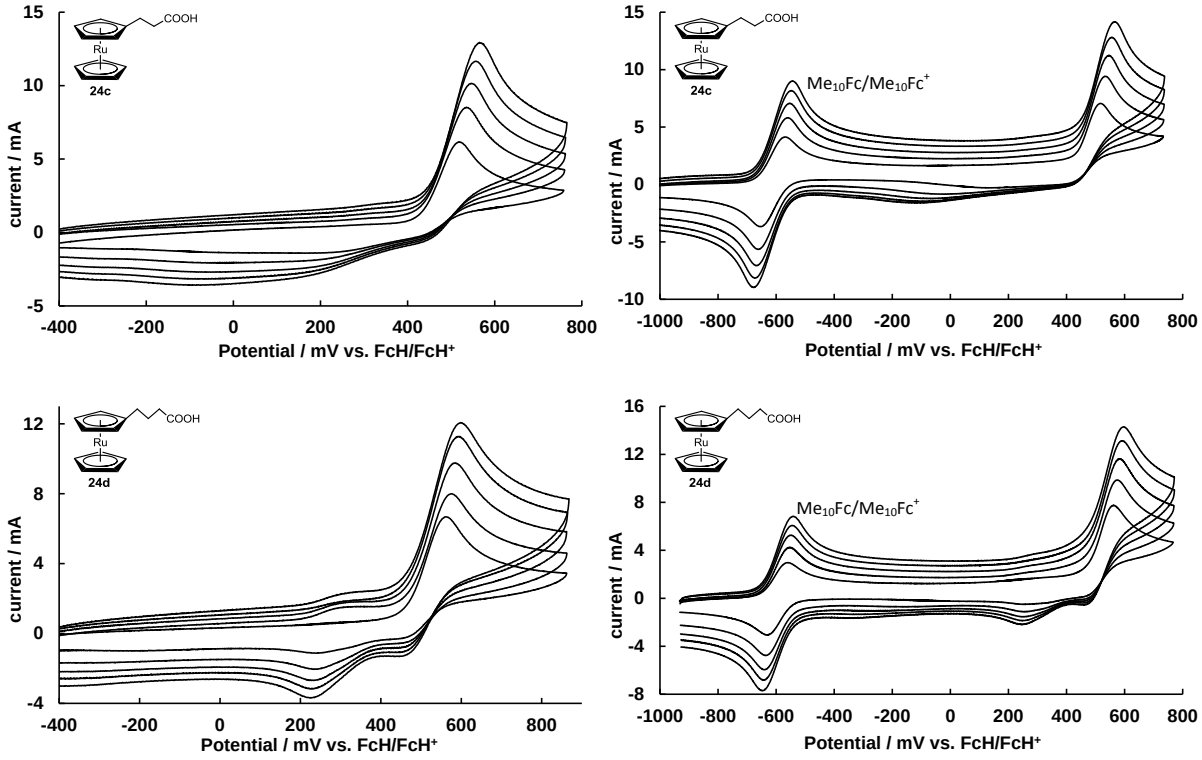

Figure 2.28 Cyclic voltammograms of 0.25 mM CH_2Cl_2 solution of 24c and 24d in the presence of $[NBu_4][B(C_6F_5)_4]$ at -40 °C show the effect of the addition of an internal standard on the reduction waves in the cathodic sweep.

To conclude, the electrochemical behaviour of the ruthenocene moiety is far more complex than that of ferrocene, which is frequently used as a redox tag to study the electronic and other properties of molecules. The electrochemical behaviour of free ruthenocene has been studied by Geiger *et al.* [99,100] and is described in good detail in the literature survey (page 23). The electrochemistry of ruthenocene involves a delicate temperature-dependent equilibrium between ruthenocenium, $\mathbf{3}^+$, and two dimers, $\mathbf{21}^{2+}$ and $\mathbf{22}^{2+}$. However, following the functionalization of ruthenocene to form ruthenocenyl derivatives, this equilibrium is disturbed to such extents that a direct correlation between the electrochemistry of ruthenocenyl derivatives and ruthenocene is very speculative. To give an all-inclusive description of the electrochemical behaviour of ruthenocene derivatives such as **24a – 24d** would require an extensive study with many technique, including the *in situ* measurements of intermediates. However, this was considered outside the boundaries of the time constrictions of this study.

3.4.2 Cyclic voltammetry of water-soluble polymer-bound ruthenocenes

The electrochemistry of polymers **4 – 7** was investigated in water. The three-electrode system utilized consisted of two Pt wires for the auxiliary and reference electrodes and a glassy carbon working electrode. The supporting electrolyte used was 0.1 M KCl and the concentration of each polymer was 0.25 mM, CV's for **4 – 7** is shown in **Figure 2.29**

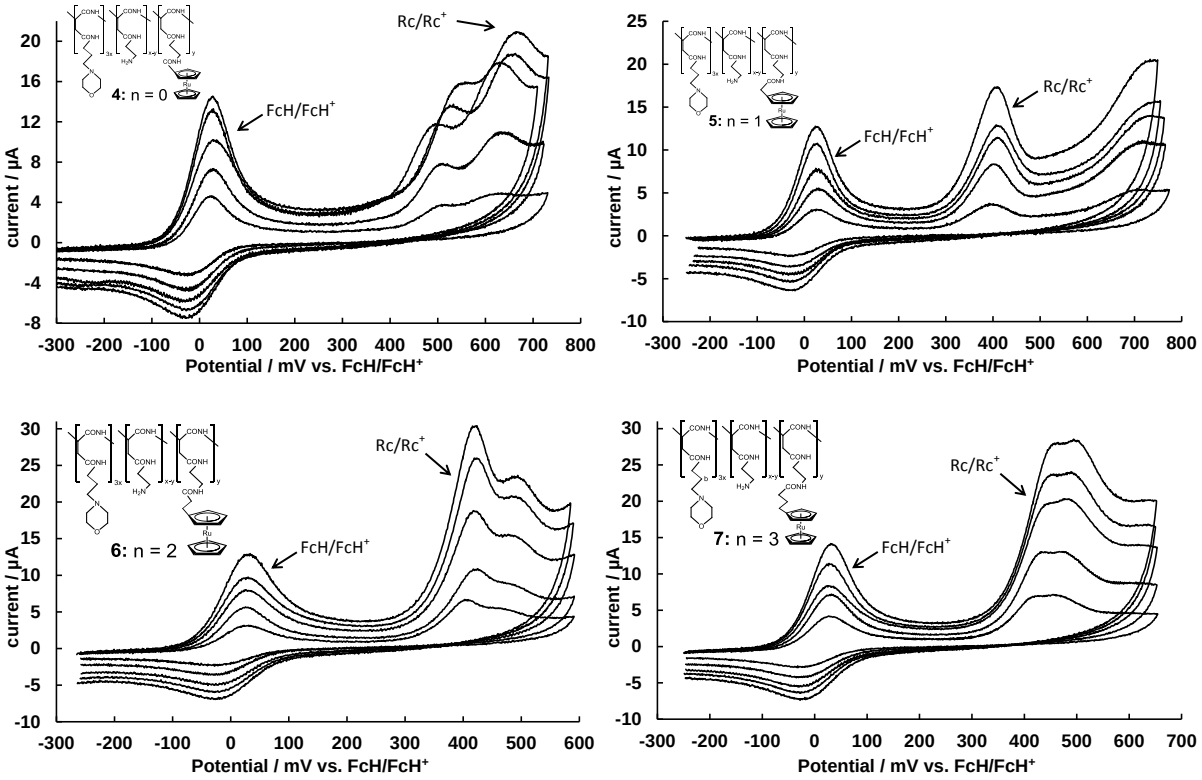

Figure 2.29 Cyclic voltammograms of 0.25 mM H_2O solutions of polymers 4 – 7 containing KCl as supporting electrolyte at 25 °C with a scan rates of 100, 200, 300, 400 and 500 mV·s^{-1}.

The anodic scan for polymers **4 – 7** shows two oxidation waves besides that of the internal reference, $[FcH]^+[PF_6]^-$. These two waves are for the oxidation of the polymer bound ruthenocenyl group and the polymer itself. It is unclear which part of the polymer it is that undergoes oxidation. The oxidation wave for the polymer is generally found between 450 and 550 mV.

The oxidation wave for the ruthenocenyl group in polymer **4** has a much higher potential (E_{pa} = 631 mV at 25 °C, ν = 100 mV·s^{-1}) than that of polymers **6, 7** and **8** due to the electron-withdrawing carbonyl group directly attached to the ruthenocenyl group. This is in analogy with the free ruthenocenyl-containing carboxylic acids. The one, two and three CH_2

separator groups on polymers **6, 7** and **8** respectively is enough to isolate the ruthenium centre of the ruthenocenyl group from the electron withdrawing carbonyl group. The oxidation wave for the free carrier polymer, **63** was observed at 648 mV see **Figure 2.30**.

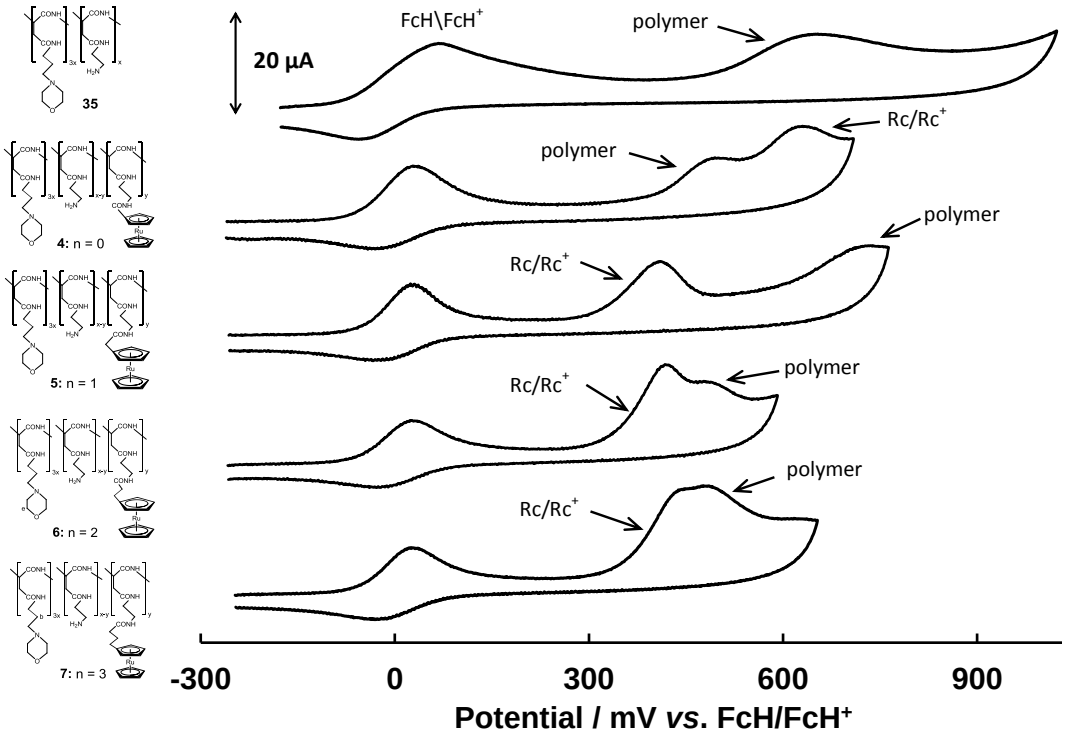

Figure 2.30 Cyclic voltammograms of 0.25 mM H_2O solutions of polymers 4 – 7 containing KCl as supporting electrolyte at 25 °C with a scan speed of 400 mV·s^{-1}.

Ferrocenium hexafluorophosphate, $[FcH]^+[PF_6]^-$ was used as internal reference in the same concentration as the analyte (0.25 mM). Unlike ferrocene and decamethylferrocene this iron(III) salt is water soluble, making it a good choice for electrochemistry performed in aqueous media. $[FcH]^+[PF_6]^-$ does not show a reversible Fe^{2+}/Fe^{3+} couple in this system, neither when the scan is started at a potential higher or lower than the redox couple.

No reduction waves were observed for the ruthenocenyl group in aqueous solution. The ruthenocene moiety is surrounded by a sea of available electron donors including water and the various amine, amide and keto groups on the polymer. In aqueous solution Ru^{3+} is expected to be reduced to Ru^{2+} chemically by the solvent before it can be electrochemically reduced. This explains the total absence of a reduction wave during the reverse cathodic cycle in the CV of **4 – 7.** In addition in the presence of nucleophiles Rc is known to oxidize very easily to Rc^{2+} containing Ru^{4+} metal centres.[99, 100, 101]

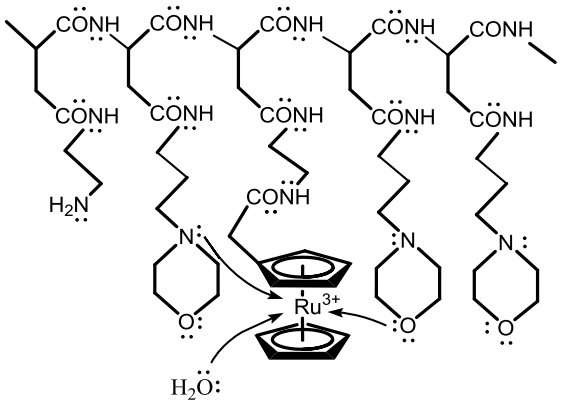

Figure 2.31 The anchored ruthenocenyl group is surrounded by a sea of electron donors which may easily reduce any Ru^{3+} back to Ru^{2+} as it forms. The available amine or either ligands from the morpholino group may also stablize Ru^{4+} if over oxidation occurs.

Table 2.5. The cyclic voltammetry data (potentials versus FcH/FcH^+) at a glassy carbon electrode (surface area = 0.071 cm^2) of 0.25 mmol dm^{-3} solutions of polymers 4 – 7 in H_2O containing 0.1 mol dm^{-3} KCl as supporting electrolyte at 25 °C.

		Rc wave		polymer wave	
Compound	scan rate	E_{pa}/	i_{pa}/	E_{pa}/	i_{pa}/
	$mV \cdot s^{-1}$	mV	µA	mV	µA
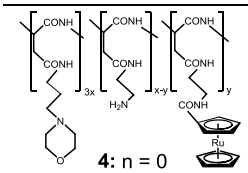 **4**: n = 0	100	631	2.23	530	2.31
	200	633	5.22	533	5.48
	300	630	8.12	520	8.87
	400	657	8.13	551	10.36
	500	668	8.53	581	12.11
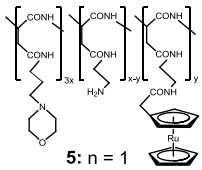 **5**: n = 1	100	397	2.74	712	2.26
	200	402	6.53	717	5.78
	300	410	9.29	734	7.49
	400	409	10.35	744	7.46
	500	407	14.04	741	11.12
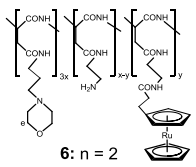 **6**: n = 2	100	426	5.34	450	1.41
	200	422	8.93	469	1.64
	300	421	15.98	478	2.18
	400	423	22.84	488	3.77
	500	421	26.63	492	4.62
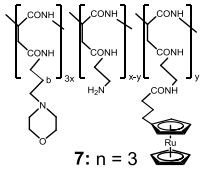 **7**: n = 3	100	424	5.13	459	2.97
	200	434	9.36	473	3.56
	300	447	16.77	481	4.22
	400	455	19.88	489	4.20
	500	460	23.57	495	4.84

This concludes the description and discussion of the research undertaken by the author. Chapter 4 will provide experimental procedures utilized by the author and Chapter 5, the final chapter in this thesis will present a short summary and future perspectives.

---

[89] O. Hofer, K. Schloegel, *J. Organomet. Chem.*, 443, **13** (1968).

[90] D. Lednicer, J.K. Lindsay, C.R. Hauser, *J. Org. Chem.*, 653, **23** (1958).

[91] J. Cason, *Org. Synth. Coll. Vol.*, 169, **3** (1955).

[92] P. Neri, G. Antoni, *Macromol. Synth.*, 25, **8** (1982).

[93] G. Giammona, B. Carlisi, G. Cavallaro, I. Donato, F. Pinio, V. Liveri, *Int. J. Pharm.*, 239, **64** (1990).

[94] E.W. Neuse, A.G. Perlwitz, *Polyamides as drug carriers: Water soluble Polymers*; eds. S.W. Shalaby, C.L. McCormick, G.B. Butler, *American Chemical Society*, Washington DC, 1991, pp 395-404.

[95] D.D. N'Da, E.W. Neuse, *J. Inorg. Organomet. Polym.*, 468, **20** (2010).

[96] J.C. Swarts, G.J. Lamprecht, E.W. Neuse, *J. Inorg. Organomet. Polym*., 143, **4** (1994).

[97] S. Kamiyama, T.M. Suzuki, T. Kimura, A. Kasahara, *Bull. Chem. Soc. Jpn.*, 909, **51** (1978).

[98] K.C. Kemp, E. Fourie, J. Conradie, J.C. Swarts, *Organomet.*, 353, **27** (2008).

[99] J.C. Swarts, A. Nafady, J.H. Roudebush, S. Trupia, W.E. Geiger. *Inorg. Chem*., 2156, **48** (2009).

[100] S. Trupia, A. Nafady, W.E. Geiger, *Inorg. Chem*., 5480, **42** (2003).

[101] M.W. Droege; W.D. Harman, H. Taube, *Inorg. Chem.*, 1309, **26** (1987).

4 Experimental

4.1 Introduction

This section provides a description of the materials, equipment, techniques and experimental procedures used in the current study.

4.2 Materials

Solid reagents (Merck, Aldrich and Fluka) employed for synthesis were used without further purification. Liquid reagents (Merck and Aldrich) were used without further purification unless otherwise stated. Organic solvents were dried according to published procedures.[102] Column chromatography was performed on Kieselgel 60 (Merck, grain size 0.040-0.063 mm). Filtration and vacuum evaporation was performed with the aid of a water aspirator. Dialyses were performed against running water in 12 000 molecular mass cut-off cellulose membrane tubing followed by freeze drying on an EZ-DRY 550Q freeze dryer at -43 °C and 63 mTorr.

4.3 Spectroscopic measurements

^{1}H NMR spectra were measured at 298 K on a Bruker Advance DPX 300NMR spectrometer. All chemical shifts are reported relative to TMS ($Si(CH_3)_4$) at 0.00 ppm. Under these conditions, the $CDCl_3$ ^{1}H NMR signal was a 7.27 ppm, while traces of water in the $CDCl_3$ is at 1.60 ppm. Selective spectra have been provided in the appendix. FTIR measurement was performed using a Bruker Tensor 27 IR spectrometer and Pike MIRacle ATR, running OPUS software (Version 1.1). Melting points were recorded on an Olympus BX51 microscope, using a LINKAM, TMS 600 hot stage, and were uncorrected. The melting points given were the onset temperature of melting and are uncorrected for standard pressure ($P \approx 650$ Torr during measurements, not 760 Torr)

XPS data were recorded on a PHI 5000 Versaprobe system with monochromatic Al Kα X-ray source. Spectra were obtained using the aluminium anode (Al Kα = 1486.6 eV) operating at 50 μm, 12.5W and 15 kV energy (97 X-ray beam). The survey scans were recorded at constant pass energy of 187.85 eV and high resolution scans at a constant pass energy of 23.5 eV. The background pressure was 2 x 10^{-8} mbar. The XPS data were analysed utilizing Multipak version 8.2c computer software using Gaussian–Lorentz fits.

4.4 Synthesis

4.4.1 2-Chlorobenzoyl ruthenocene, 23

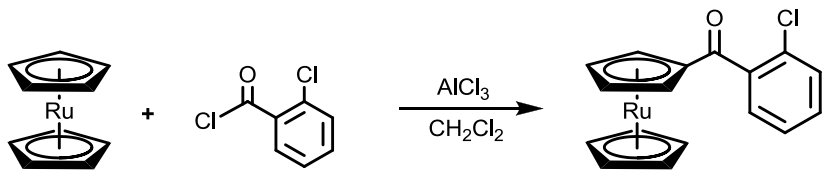

3 **23**

Ruthenocene, **3** (2 g, 8.62 mmol) and 2-chlorobenzoyl chloride (1.5 g, 9 mmol) were added to dichloromethane (40 mL) while stirring under an argon atmosphere. After the solution was chilled thoroughly, solid anhydrous aluminium chloride (1.72, 12.9 mmol) was added in small portions at a rate so that the reaction mixture temperature did not exceed 5 °C. Stirring continued for 60 minutes in an ice bath and then for 16 hours at room temperature. The reaction mixture was cooled in ice. Ice water (80 mL) was added cautiously and the resulting mixture stirred vigorously for 30 minutes before the aqueous layer was extracted with dichloromethane (3 x 200 mL). The organic extracts were combined and washed with an equal volume of water, then with 10 % aqueous NaOH (140 mL), dried over $MgSO_4$ and the solvent removed under reduced pressure to yield 2.03 g (64%), of **23,** as dark yellow crystals. Melting point 110 °C. IR ν /cm^{-1} = 1645 (C=O), Spectrum 27. ^{1}H NMR δ_H (300MHz, $CDCl_3$)/ppm: 4.67 (s, 5H, C_5H_5); 4.86 (t, 2H, C_5H_4); 5.03 (t, 2H, C_5H_4); 7.3-7.5 (m, 4H, C_6H_4), Spectrum 1.

4.4.2 Ruthenocenoic acid, 24a

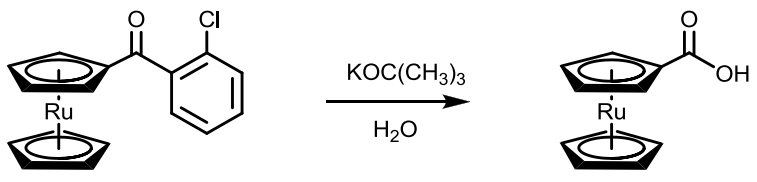

23 **24a**

2-Chlorobenzoyl ruthenocene, **23** (1.75 g, 4.6 mmol) was added to a mixture of potassium tertiary butoxide (13 g, 115 mmol) and water (0.612 mL, 34 mmol) in dimethoxyethane (100 mL) under an argon atmosphere. This produced a yellow slurry which was refluxed for 24 hours. After cooling the mixture, ice water (300 mL) was added and the resulting solution was washed with ether (3 x 100 mL). The aqueous phases were combined and acidified with concentrated hydrochloric acid. The residue was collected by filtration, washed thoroughly with water and air dried, yielding 1.01 g (80 %) of **24a** as light yellow crystals. Melting point 212 °C. IR ν /cm^{-1} = 1659 (C=O), Spectrum 28. ^{1}H NMR δ_H (300MHz, $CDCl_3$)/ppm: 4.64 (s, 5H, C_5H_5); 4.80 (t, 2H, C_5H_4); 5.11 (t, 2H, C_5H_4), Spectrum 2.

4.4.2 *N,N*-Dimethylaminomethyl ruthenocene, 16

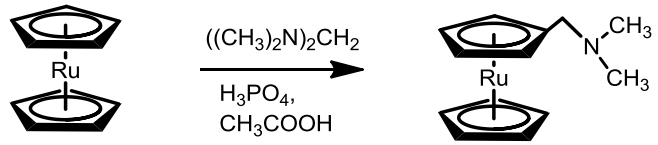

3 **16**

A solution of phosphoric acid (10 g, 100 mmol) and acetic acid (100 mL) was flushed with Argon for 20 minutes. The solution was cooled in an ice-bath, before bis(dimethylamino)methane (1.5 g, 1.47 mmol) was added drop-wise. Ruthenocene, **3** (2 g, 8.6 mmol) was added under argon and the resulting suspension was refluxed for 5 hours. The reaction mixture was allowed to cool to room temperature, diluted with water (20 mL) and the unreacted ruthenocene removed by extracting the solution with diethyl ether (3 x 40 mL). The aqueous solution was cooled in ice water and made alkaline by addition of sodium hydroxide solution (30 mL, 10 M). The tertiary amine separated from the alkaline solution as an oil. The mixture was extracted with diethyl ether (3 x 40 mL), washed with water, the organic layer dried over $MgSO_4$ and the solvent removed under reduced pressure to yield 1.39 g (56 %) of **16** as a light yellow oil. ^{1}H NMR δ_H (300MHz, $CDCl_3$)/ppm: 2.21 (s, 6H, 2xCH_3); 3.09 (s, 2H, CH_2); 4.49-4.52 (m, 2H of C_5H_4 + 5H of C_5H_5); 4.60 (m, 2H, C_5H_4), Spectrum 3.

4.4.3 *N,N,N*-Trimethylaminomethyl ruthenocene iodide, 61

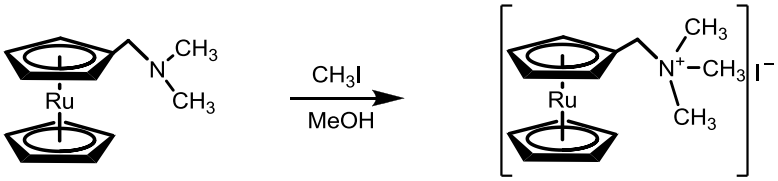

16 **61**

Methyl iodide (2.06 g, 14.5 mmol) was added to a stirred solution of N,N-dimethylaminomethyl ruthenocene, **16** (1.39 g, 4.82 mmol) in methanol (10 mL). The solution was heated on a rotary evaporator set at 80 °C for 30 min. While adding methanol the solution was cooled to room temperature and diethyl ether (100 mL) added. The ammonium salt, **61,** was filtered, washed with diethyl ether and air dried to give 1.49 g (72 %) as a yellow powder. Melting point 169 °C. ^{1}H NMR δ_H (300MHz, $CDCl_3$)/ppm: 3.32 (s, 9H, $(CH_2)_3$); 4.57 (s, 2H, CH_2); 4.66 (s, 5H, C_5H_5); 4.71 (t, 2H, C_5H_4); 4.87 (t, 2H, C_5H_4), Spectrum 4.

4.4.4 Ruthenocenylacetonitrile, 62

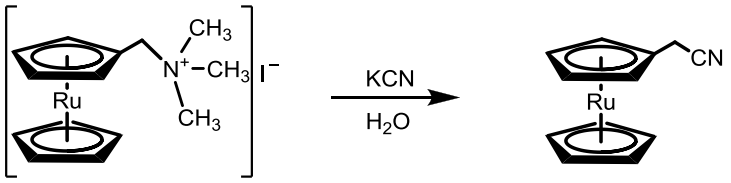

61 **62**

A solution of N,N,N-trimethylaminoruthenocene iodide, **61** (500 mg, 1.162 mmol) and potassium cyanide (650 mg, 10 mmol) in water (10 mL) was refluxed for 3 hours. The solution was cooled to room temperature and the light yellow precipitate extracted with ether (3 x 20 mL). The ether extracts were combined, washed with water, dried over $MgSO_4$ and the solvent removed under reduced pressure on a rotary evaporator to yield 220 mg (70 %) of **62** as a brown-yellow powder. Melting point 91 °C. IR ν /cm^{-1} = 2252 (C≡N), Spectrum 31. ^{1}H NMR δ_H (300MHz, $CDCl_3$)/ppm: 3.38 (s, 2H, CH_2); 4.53 (t, 2H, C_5H_4); 4.61 (s, 5H, C_5H_5); 4.69 (t, 2H, C_5H_4), Spectrum 5.

4.4.5 2-Ruthenocenylethanoic acid, 24b

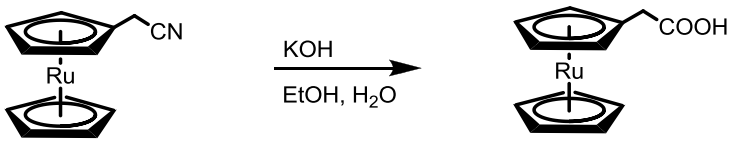

62 **24b**

To a solution of potassium hydroxide (1 g, 17.8 mmol) in water (10 mL), a suspension of the nitrile, **62** (200 mg, 0.74 mmol) in ethanol (5 mL) was added and refluxed for 5 hours until the evolution of ammonia had ceased. Most (> 95 %) of the ethanol was removed under reduced pressure. The residual suspension was dissolved in water (50 mL), extracted with ether (2 x 50 mL) and filtered. The solution was acidified with 2 M HCl and the precipitate filtered, washed and air dried to yield 110 mg (51 %) of **24b** as a white powder. Melting

point 140 °C. IR ν /cm^{-1} = 1707 (C=O), 1692 (C=O), Spectrum 32. ^{1}H NMR δ_H (300MHz, $CDCl_3$)/ppm: 3.38 (s, 2H, CH_2); 4.54 (t, 2H, C_5H_4); 4.61 (s, 5H, C_5H_5); 4.69 (t, 2H, C_5H_4), Spectrum 6.

4.4.6 Ruthenocene carboxaldehyde, 14

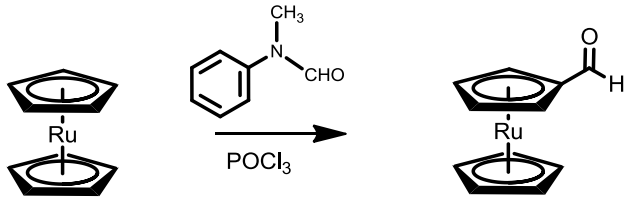

3 **14**

A solution of N-methylformanilide (3.15 g 23.3 mmol) and phosphorous oxychloride (2.37 g, 15.5 mmol, 1.45 mL) was stirred vigorously while ruthenocene, **3** (1.8 g, 7.76 mmol) was added in small portions over 30 minutes under argon atmosphere. A red solid-viscous suspension formed after 30 minutes of stirring. The mixture was stirred for 1 hour at room temperature and then at 65 °C for 2 hours never exceeding 70 °C. Hereafter the mixture was cooled to 0 °C before sodium acetate (6 g) dissolved in water (50 mL) was added slowly. Stirring continued overnight before the reaction mixture was extracted in ether (3 x 50 mL). The ether extracts were combined and washed with equal amounts of HCl (1 M), water, saturated sodium carbonate solution and again with water (all saturated with sodium chloride). The organic phase was dried and the solvent removed. The product was purified by column chromatography with hexane:ether (3:4) as eluent yielding 1.49 g (74 %) of **14** as yellow crystals. Melting point 100 °C. IR ν /cm^{-1} = 1670 (C=O), 1655 (C=O), Spectrum 33. ^{1}H NMR δ_H (300MHz, $CDCl_3$)/ppm: 4.65 (s, 5H, C_5H_5); 4.86 (t, 2H, C_5H_4); 5.09 (t, 2H, C_5H_4); 9.72 (s, 1H, C<u>H</u>O), Spectrum 7.

4.4.7 3-Ruthenocenylpropenoic acid, 26

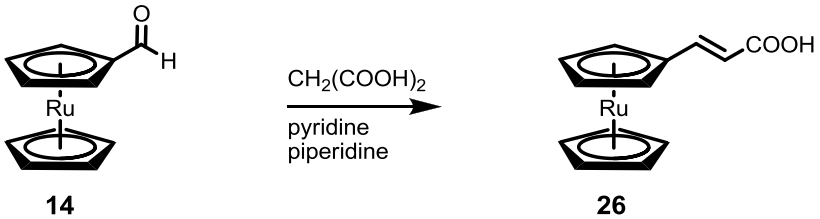

14 **26**

Ruthenocene carboxaldehyde, **14** (1.5 g, 5.78 mmol), malonic acid (1.785 g, 17 mmol) and piperidine (0.56 mL) were dissolved in pyridine and heated in an oil bath at 110 °C for 2 hours under an argon atmosphere. The cooled solution was diluted with water and extracted with chloroform. The chloroform extracts were washed with 1 M HCl (2 x 100 mL) and

water (2 x 100 mL) before the acrylic acid derivative was extracted with ice cooled 2 M NaOH (200 ml). While effectively cooling the solution with ice the water phase was acidified with 1 M HCl and the precipitate filtered, washed with water and air dried to yield 1.58 g (90 %) of **26** as a yellow powder. Melting point 227 °C. IR ν /cm^{-1} = 1671 (C=O), 1615 (C=O), Spectrum 34. ^{1}H NMR δ_H (300MHz, $CDCl_3$)/ppm: 4.56 (s, 5H, C_5H_5); 4.72 (t, J_{HH}=15Hz, 2H, C_5H_4); 5.87 (t, J_{HH}=15Hz, 2H, C_5H_4), 5.97 (d, 1H, CH=C<u>H</u>COOH); (d, 1H, C<u>H</u>=CHCOOH), Spectrum 8.

4.4.8 3-Ruthenocenylpropanoic acid, 24c

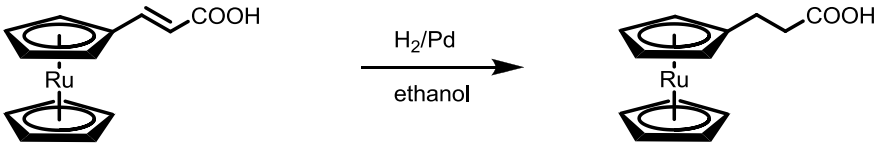

26 **24c**

3-Ruthenocenylpropenoic acid, **26** (250 mg, 0.82 mmol) and palladium on activated charcoal (30 mg) was suspended in absolute ethanol (50 mL). The suspension was stirred under a 10 bar hydrogen atmosphere for 20 hours before the reaction mixture was filtered through 2 cm of silica gel. Equal volumes of water and ice were added to the yellow ethanolic mixture. The solution was extracted with diethyl ether (2 x 250 mL) the combined ether extracts were thoroughly washed with water to remove the excess ethanol. The solution was dried over $MgSO_4$ and evaporated under reduced pressure to yield 0.177 g (71%) of **24c** an off-white powder. Melting point 156 °C. IR ν /cm^{-1} = 1693 (C=O), Spectrum 35. ^{1}H NMR δ_H (300MHz, $CDCl_3$)/ppm: 2.54 (m, 4H, <u>CH_2</u><u>CH_2</u>COOH); 4.45 (t, 2H, C_5H_4); 4.51-4.53 (m, 7H, C_5H_4 + C_5H_2), Spectrum 9.

4.4.9 3-Ruthenocenoylpropanoic acid, 25

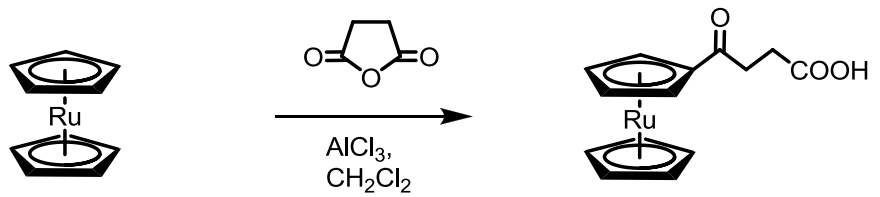

3 **25**

Succinic anhydride, **43** (250 mg, 2.15 mmol) dissolved in dichloromethane (25 mL) was added to a mixture of ruthenocene **3** (250 mg, 2.15 mmol) and aluminium chloride (0.76 g, 5.6 mmol) in dichloromethane (25mL) under a nitrogen atmosphere. The reaction mixture was refluxed for 24 hours. After cooling, ice cold water (40 mL) was added and the aqueous layer extracted twice with dichloromethane. The combined dichloromethane extracts were

thoroughly washed with water. The organic phase was then extracted twice with equal amounts of 2 M NaOH. While cooling the solution with ice the water phase was acidified with 1 M HCl and the precipitate filtered, washed with water and air dried to liberate 1.1 g (74 %) of **25** as orange crystals. Melting point 202 °C. IR ν /cm^{-1} = 1707 (C=O, acid), 1659 (C=O, keto), Spectrum 36. ^{1}H NMR δ_H (300MHz, $CDCl_3$)/ppm: 2.71 (t, J_{HH}=6.5Hz, 2H, $\underline{CH_2}COOCH_3$); 3.03 (t, J_{HH}=6.5Hz, 2H, $C_5H_4CO\underline{CH_2}$); 4.62 (s, 5H, C_5H_5); 4.82 (t, 2H, C_5H_4); 5.16 (t, 2H, C_5H_4),

4.4.10 3-(Carbomethoxy)propionic acid, 44

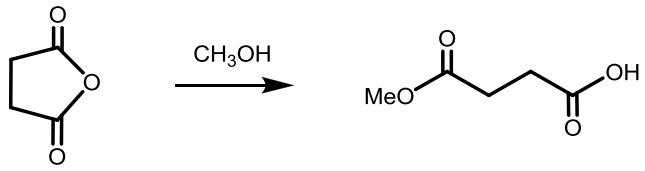

43 **44**

A mixture of succinic anhydride, **43** (10 g, 0.1 mol) and methanol (5 mL, 0.12 mol) was brought to a reflux on a steam bath. After 30 minutes the mixture was swirled frequently until it became homogeneous. The flask was then half emerged in the steam bath for a further 30 minutes. The excess methanol was removed under vacuum and the finely crushed powder dried to constant weight under vacuum (3 days) to give 11.71 g (89 %) of **44** as a white powder. Melting point 56 °C. IR ν /cm^{-1} = 1725 (C=O, ester), 1680 (C=O, acid), Spectrum 37. ^{1}H NMR δ_H (300MHz, $CDCl_3$)/ppm: 2.67 (m, 4H, CH_2CH_2); 3.70 (t, 3H, CH_3), Spectrum 11.

4.4.11 3-(Carbomethoxy)propionyl chloride, 45

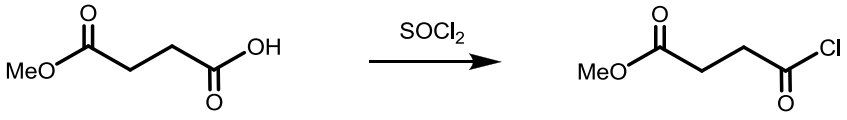

44 **45**

3-Carbomethoxypropionic acid, **44** (7 g, 53 mmol) and thionyl chloride (8 ml, 110 mmol) were heated in a bath at 30° - 40°C for 3 hours in a round bottom flask equipped with a condenser. The excess thionyl chloride was removed under reduced pressure, and the 3-carbomethoxypropionyl chloride distilled under reduced pressure to yield 7.23 g (91 %) of **45** as a colourless liquid. IR ν /cm^{-1} = 1786 (C=O, acid chloride), 1733 (C=O, ester), Spectrum 38. ^{1}H NMR δ_H (300MHz, $CDCl_3$)/ppm: 2.71 (t, 2H, $\underline{CH_2}CH_2C(O)Cl$); 3.24 (t, 2H, $CH_2\underline{CH_2}C(O)Cl$); 3.74 (s, 3H, CH_3), Spectrum 12.

4.4.12 Methyl 3-ruthenocenoyl propanoate, 59

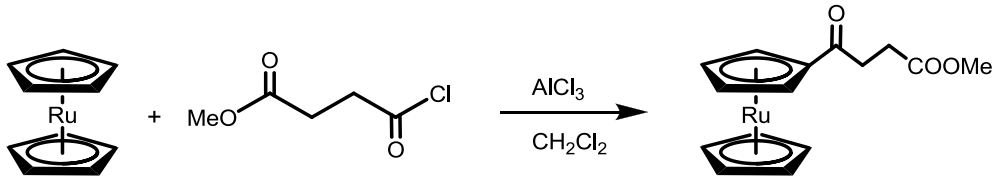

3 **45** **59**

Ruthenocene, **3** (1 g, 4.3 mmol) and aluminium chloride (0.76 g, 5.6 mmol) were degassed for 10 minutes. Dichloromethane (25 mL) was added, the reaction stirred and a maroon colour observed. The acid chloride, **45** (0.84 g, 5.6 mmol) was added and the solution was refluxed under an argon atmosphere for 24 hours. After cooling, ice cold water was added and the aqueous layer extracted twice with dichloromethane. The combined dichloromethane extracts were thoroughly washed with water. The solution was dried over $MgSO_4$ and the solvent removed under reduced pressure. Column chromatography of the residue using hexane:ether (1:1) as eluent gave 1.1 g (74 %) of **59** as orange crystals. Melting point 71 °C. IR ν /cm^{-1} = 1725 (C=O, ester), 1664 (C=O, keto), Spectrum 39. ^{1}H NMR δ_H (300MHz, $CDCl_3$)/ppm: 2.65 (t, J_{HH}=6.7Hz, 2H, $\underline{CH_2}COOCH_3$); 3.00 (t, J_{HH}=6.7Hz, 2H, $C_5H_4CO\underline{CH_2}$); 3.72 (s, 3H, OCH_3); 4.64 (s, 5H, C_5H_5); 4.80 (t, 2H, C_5H_4); 5.15 (t, 2H, C_5H_4), Spectrum 13.

4.4.13 Methyl 4-ruthenocenyl butanoate, 60

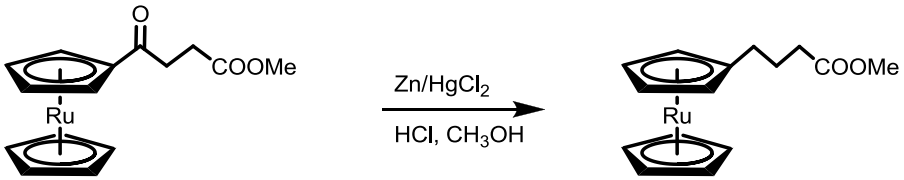

59 **60**

Zinc granules (10 g) were cut to pieces smaller than 5 mm^3. This was washed with HCl (2 M) for 5 minutes followed by running water for 5 minutes. The washed zinc granules was then added to $HgCl_2$ (0.8 g) dissolved in a mixture of concentrated HCl (0.5 mL) and water (11 cm^3). The mixture was shaken for 10 minutes before the liquid was decanted. The amalgam was then washed with water, methanol, HCl (2 M) and again with water.

3-Ruthenocenyl propionic acid, **59** (240 mg, 0.7 mmol) was added to a mixture containing concentrated hydrochloric acid (1.875 mL), water (12.5 mL), methanol (7.5 mL) and zinc amalgam (2.5g) under nitrogen for 5 days. During this time the reaction was topped up with conc. HCl (0.75 mL) and methanol to the original level every 12 hours. The product was extracted by dichloromethane (3 x 50 mL) and the dichloromethane layer washed with water.

The dichloromethane layer was dried over $MgSO_4$ and the solvent removed under reduced pressure to yield 171 mg (74 %) of **60** as a yellow oil. IR ν /cm^{-1} = 1736 (C=O, ester), Spectrum 40. ^{1}H NMR δ_H (300MHz, $CDCl_3$)/ppm: 1.78 (p, 2H, $C_5H_4CH_2\underline{CH_2}CH_2COOCH_3$); 2.22 (t, 2H, $\underline{CH_2}$); 2.35 (t, 2H, CH_2); 3.68 (s, 3H, OCH_3); 4.44 (t, 2H, C_5H_4); 4.50 (t, 2H, C_5H_4); 4.51 (s, 5H, C_5H_5), Spectrum 14.

4.4.14 4-Ruthenocenyl butanoic acid, 24d

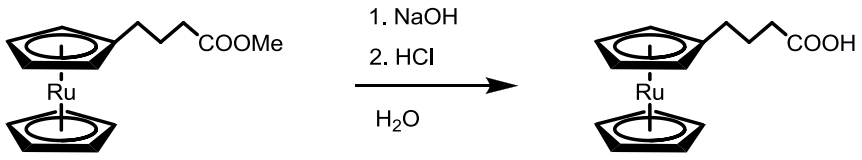

60 **24d**

The ester, **60** (150 mg, 0.45 mmol) was dissolved in ethanol (25 mL) followed by the addition of sodium hydroxide solution (25 mL, 2 M). The solution was stirred for 1 hour at room temperature followed by the addition of ice (25 mL) and washed with cold diethyl ether (3 x 50 mL). While cooling the solution by adding fresh ice chunks, the water phase was acidified with 1 M HCl and the precipitate filtered, washed and air dried to liberate 132 mg (93 %) of **24d** as an off-white powder. Melting point 112 °C. IR ν /cm^{-1} = 1702 (C=O, acid), Spectrum 41. ^{1}H NMR δ_H (300MHz, $CDCl_3$)/ppm: 1.78 (p, 2H, $C_5H_4CH_2\underline{CH_2}CH_2COOH$); 2.25 (t, 2H, CH_2); 2.41 (t, 2H, CH_2); 4.44 (t, 2H, C_5H_4); 4.50 (m, 7H, C_5H_4+C_5H_4), Spectrum 15.

4.5 Synthesis of polymeric carriers and the anchoring of ruthenocene

4.5.1 Poly-*DL*-succinimide, 32

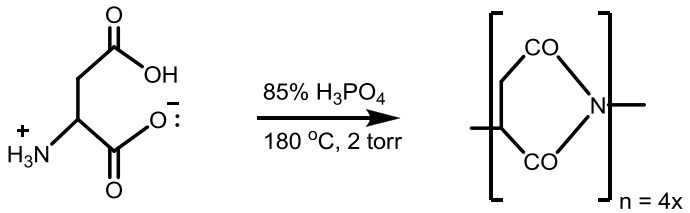

31 **32**

Finely powdered *DL*-aspartic acid, **31** (10 g, 75.2 mmol) and 85 % orthophosphoric acid (10 g, 102 mmol) were mixed in a 250 cm^3 round bottom flask. The flask (connected to a rotary evaporator fitted with a vacuum pump and manometer) was carefully submerged at atmospheric pressure into an oil bath preheated to 200 °C with slow rotation. After 5 minutes of rotation, the oil bath temperature was lowered slightly and maintained between 170 and

190 °C for 2.5 hours, while the pressure was reduced below 2 Torr. After the reaction mixture was cooled to *ca.* 50 °C, DMF (60 mL) was poured onto the warm reaction mixture and was rotated slowly on the rotary evaporator overnight at room temperature to afford a homogeneous, light brown solution. This solution was poured, with vigorous stirring, into a beaker containing water (500 mL), and the resulting polymer filtered and thoroughly washed with water (5 x 250 mL). The solid was ground under liquid nitrogen and dried under reduced pressure over 2 days to yield 7.1 g (97 %) of **32** as a white powder. Melting point °C. IR ν /cm^{-1} = 1709 (C=O), Spectrum 42. ^{1}H NMR δ_H (300MHz, DMSO)/ppm: 5.24 (s,1H, CH) 3.18 (s, 1H, CH_2) 2.68 (s, 1H, CH_2), Spectrum 16.

4.5.2 Poly-*α,β-DL*-[*N*-(3-(morpholin-4-yl)propyl)aspartamide-co-*N*-(2-aminoethyl)aspartamide, 35

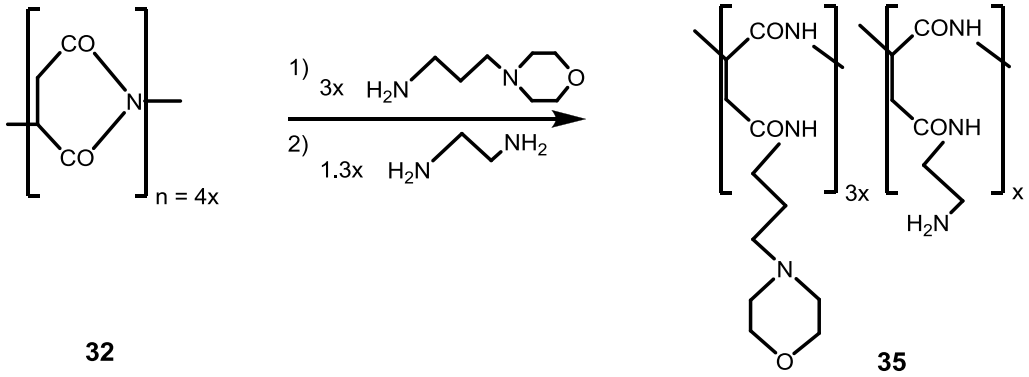

32 **35**

N-(3-aminopropyl)morpholine (1.0817 g, 7.5 mmol) in anhydrous DMF (4 mL) was added to a solution of polysuccinimide, **32** (0.97 g, 10 mmol) in anhydrous DMF (8 mL) over a period of 10 minutes at 0 °C. The solution was stirred for 25 minutes at 0 °C and then for a further 5 hours a room temperature. After cooling the solution again to 0 °C, ethylene diamine (0.6 g, 10 mmol) in DMF (4 mL) was slowly added over a period of 20 minutes at 0 °C, after which stirring continued at room temperature for 5 hours. The product was precipitated from solution by ethanol:ether (1:3, 200 mL), filtered and redissolved in water (120 mL). Dialysis against running tap water for 19 hours in 12 000 molecular mass cut-off membrane tubing followed by freeze-drying gave 1.150 g (52 %) of **35** as a white fluffy powder. Melting point > 350 °C. IR ν /cm^{-1} = 1643 (C=O, amide); 1529 (N-H, amide); 1113 (C-O-C), Spectrum 43. ^{1}H NMR δ_H (300MHz, D_2O)/ppm: 1.64 (s, 6H, b-CH_2); 2.32 (s, 6H, c-CH_2); 2.46 (s, 12H, d-CH_2); 2.55-3.00 (m, 12H, asp-CH_2+a′-CH_2+c′-CH_2); 3.14 (s, 6H, a-CH_2); 3.67 (s, 12H,e-CH_2), Spectrum 17. ^{1}H NMR δ_H (300MHz, DMSO)/ppm: 1.55 (s, 6H, b-CH_2); 2.24 (s, 6H, c-CH_2); 2.31 (s, 12H, d-CH_2); 2.40-2.87 (m, 12H, asp-CH_2 +a′-CH_2+c′-CH_2); 3.07 (m, 6H, a-CH_2); 3.55 (s, 12H, e-CH_2); 4.50 (bs, 4H, asp-CH); 7.38-8.94 (m, 8H,CONH), Spectrum 18.

^{1}H NMR δ_H (300MHz, DMSO + 5 % D_2O)/ppm: 1.51 (s, 6H, b-CH_2); 2.13-2.33 (m, 18H, c-CH_2 + d-CH_2); 2.63 (m, 12H, asp-CH_2 + a´-CH_2 + c´-CH_2); 3.02 (m, 6H, a-CH_2); 3.51 (s, 12H,e-CH_2); 4.47 (bs, 4H, asp-CH); 7.5- 9.2 (b, 8H, HNCO), Spectrum 19.

4.5.3 Polymers 4, 5, 6 and 7

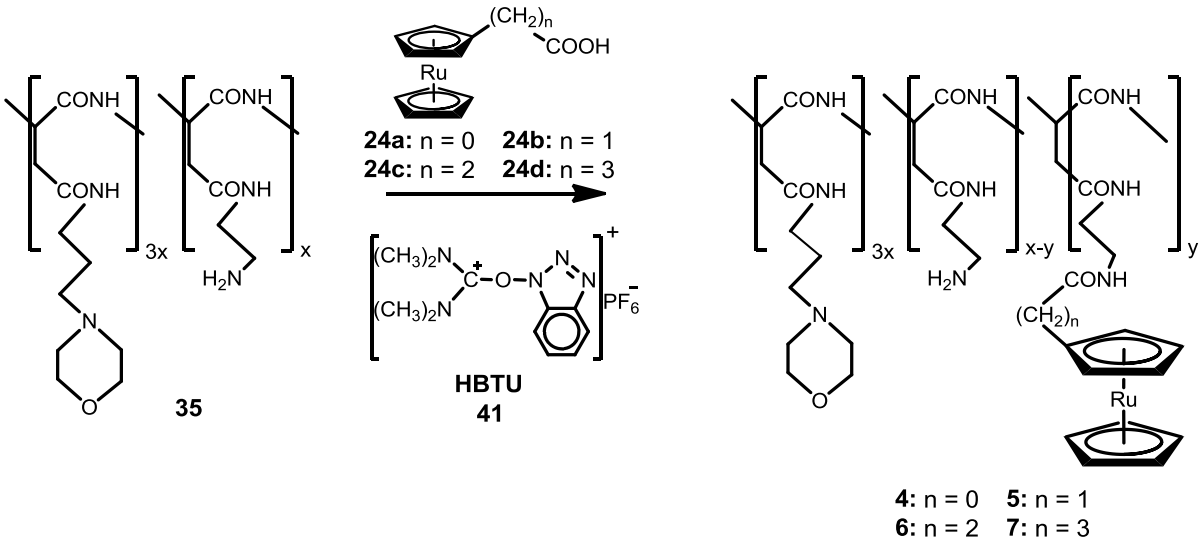

Note: The polymers **4**, **5**, **6** and **7** were all synthesised by exactly the same method. Therefore only the procedure for **4** will be given as a representative sample. Yields, attachment ratios and characterisation data for all the polymers follow after the synthetic procedure.

Polymer **4:** To a solution of **35** (0.22 g, 0.25 mmol) in water (1 mL) was added (in this order), triethylamine (35 mg, 0.048 mL, 0.35 mmol), a solution of ruthenocenic acid (0.068 g, 0.25 mmol) in DMF (1 mL) and *O*-benzotriazolyl-*N*,*N*,*N*`,*N*`-tetramethyluronium hexafluorophosphate, HBTU (0.114 g, 0.3 mmol). The mixture was stirred for 2 hours at room temperature during which time the heterogeneous mixture almost homogenised. Water (10 mL) was added to the reaction mixture before it was centrifuged, dialysed for 24 hours and freeze-dried to obtain **4**. Yield 0.155 g (58 %), y = 0.7. Melting point 163-167 °C. IR ν /cm^{-1} = 1645 (C=O, amide); 1531 (N-H, amide); 1114 (C-O-C), Spectrum 44. ^{1}H NMR δ_H (300MHz, DMSO + 5 % D_2O)/ppm: 1.51 (s, 6H, b-CH_2); 2.11-2.35 (m, 18H, c-CH_2 + d-CH_2); 2.37-2.91 (m, 12H, asp-CH_2 + a´-CH_2 + c´-CH_2); 2.91-3.83 (m, 6H, a-CH_2); 3.50 (s, 12H, e-CH_2); 4.31-4.67 (m, 11H, C_5H_5 + C_5H_4 + asp-CH); 5.05 (s, 2H, C_5H_4), Spectrum 20.

Characterisation data for polymer **5**. Yield 0.131 g (47 %), y = 0.85. Melting point 161-166 °C. IR ν /cm^{-1} = 1646 (C=O, amide); 1534 (N-H, amide); 1114 (C-O-C), Spectrum 45. ^{1}H NMR δ_H (300MHz, DMSO + 5 % D_2O)/ppm: 1.56 (s, 6H, b-CH_2); 2.16-2.40 (m, 18H, c-CH_2

+ d-CH_2); 2.42-2.81 (m, 8H, asp-CH_2 + a′-CH_2 + c′-CH_2 + α-CH_2); 2.88 (s, 6H, a-CH_2); 2.95-3.20 (m, 6H, a′-CH_2 + α-CH_2 + c′-CH_2); 3.56 (s, 12H, e-CH_2); 4.36-4.74 (m, 13H, C_5H_5 + C_5H_4 + asp-CH), Spectrum 21.

Characterisation data for polymer **6**. Yield 0.139 g (48 %), y = 0.98. Melting point 158-162 °C. IR ν /cm^{-1} = 1645 (C=O, amide); 1535 (N-H, amide); 1115 (C-O-C), Spectrum 46. ^{1}H NMR δ_H (300MHz, D_2O)/ppm: 1.64 (bs, 6H, b-CH_2); 2.33 (s, 6H, c-CH_2) 2.46 (s, 12H, d-CH_2); 2.54-2.98 (m, 12H, asp-CH_2 + a′-CH_2 + c′-CH_2 + α-CH_2 + β-CH_2); 3.13 (s, 6H, a-CH_2); 3.61 (s, 12H, e-CH_2), Spectrum 22. ^{1}H NMR δ_H (300MHz, DMSO)/ppm: 1.52 (s, 6H, b-CH_2); 2.11-2.86 (m, 34H, c-CH_2 + d-CH_2 + a′-CH_2 + c′-CH_2 + α-CH_2 + β-CH_2 + asp-CH_2); 2.92-3.14 (m, 6H, a-CH_2); 3.52 (s, 12H, e-CH_2); 4.34-4.60 (m, 13H, C_5H_5 + C_5H_4+asp-CH), Spectrum 23.

Characterisation data for polymer **7.** Yield 0.141 g (49 %), y = 0.91. Melting point 159-164 °C. IR ν /cm^{-1} = 1644 (C=O, amide); 1529 (N-H, amide); 1114 (C-O-C), Spectrum 47. ^{1}H NMR δ_H (300MHz, D_2O)/ppm: 1.40-1.76 (bs, 8H, b-CH_2 + β-CH_2); 1.95-2.15 (m, 4H, α-CH_2 + γ-CH_2); 2.17-2.46 (m, 18H, c-CH_2 + d-CH_2); 2.46-2.95 (bs, 12H, asp-CH_2 + a′-CH_2 + c′-CH_2); 2.95-3.36 (m, 6H, a-CH_2); 3.61 (s, 12H, e-CH_2), Spectrum 24. ^{1}H NMR δ_H (300MHz, DMSO)/ppm: 1.52 (m, 8H, b-CH_2 + β-CH_2); 2.03-2.11 (m, 4H, α-CH_2 + γ-CH_2); 2.11-2.38 (m, 18H, c-CH_2 + d-CH_2); 2.38-2.86 (m, 12H, asp-CH_2 + a′-CH_2 + c′-CH_2) 2.92-3.14 (m, 6H, a-CH_2); 3.52 (s, 12H, e-CH_2); 4.34-4.60 (m, 13H, C_5H_5 + C_5H_4 + asp-CH), Spectrum 25.

4.6 Other compounds

4.6.1 Ferrocenium hexafluorophosphate, 19

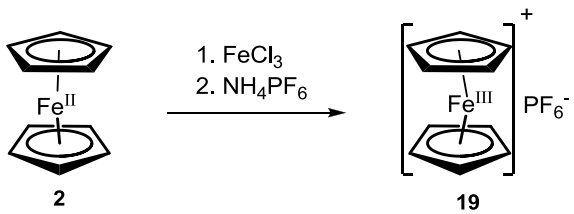

2 **19**

Anhydrous $FeCl_3$ (5.9 g, 36 mmol) was added to a stirred solution of ferrocene (5.0 g, 26.9 mmol) in a mixture of water (100 mL) and acetone (40 mL) at room temperature. After 15 minutes the deep blue solution was filtered through celite, followed by the addition of

ammonium hexafluorophosphate (5.8 g, 35.6 mmol). After 5 minutes ethanol (5mL) was added to aid the precipitation of the blue solid which was then removed by filtration to yield 5.12 g (57 %) of **19** as blue crystals. IR ν /cm^{-1} = 811 (P-F, stretch); 1419 (C=C); 3200 (C-H), Spectrum 48. Fe^{3+} is paramagnetic therefore no NMR spectra were measured.

4.6.2 Tetrabutylammonium tetrakis(pentafluorophenyl)borate, $[NBu_4][B(C_6F_5)_4]$

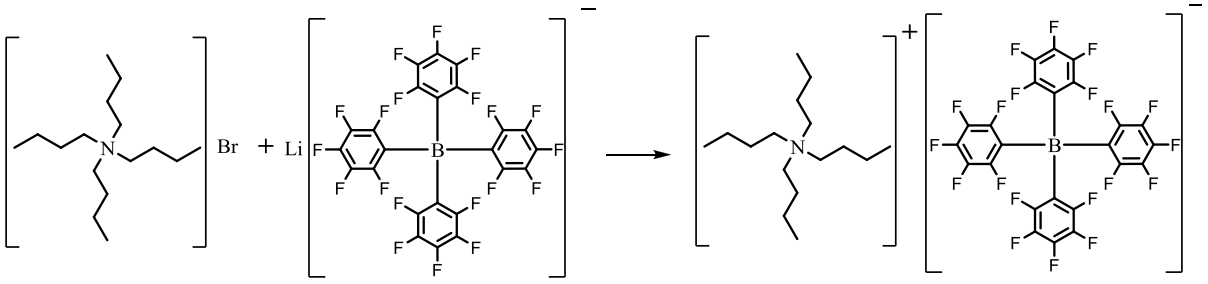

Lithium tetrakis(pentafluorophenyl)borate (5.5 g, 10.1 mmol) was dissolved in methanol (11 mL). Tetrabutylammonium bromide (2.9 g, 8.87 mmol) dissolved in methanol (6 mL) was added drop-wise at room temperature over 30 minutes, while stirring, to the lithium solution. The solution was closed with a septum and kept at 0 °C for 30 minutes. Thereafter the solution was left overnight at -25 °C. An off-white precipitate from a brown liquid was obtained by filtration and washed with methanol (10 ml at -25 °C). The solid was dissolved in excess dry dichloromethane (30 mL), $MgSO_4$ added and the mixture, covered with a septum, stirred for 2 hours at room temperature. The $MgSO_4$ was filtered off, washed with dichloromethane and the solvent removed under vacuum to yield (65%) as white crystals. ^1H NMR δ_H (300MHz, $CDCl_3$)/ppm: 0.97 (t, 3H, CH_3); 1.35 (m, 2H, $\underline{CH_2}CH_3$); 1.54 (m, 2H, $\underline{CH_2}CH_2CH_3$); 3.01 (m, 2H, $\underline{CH_2}CH_2$ CH_2CH_3); Spectrum 26.

4.7 Electrochemistry

Cyclic voltammetry (CV), linear sweep voltammetry (LSV) and square wave voltammetry (SWV) was carried out using a Princeton Applied Research PARSTAT 2273 voltammograph and recorded using PowerSuite (Version 2.58). A three electrode configuration was used. Platinum wires were used for both the reference and auxiliary electrodes. A glassy carbon working electrode (surface area 3.14 mm^2) was utilized after polishing on a Buhler polishing mat first with 1 micron and then with ¼ micron diamond paste.

4.7.1 Electrochemistry in organic solvents

Voltammograms in organic solvents were performed inside an M Braun Lab master SP glovebox filled with high purity argon (H_2O and O_2 < 10 ppm). Spectrochemical grade dichloromethane (Aldrich) was used in a 1 cm^3 cell. Tetrabutylammonium tetrakis(pentafluorophenyl)borate, $[NBu_4][B(C_6F_5)_4]$, was used as a supporting electrolyte (0.1 M). The concentration of all analyte solutions was 0.25 mM. Analysis was performed at -40, -10 and 25 ±1 °C. Temperature was regulated with a closed circulatory ethanol stream isolated from the atmosphere inside the glove box.

4.7.2 Electrochemistry in aqueous media

Aqueous electrochemistry of all ruthenocene-containing polymers was performed in distilled water containing 0.1 M KCl as supporting electrolyte. Analysis was performed at 25 °C under a blanket of argon. Analyte concentrations were 0.25 mM. Ferrocenium hexafluorophosphate was used as internal standard at 0 mV.

---

[102] B.S. Furniss, A.J. Hannaford, P.W.G. Smith, A.R. Tatchell, *Vogel's Textbook of Practical Organic Chemistry*,4th Edition, Longman, New York, p264-318.

5 Summary and future perspectives

5.1 Summary

This research project focussed on the synthesis, characterisation and electrochemical aspects of ruthenocene-containing water-soluble polymers.

First, a series of ruthenocene-containing carboxylic acids of the form $Rc(CH_2)_nCOOH$ (n = 0 – 3), where Rc = $Ru^{II}(\eta^5\text{-}C_5H_5)(\eta^5\text{-}C_5H_4)$, were synthesised in multistep reactions. The two-step reaction to obtain RcCOOH is known and also the three-step reaction toward $RcCH_2CH_2COOH$. However, to obtain $RcCH_2COOH$ as well as $Rc(CH_2)_3COOH$, a new four-step and five-step synthetic route had to be developed. The synthetic route to produce $Rc(CH_2)_3COOH$ resulted in a yield of 69 % for the overall five-step synthesis. In total sixteen different ruthenocene derivatives had to be synthesized, eight of which were new.

Since none of the ruthenocene derivatives are water-soluble, a carrier polymer possessing good water solubility was synthesized. For this a polyaspartamide derivative, poly-*α,β-DL*-[*N*-(3-(morpholin-4-yl)propyl)aspartamide-co-*N*-(2-aminoethyl)aspartamide was synthesised bearing biodegradable amide connecting groups. This polymer possessed amine-terminated side chains which can act as anchoring sites for the water-insoluble ruthenocene-containing carboxylic acids.

The four ruthenocene-containing carboxylic acids were then covalently anchored to the amine-terminated side chains of the polyaspartamide carrier polymer to give four new ruthenocenyl-polymer conjugates **4-7.** To the best of the authors knowledge these polymers are the only known water-soluble ruthenocene peptide macromolecular conjugates.

The techniques utilised for the characterisation of these ruthenocenyl-containing polymers and their precursors included elemental analysis, XPS, ^{1}H NMR spectroscopy, IR spectroscopy and electrochemical analysis.

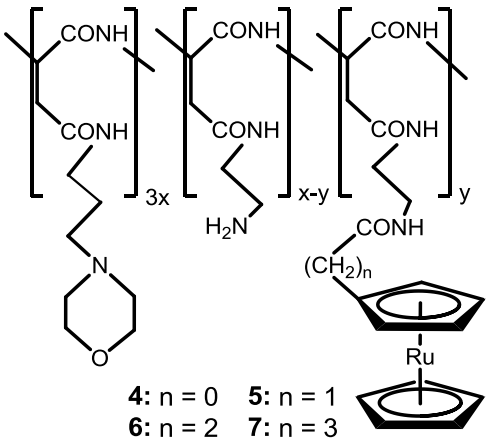

Figure 5.1 Structure of ruthenocene-containing water-soluble polymers

A cyclic voltammetry study was carried out on all of the ruthenocene-containing carboxylic acids in CH_2Cl_2/0.1 M $[NBu_4][B(C_6F_5)_4]$. Despite the use of this non-coordinating solvent/electrolyte system, none of the ruthenocene-containing carboxylic acids exhibited a chemical reversible Rc/Rc^+ couple. Various follow-up chemical reactions of the electrochemical generated Rc^+ derivatives containing a Ru^{3+} cation were observed. A key finding was that one CH_2 spacer between the ruthenocenyl group and the COOH group were enough to eliminate any significant communication between these two functional groups. The formal reduction potentials of the free carboxylic acids varied between $484 \leq E^{o'} \leq 776$ mV vs. FcH/FcH^+, with $E^{o'}$ (RcCOOH) 260 mV larger than that of $Rc(CH_2)_3COOH$. Complexes $Rc(CH_2)_nCOOH$ with n = 1, 2 and 3 were oxidised within 32mV potential range with $Rc(CH_2)_3COOH$ having an observed formal reduction potential of $E^o = ′516$ mV vs. FcH/FcH^+.

Electrochemistry in water as solvent was conducted on the ruthenocene-polymer conjugates **4 - 7**. The oxidation potential values of the polymer bound ruthenocene moiety ranged between E_{pa} = 397 and 631 mV. The latter, highest, oxidation potential belongs to polymer **4** having no separator (*i.e.* CH_2 groups) between the ruthenocenyl and CONH functional groups. The polymer itself (i.e. no ruthenocenyl groups bound to it) shows an irreversible oxidation wave at 648 mV vs. FcH/FcH^+.

5.2 Future perspective

In this study the author has developed a method to anchor carboxylic acid ruthenocene derivatives to a water-soluble drug carrier. However, cytotoxic test of the newly synthesized ruthenocenyl-containing polymers could not be completed in the time-span of this study. The comparison of the cytotoxic activity of the free ruthenocene derivatives with that of the ruthenocenyl-polymer conjugates would reveal if anchoring of ruthenocene onto a polymeric drug carrier gives enhanced pharmacological activity. A relationship between the oxidation potential of ruthenocenyl-containing compounds and their bioactivity may prove valuable in the design of new types of ruthenocene containing drugs.

In addition, a synergistic effect was observed both in catalyses and anticancer drug activity once ferrocene is combined in the same complex bearing either a rhodium(I) [103] or a titanium(IV)[104] metal centre. It would be of interest to investigate if the ruthenocene core has the same or a different effect than ferrocene on oxidative addition reactions involving a rhodium(I) core ligated to a ruthenocene-containing ligand. Ziegler-Natta polymerisation catalytic studies involving mixed-metal titanium-ruthenocene complexes will also reveal if the ruthenocenyl group has a beneficial effect on Ziegler-Natta polymerisation catalysist or not. Further, osmocene is a much more stable metallocene when oxidised to the 17-electron osmocenium derivative than the oxidised ruthenocenium 17-electron species. Once osmocene carboxylic acid derivatives have been made, it may be possible to isolate one or more of the chemical follow-up products after oxidation to characterize them spectroscopically, by crystallography and elemental analyses. Such a study would enhance the understanding of the present ruthenocene carboxylate systems substantially.

Finally, I would like to express my satisfaction with the results of this study and would like to dedicate this work to my parents who not only introduced me to science but also allowed me to pursue my dreams and supported me throughout this study.

Q.E.D.

---

[103] J. Conradie, J. C. Swarts, *Dalton. Trans.*, 5844, 40 (2011)

[104] J.C. Swarts, E. Erasmus, Unpublished results

Appendix

[1]H NMR Spectra

Spectrum 1: 2-chlorobenzoyl ruthenocene, 23 in $CDCl_3$

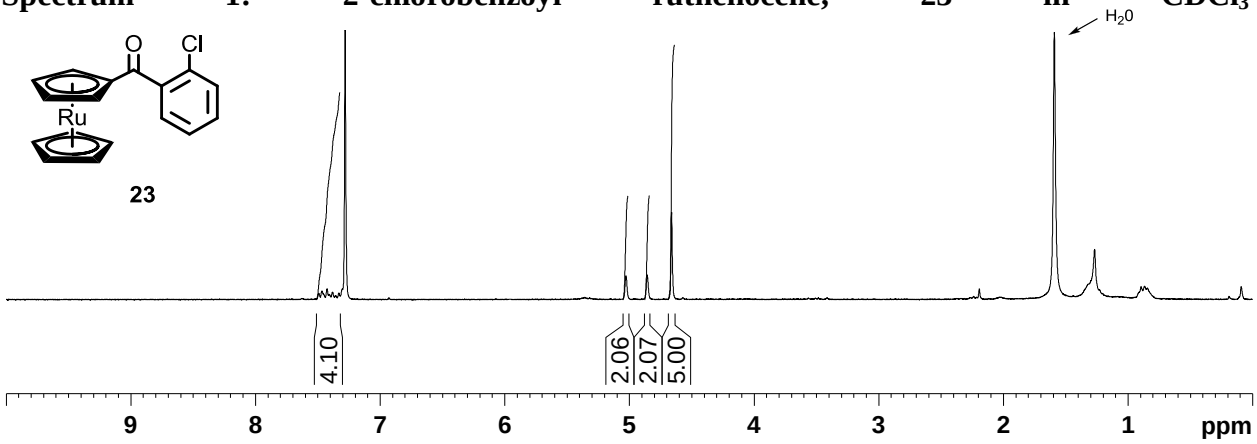

Spectrum 2: Ruthenocenoic acid, 24a in $CDCl_3$

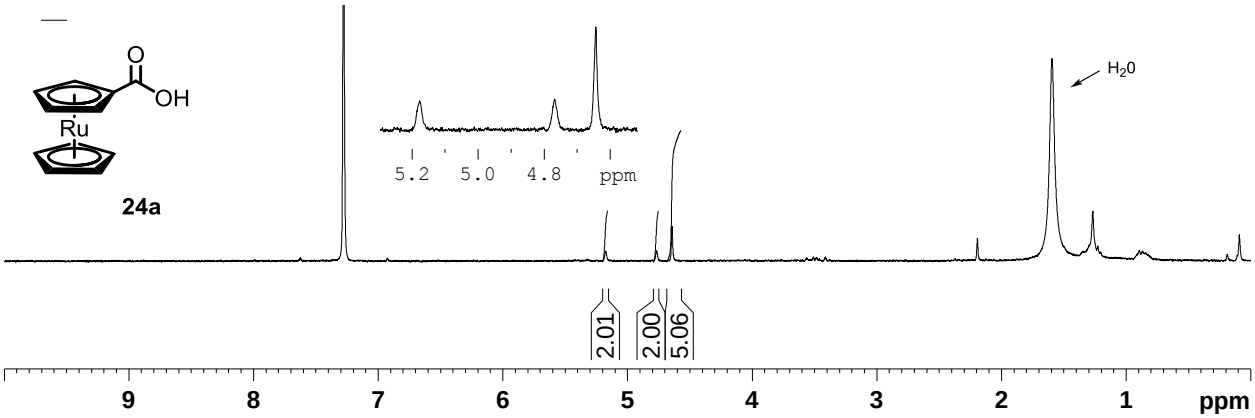

Spectrum 3: N,N-dimethylaminomethyl ruthenocene, 16 in $CDCl_3$

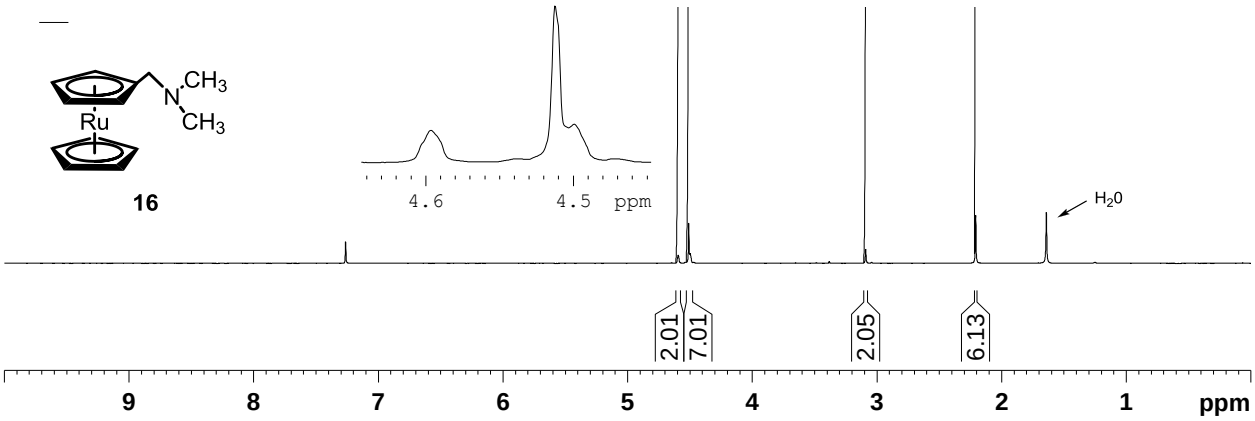

Spectrum 4: N,N,N - trimethylaminomethyl ruthenocene iodide, 61 in $CDCl_3$

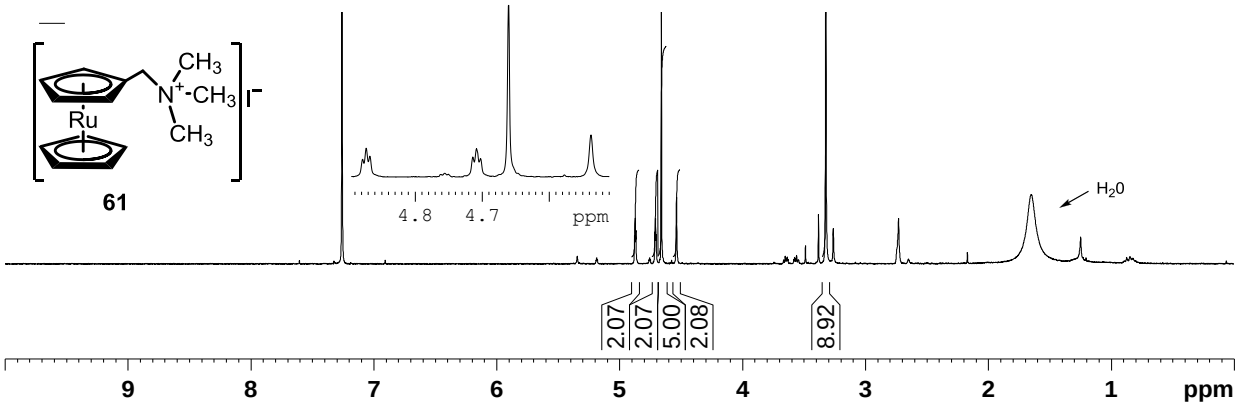

Spectrum 5: Ruthenocenylacetonitrile, 62 in $CDCl_3$

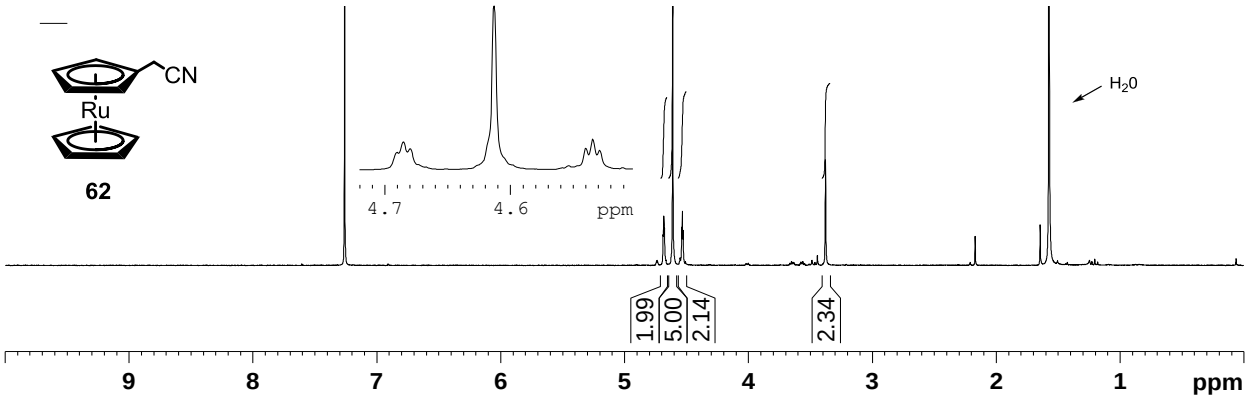

Spectrum 6: Ruthenocenylacetic acid, 24b in $CDCl_3$

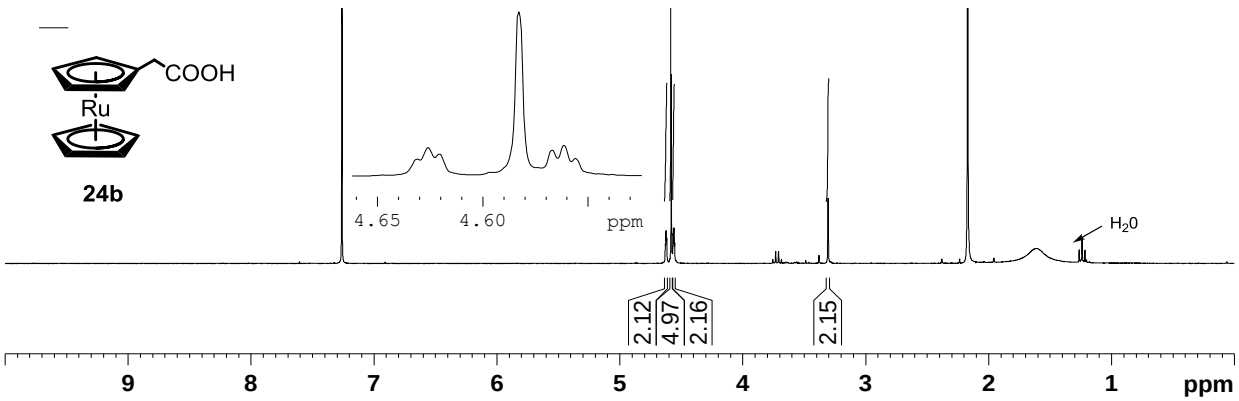

Spectrum 7: Ruthenocene carboxaldehyde, 14 in $CDCl_3$

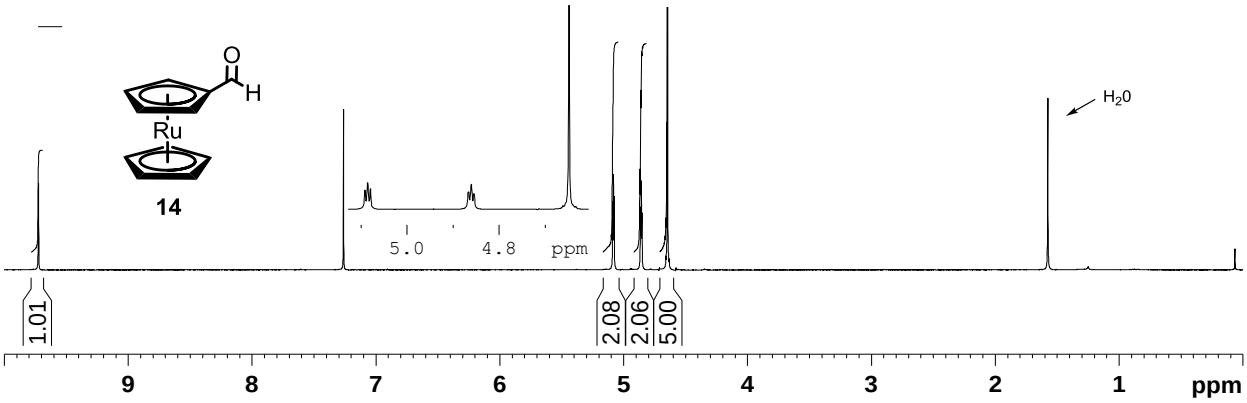

Spectrum 8: 3-ruthenocenylacrylic acid, 26 in $CDCl_3$

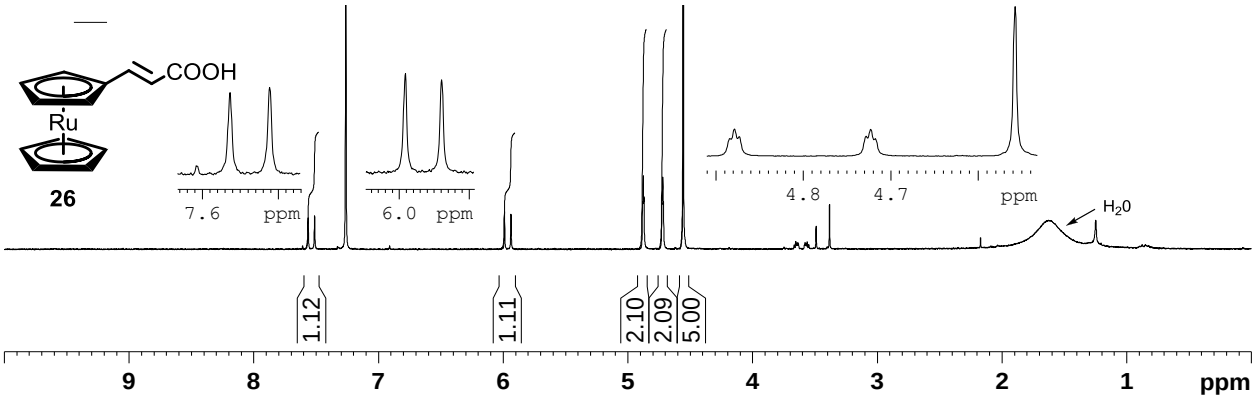

Spectrum 9: 3-ruthenocenylpropanoic acid, 24c in $CDCl_3$

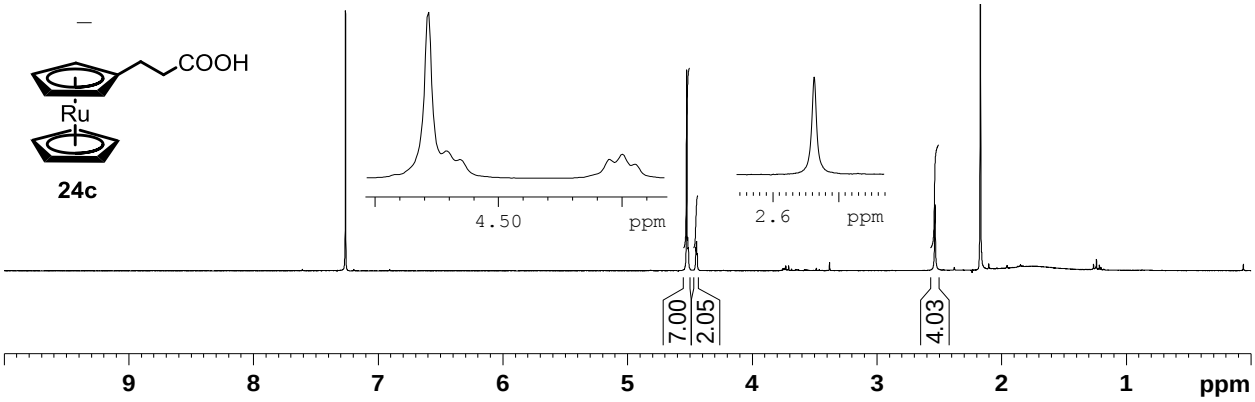

Spectrum 10: 3-ruthenocenoylpropanoic acid, 25 in $CDCl_3$

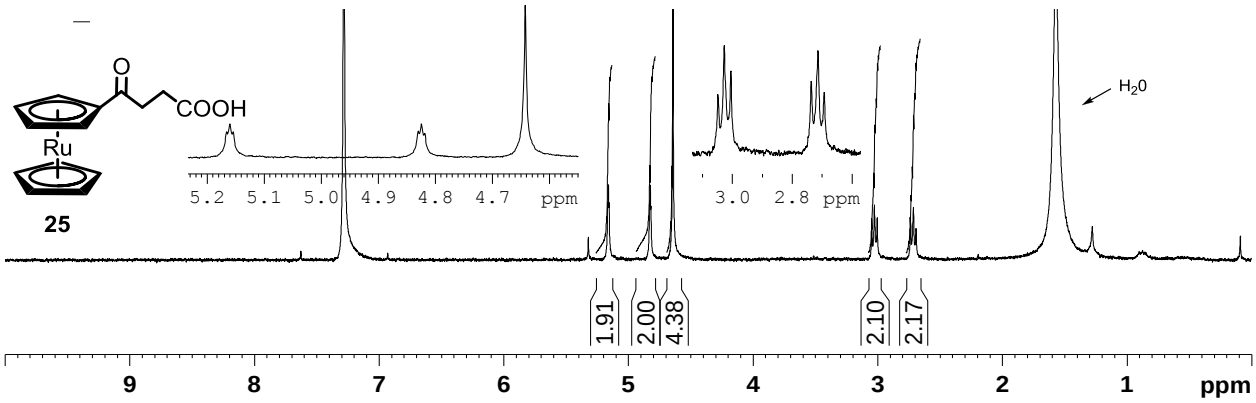

Spectrum 11: 3-(carbomethoxy) propionic acid, 44 in $CDCl_3$

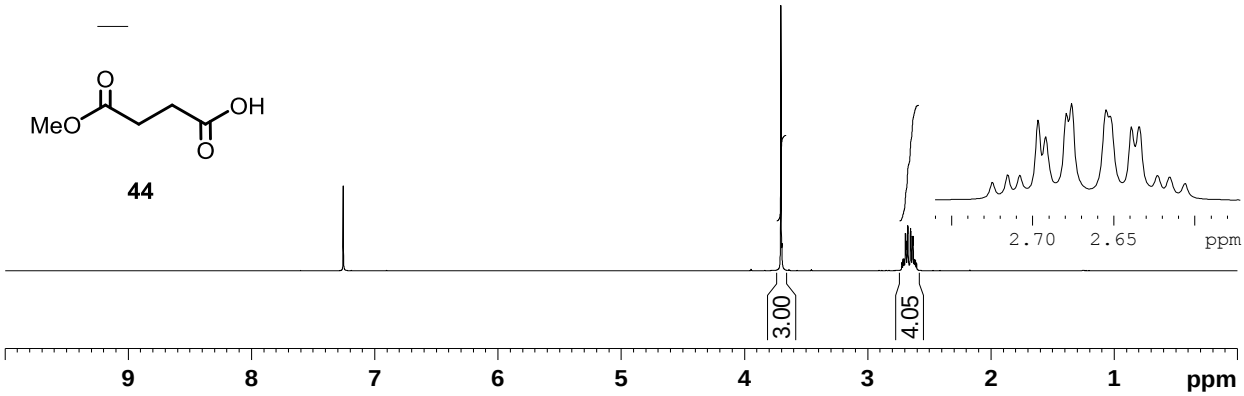

Spectrum 12: 3-(carbomethoxy)propionyl chloride, 45 in $CDCl_3$

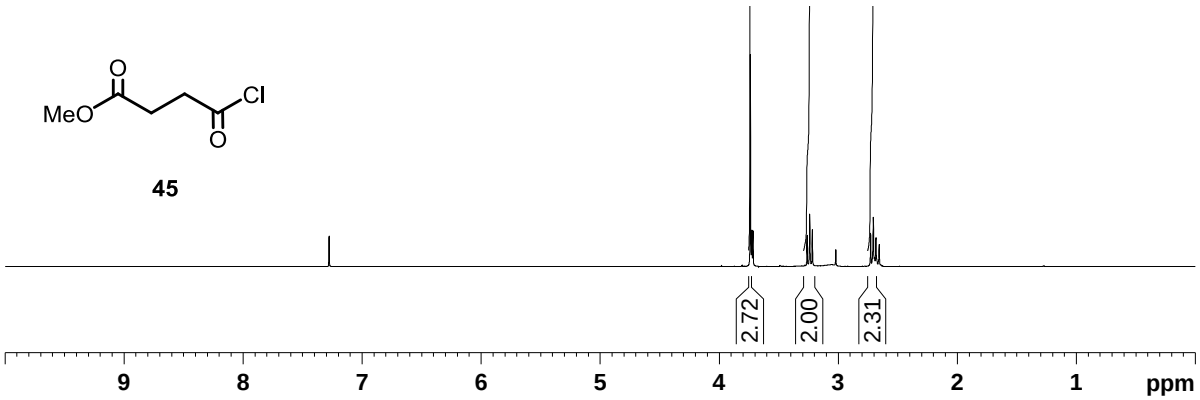

Spectrum 13: Methyl 3-ruthenocenoylpropanoate, 59 in $CDCl_3$

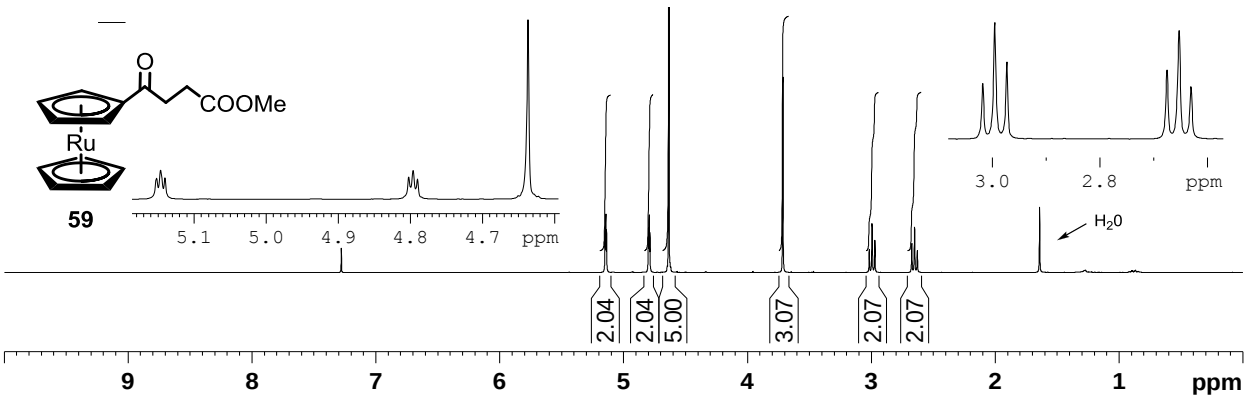

Spectrum 14: Methyl 4-ruthenocenylbutanoate, 60 in $CDCl_3$

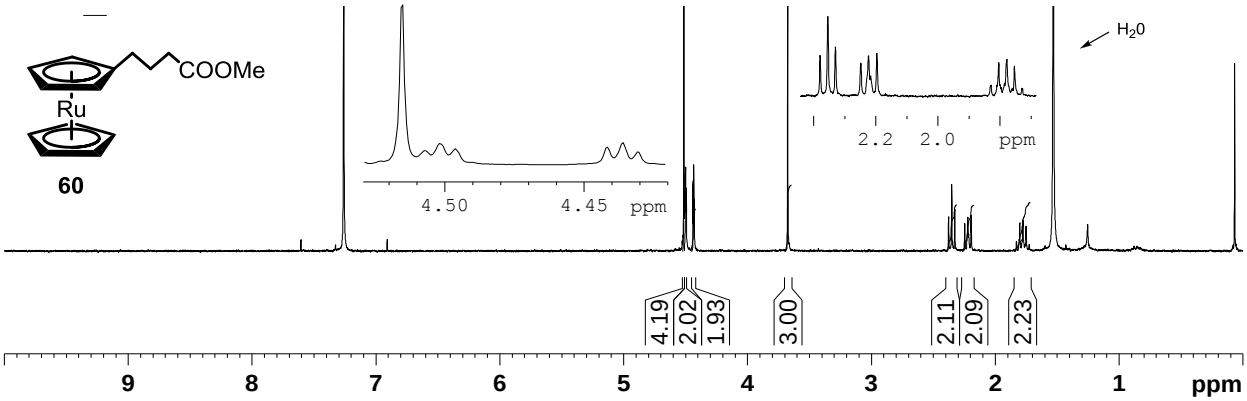

Spectrum 15: 4-ruthenocenylbutanoic acid, 24d in $CDCl_3$

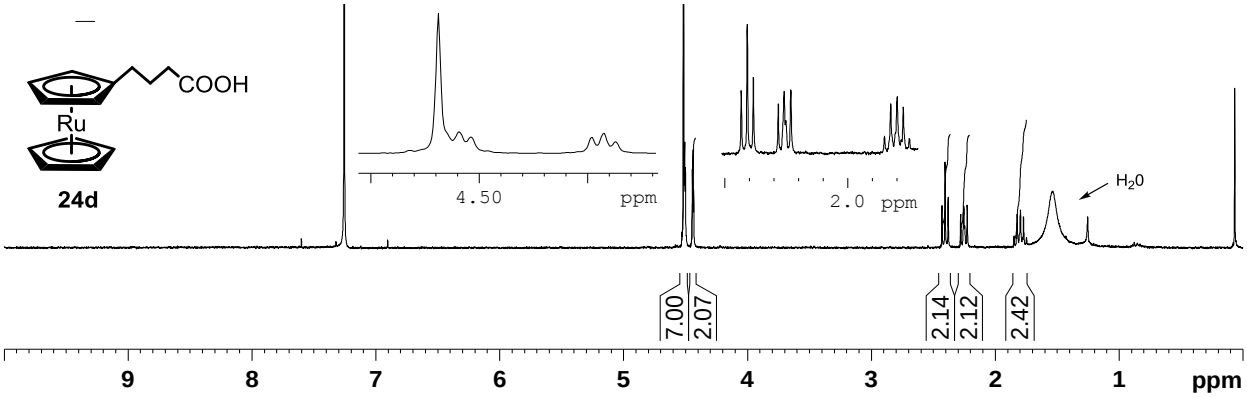

Spectrum 16: Poly-DL-succinimide, 32 in DMSO-d_6

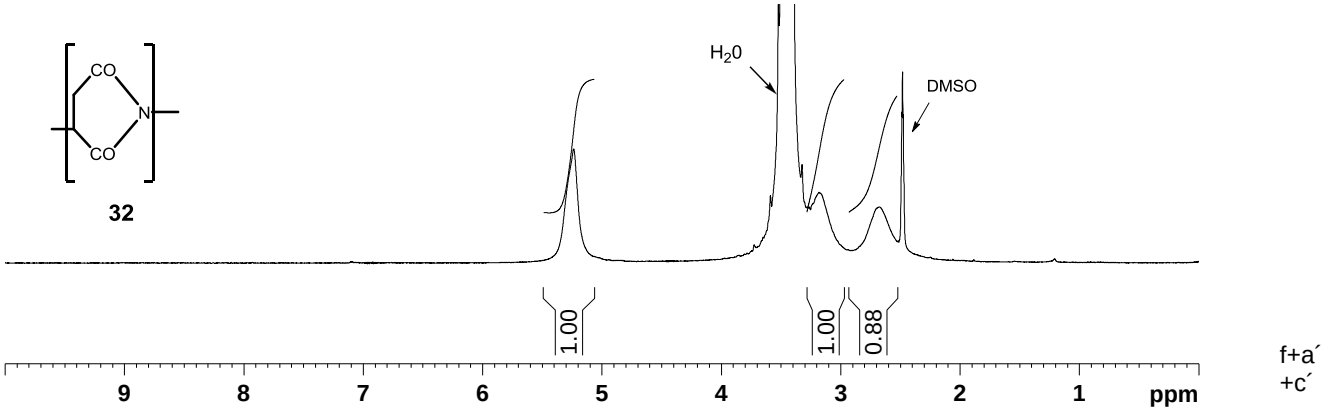

Spectrum 17: poly-α,β-DL-[N-(3-(morpholin-4-yl)propyl)aspartamide-co-N-(2-aminoethyl)aspartamide, 35 in D_2O

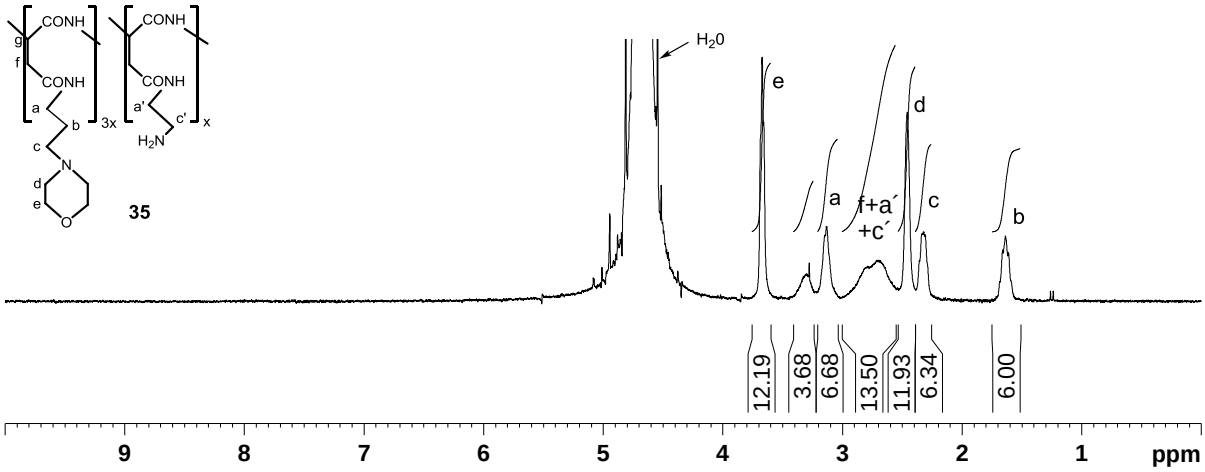

Spectrum 18: poly-α,β-DL-[N-(3-(morpholin-4-yl)propyl)aspartamide-co-N-(2-aminoethyl)aspartamide, 35 in DMSO-d_6

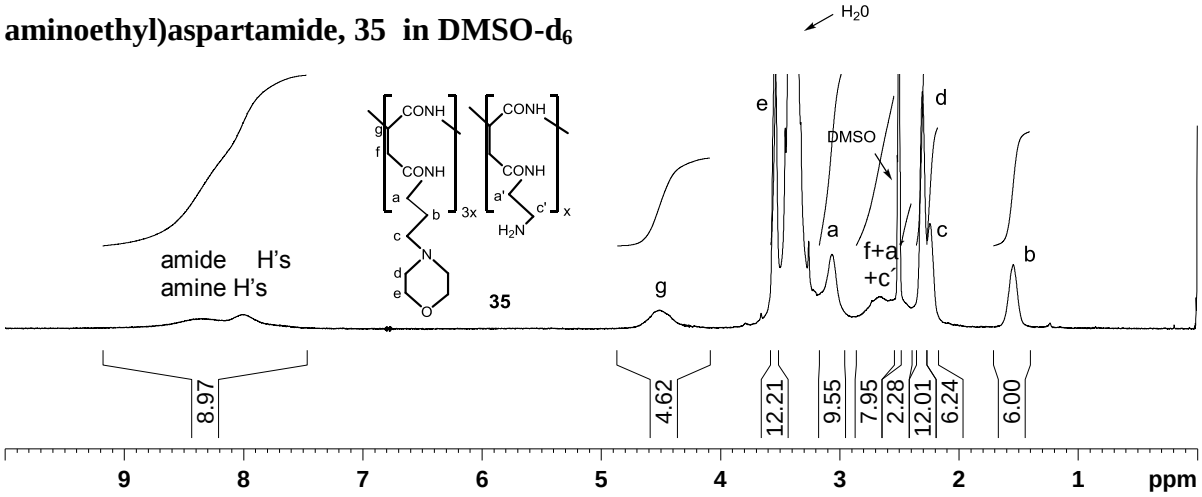

Spectrum 19: poly-α,β-DL-[N-(3-(morpholin-4-yl)propyl)aspartamide-co-N-(2-aminoethyl)aspartamide, 35 in DMSO-d_6 with 5 % D_2O

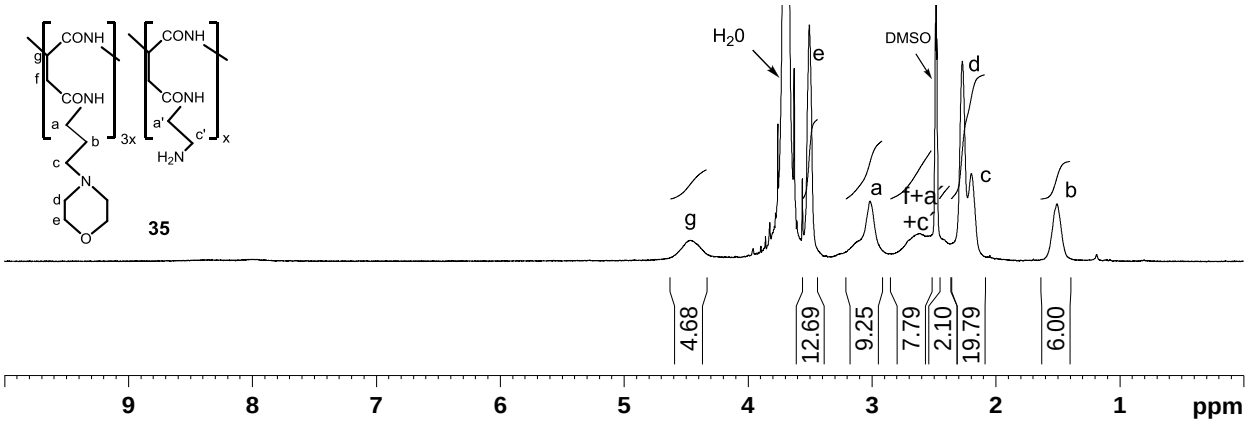

Spectrum 20: Polymer 4 in DMSO-d_6 with 5 % D_2O

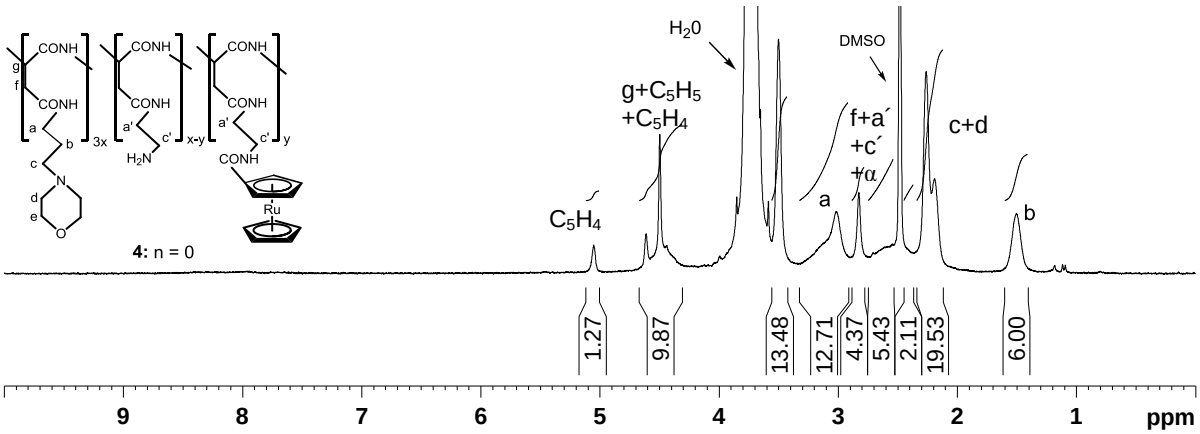

Spectrum 21: Polymer 5 in DMSO-d_6 with 5 % D_2O

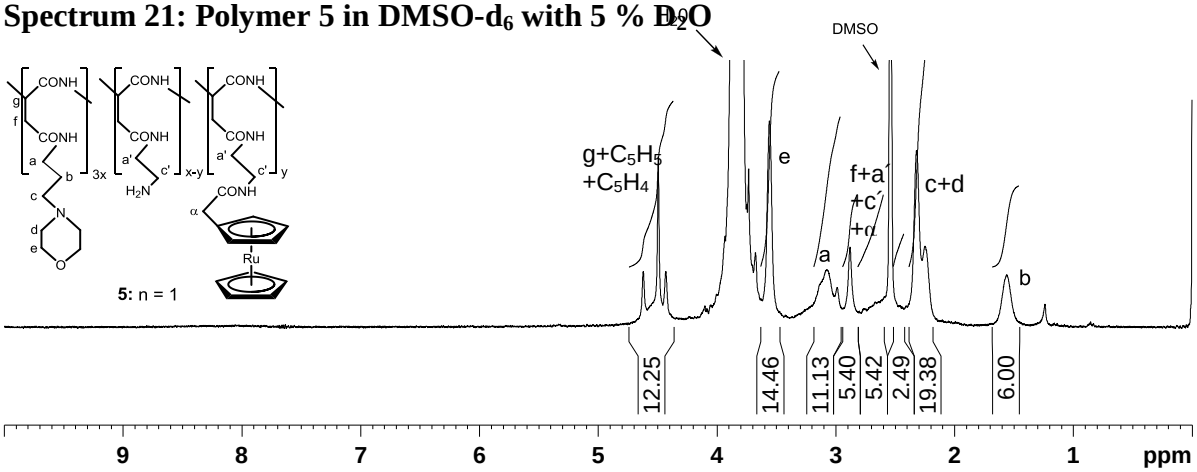

Spectrum 22: Polymer 6 in D_2O

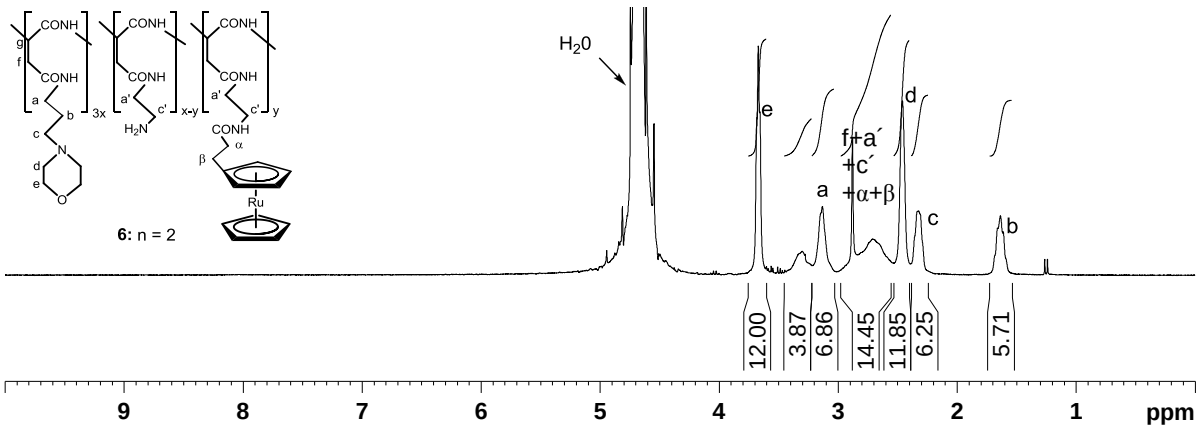

Spectrum 23: Polymer 6 in DMSO-d_6

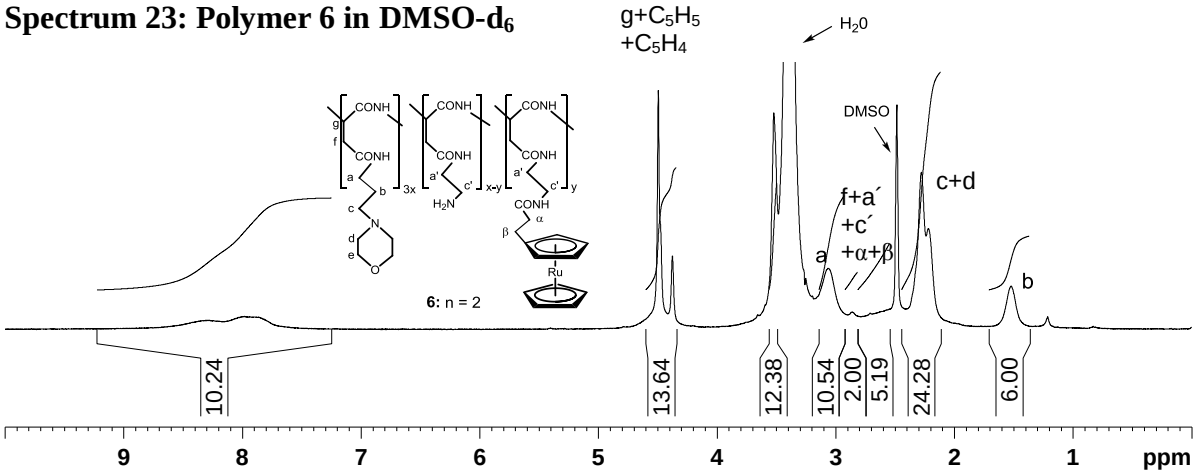

Spectrum 24: Polymer 7 in D_2O

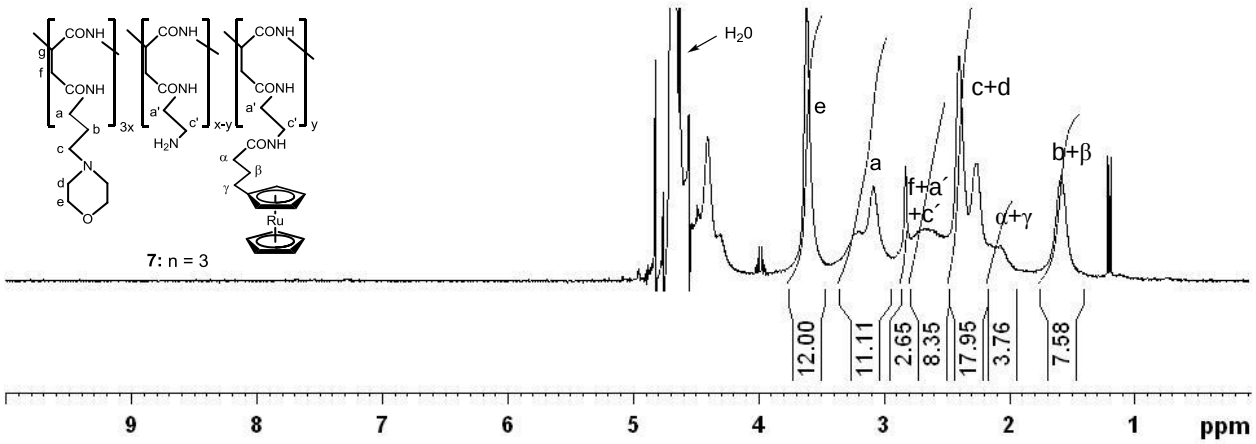

Spectrum 25: Polymer 7 in DMSO-d_6

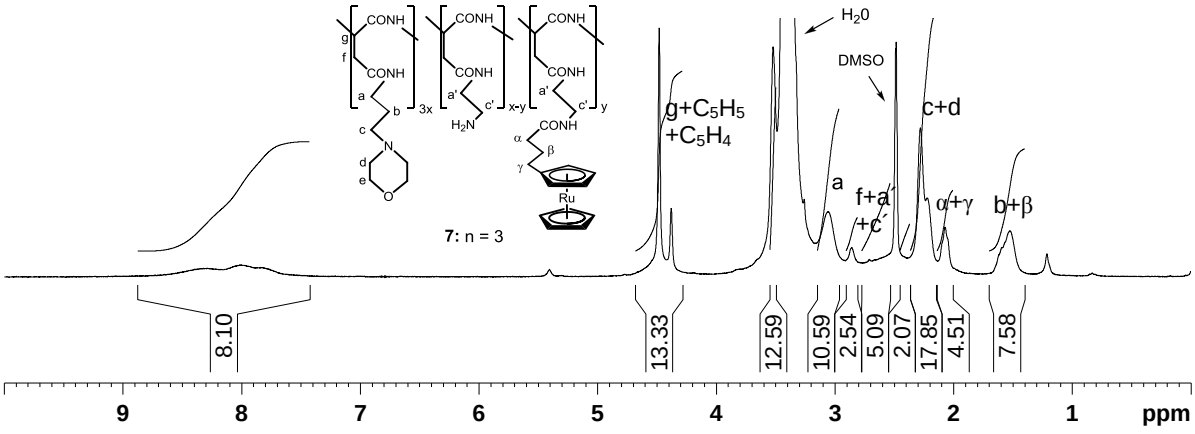

Spectrum 26 Tetrabutylamonion tetrakispentafluorophenylborate

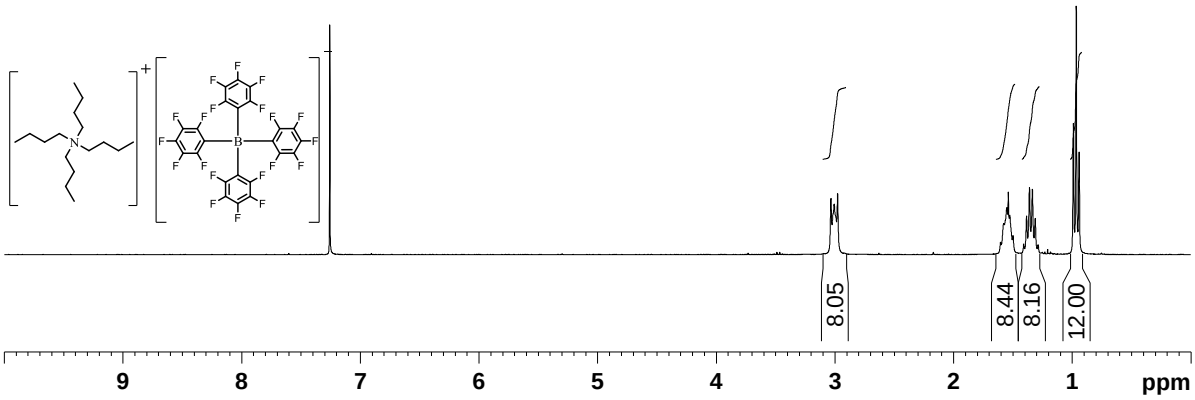

IR Spectra

Spectrum 27: 2-chlorobenzoyl ruthenocene, 23

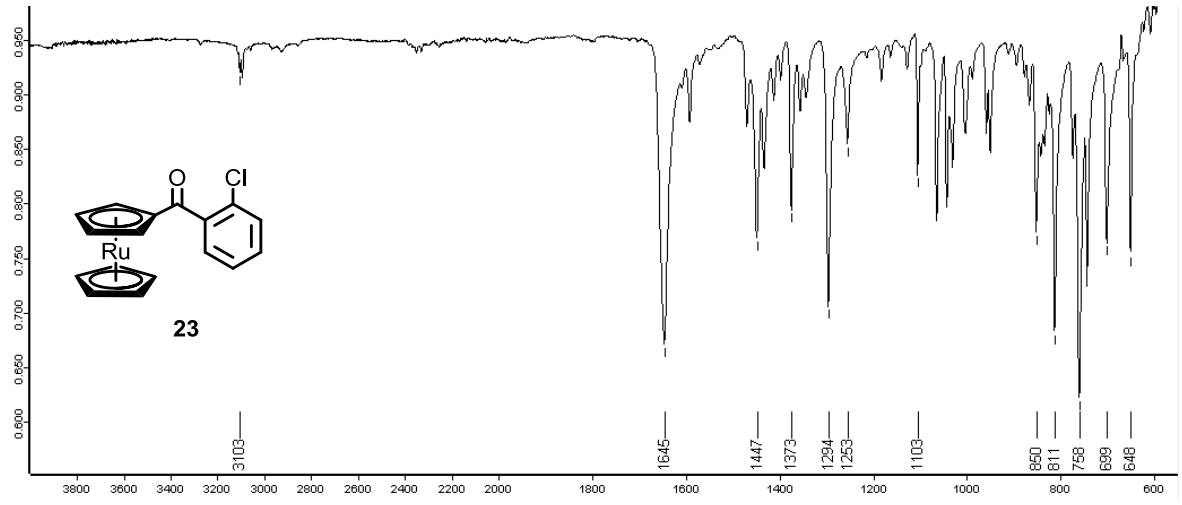

Spectrum 28: Ruthenocenoic acid, 24a

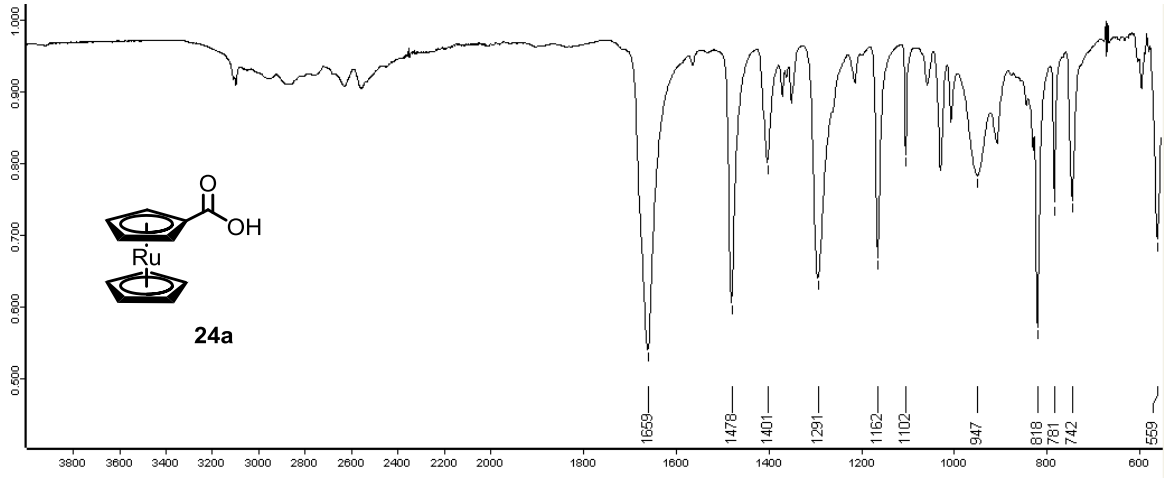

Spectrum 30: N,N,N - trimethylaminomethyl ruthenocene iodide, 61

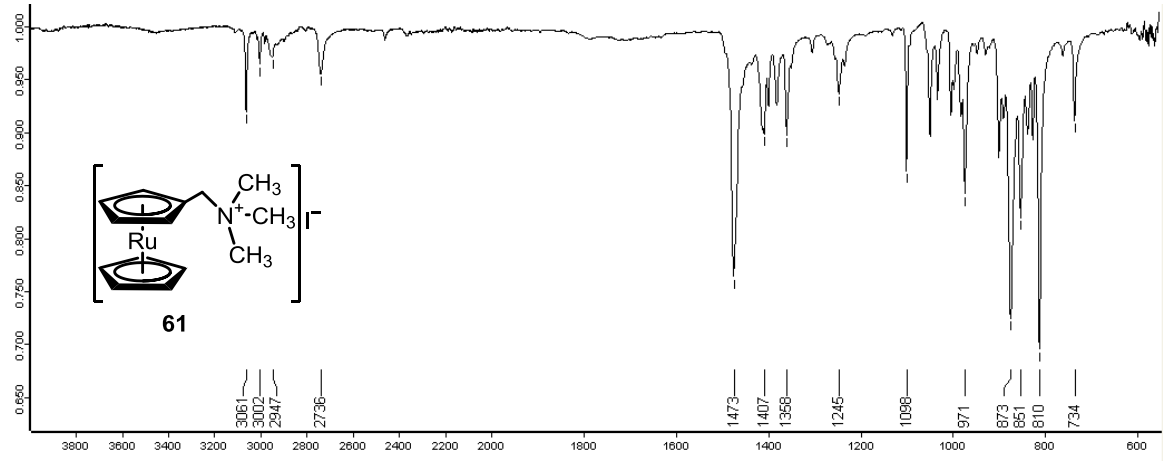

Spectrum 31: Ruthenocenylacetonitrile, 62

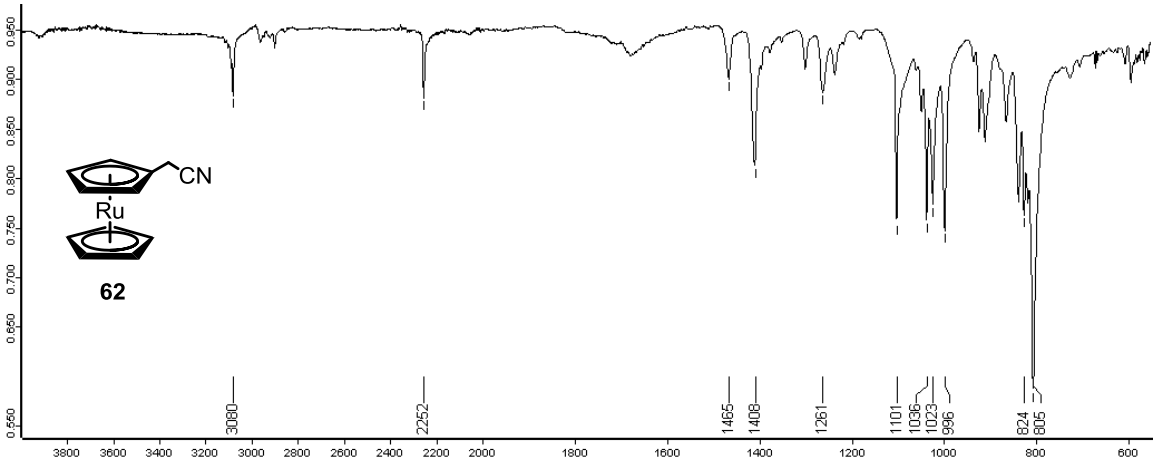

Spectrum 32: Ruthenocenylacetic acid, 24b

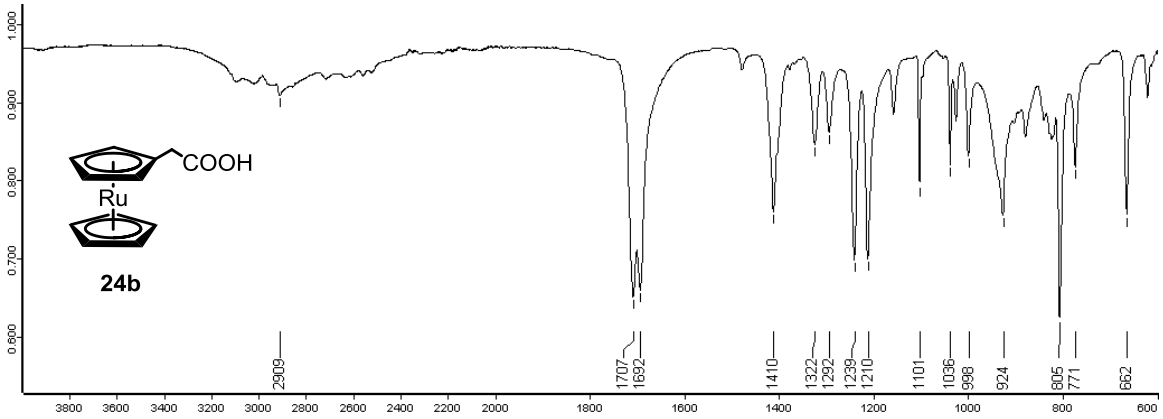

Spectrum 33: Ruthenocene carboxaldehyde, 14

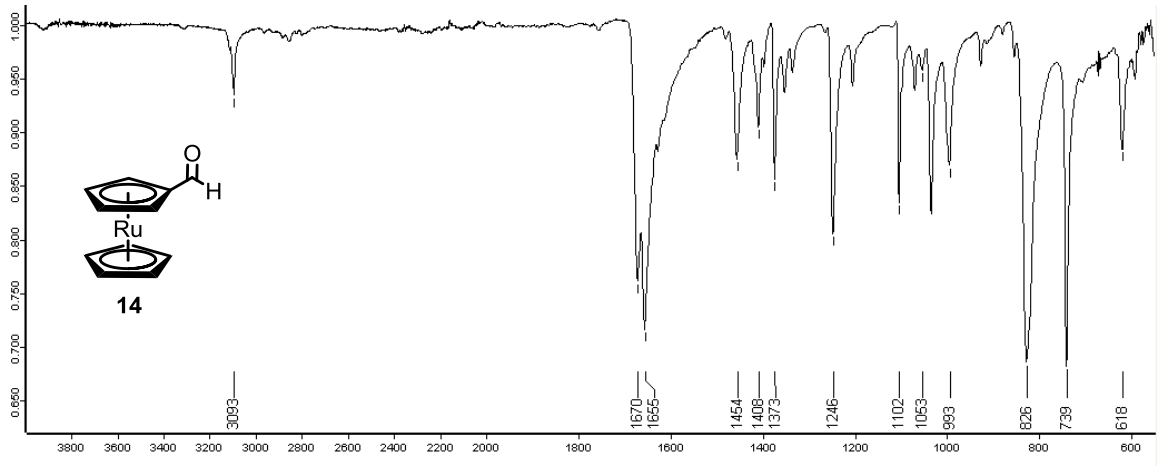

Spectrum 34: 3-ruthenocenylacrylic acid, 26

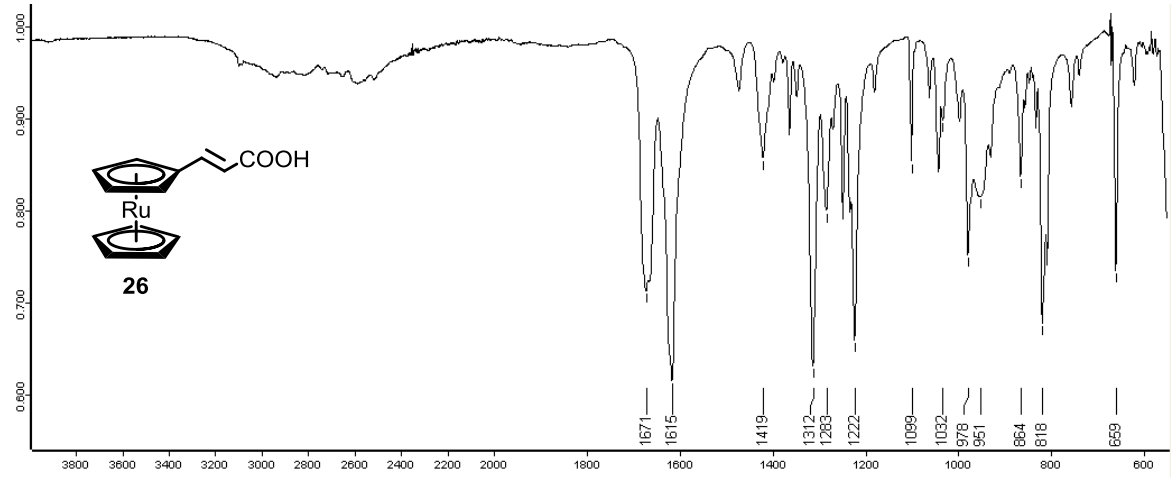

Spectrum 35: 3-ruthenocenylpropanoic acid, 24c

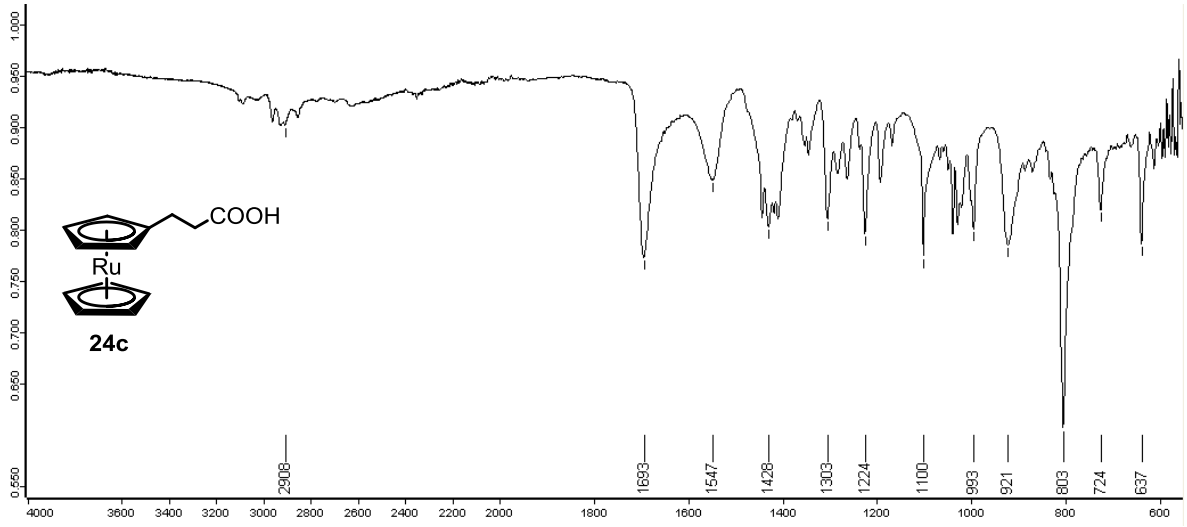

Spectrum 36: 3-ruthenocenoylpropanoic acid, 25

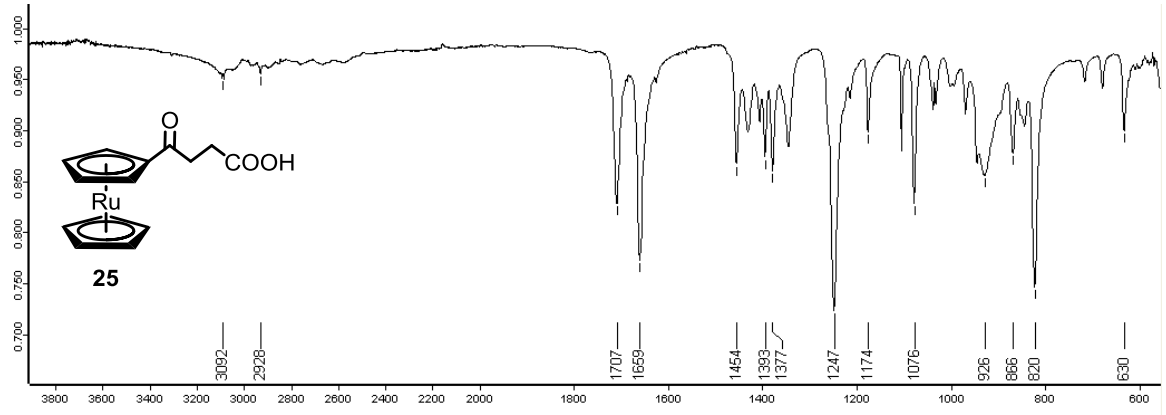

Spectrum 37: Methyl hydrogen succinate, 44

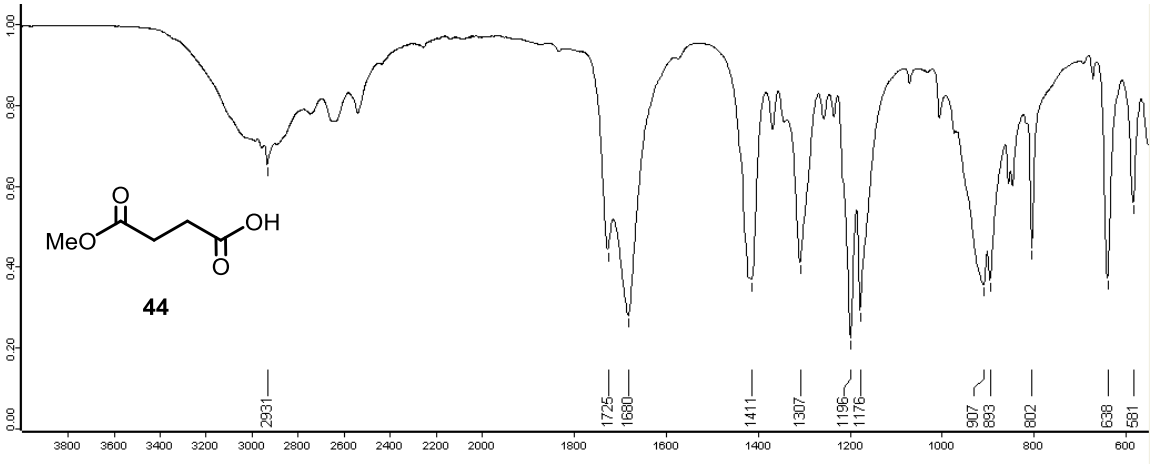

Spectrum 38: β-carbomethoxypropionyl chloride, 45

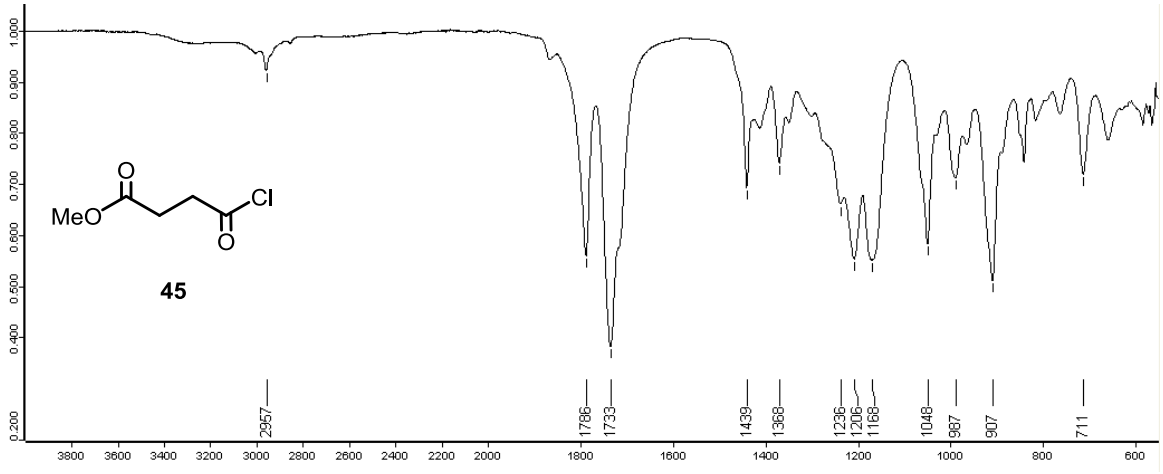

Spectrum 39: Methyl 3-ruthenocenoyl propanoate, 59

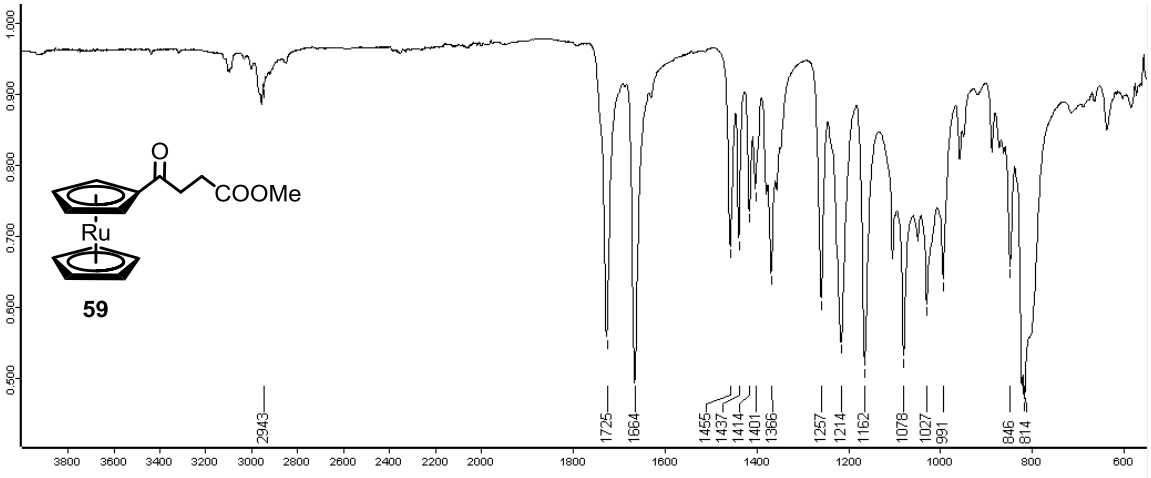

Spectrum 40: Methyl 4-ruthenocenyl butanoate, 60

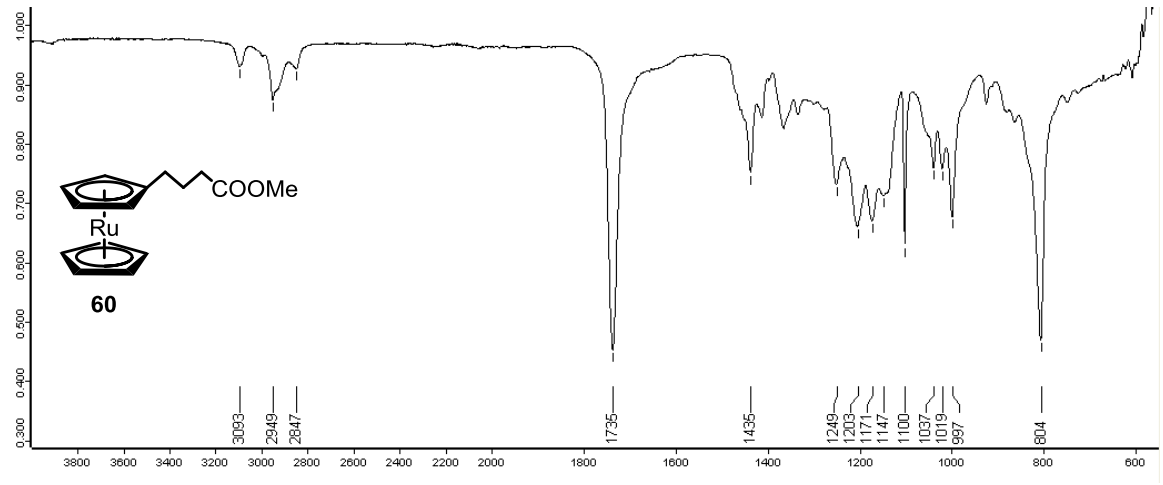

Spectrum 41: 4-ruthenocenyl butanoic acid, 24d

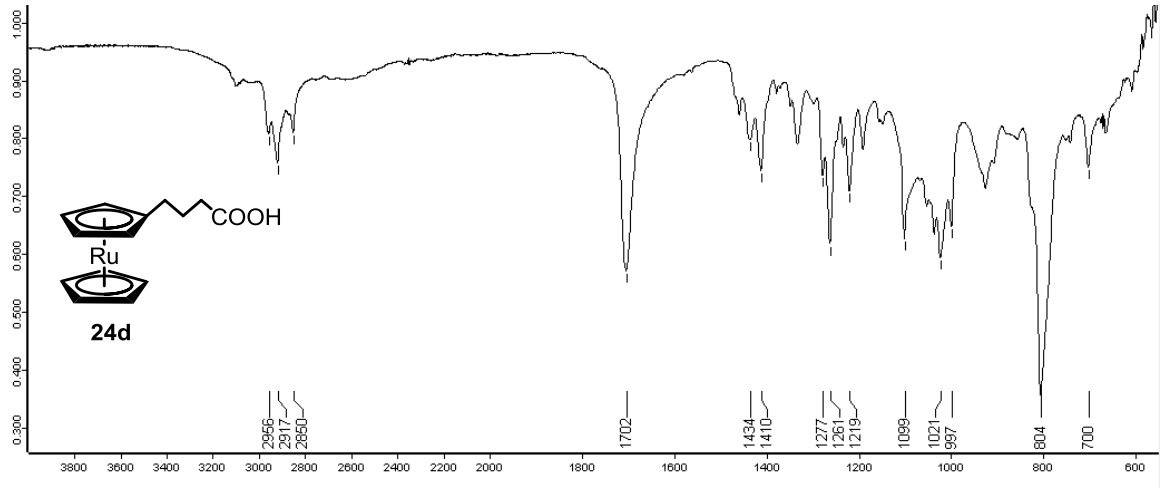

Spectrum 42: Poly-DL-succinimide, 32

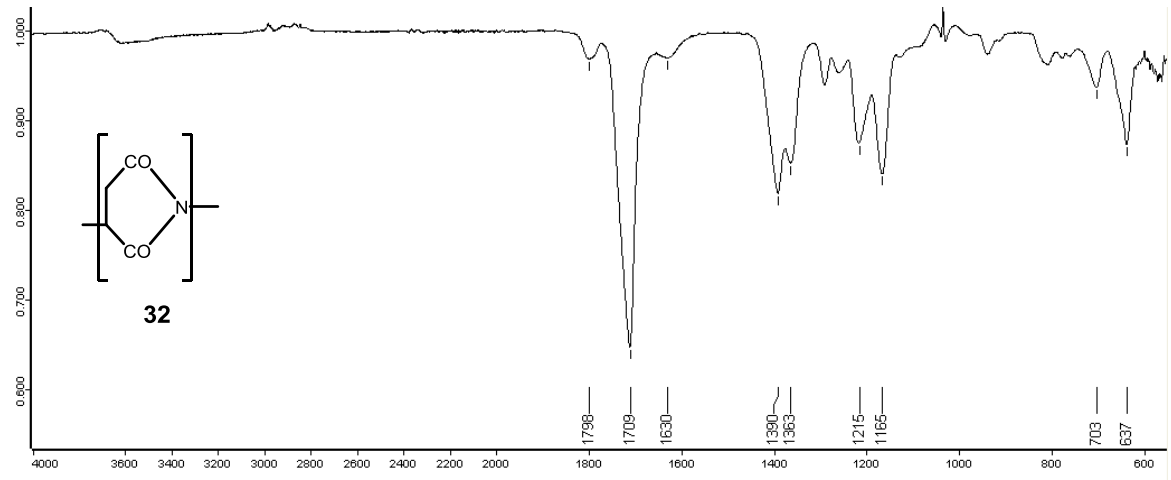

Spectrum 43: poly-α,β-DL-[N-(3-(morpholin-4-yl)propyl)aspartamide-co-N-(2-aminoethyl)aspartamide, 35

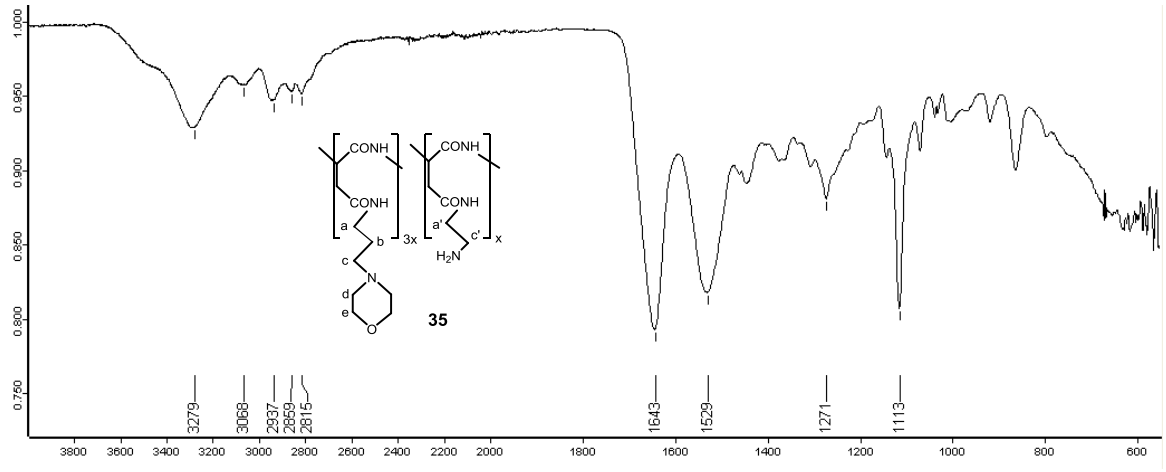

Spectrum 44: Polymer 4

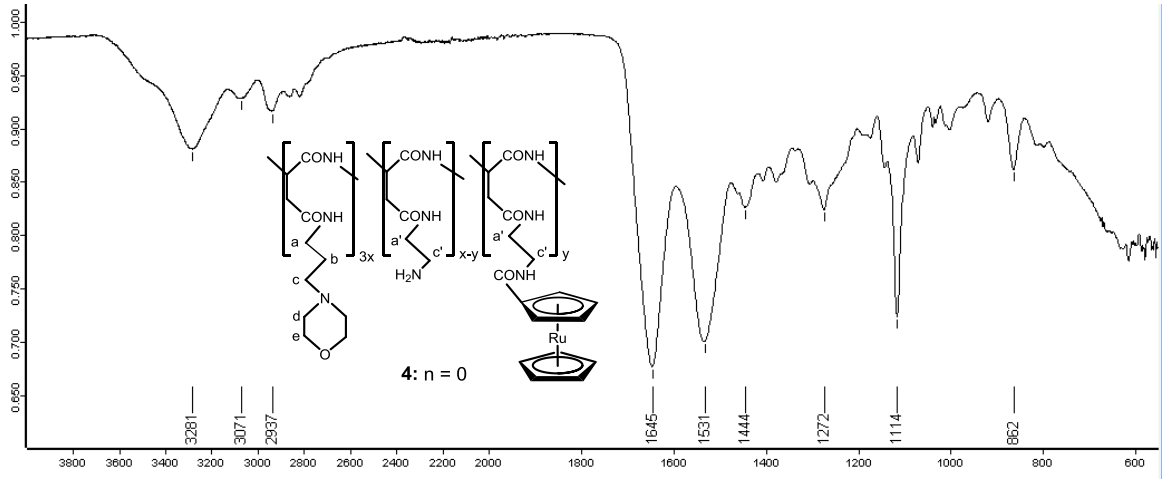

Spectrum 45: Polymer 5

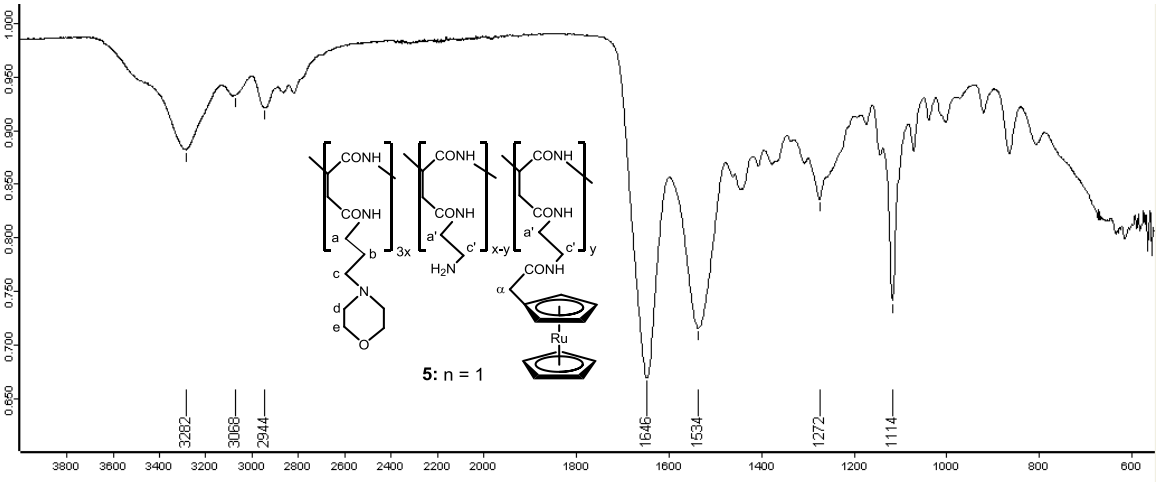

Spectrum 46: Polymer 6

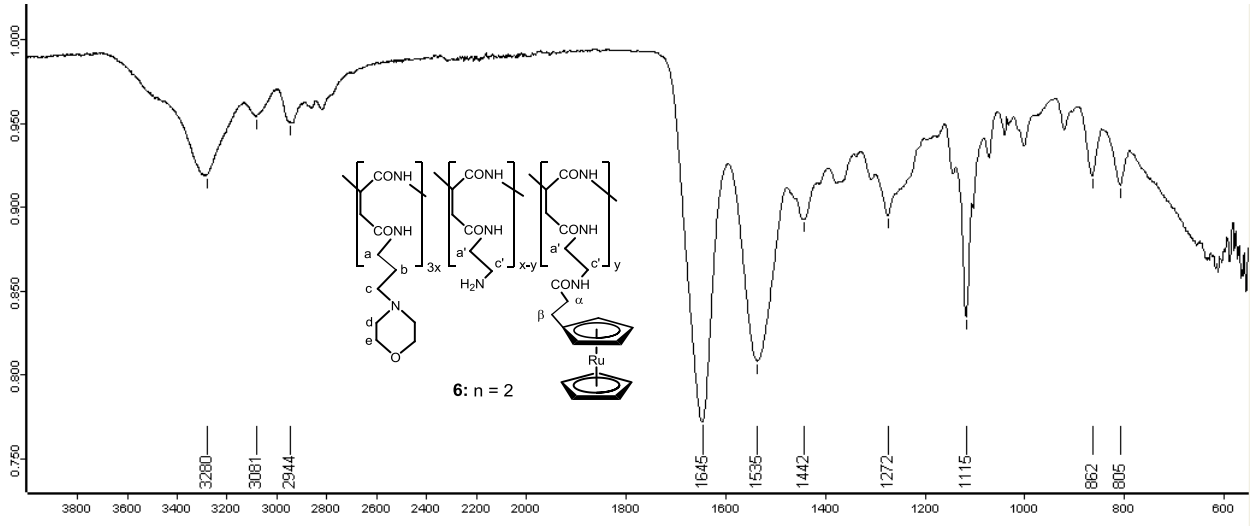

Spectrum 47: Polymer 7

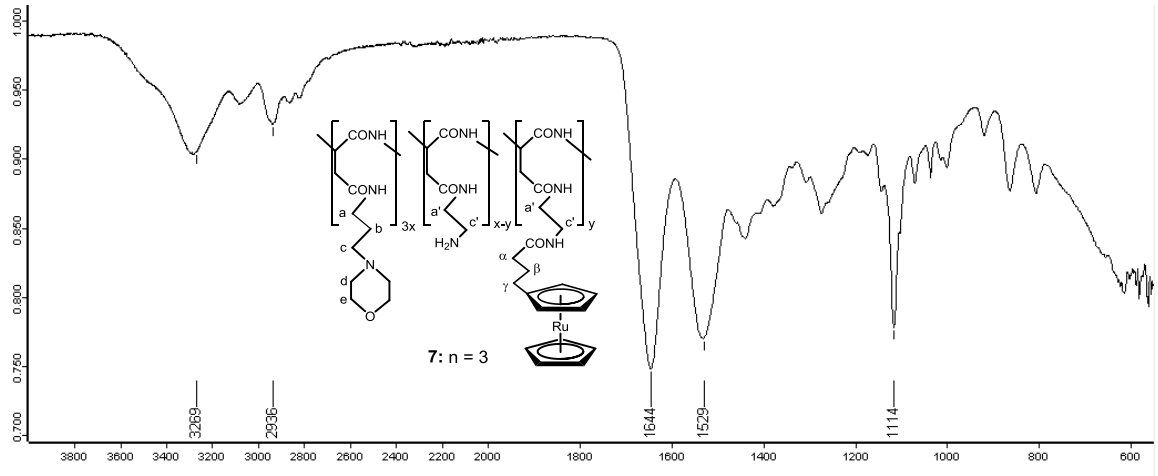

Spectrum 48: Ferrocenium hexafluorophosphate, 19

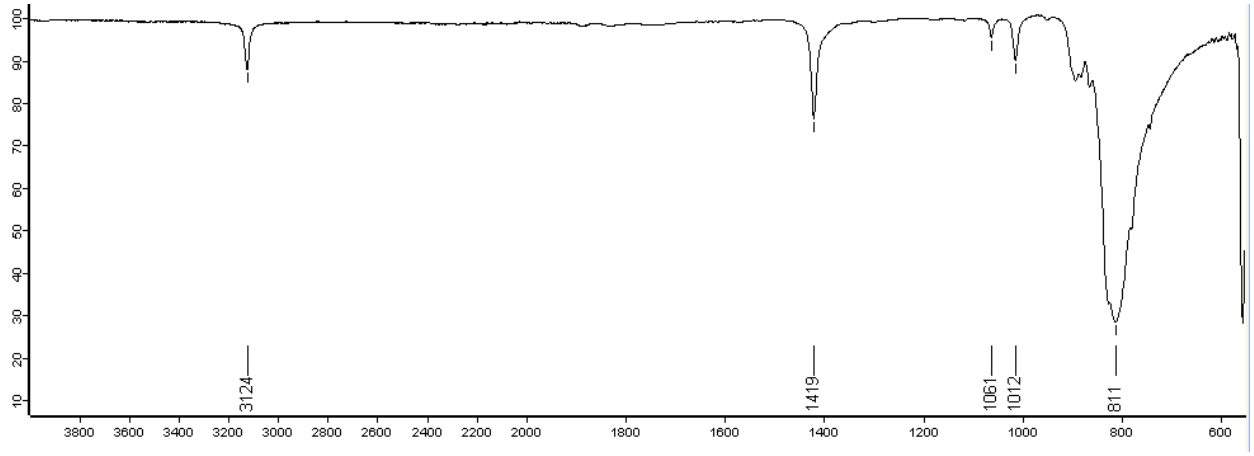

XPS survey scans

Spectrum 49: Ruthenocenylacetic acid, 24b

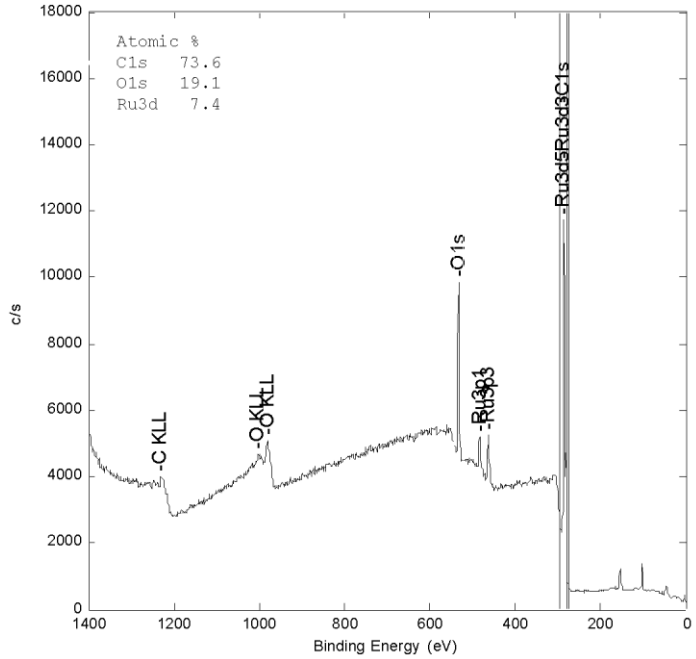

Spectrum 50: poly-α,β-DL-[N-(3-(morpholin-4-yl)propyl)aspartamide-co-N-(2-aminoethyl)aspartamide, 35

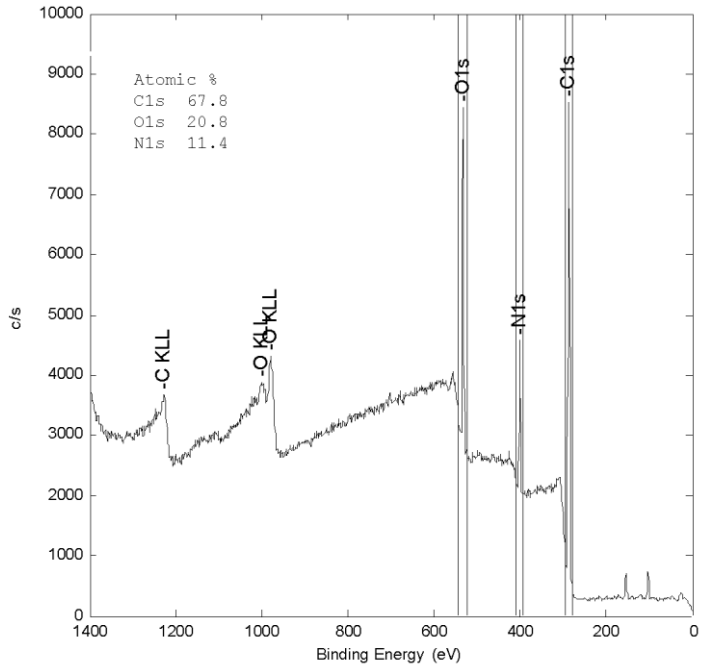

Spectrum 51: Polymer 6

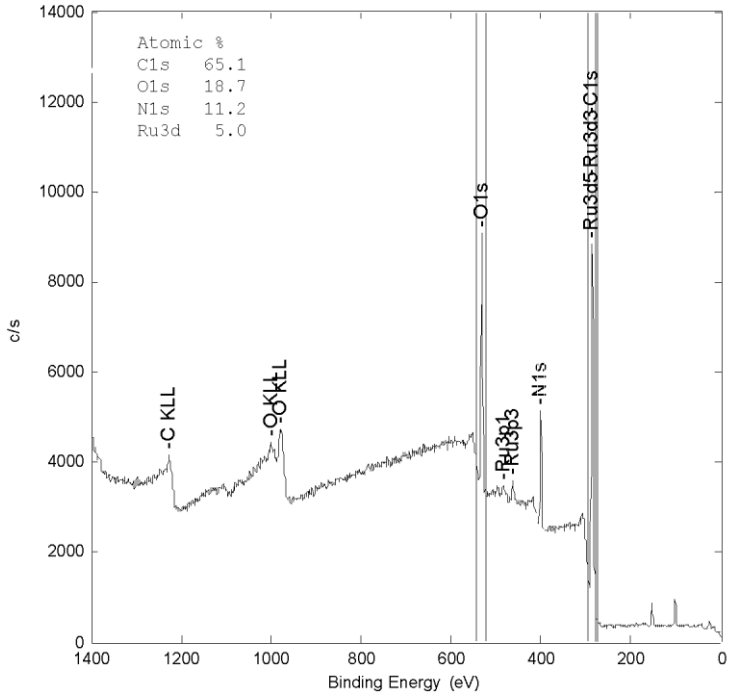

Ek verklaar dat die verhandeling wat hierby vir die kwalifikasie Magistergraad (Chemie) aan die Universiteit van die Vrystaat deur my ingedien word, my selfstandige werk is en nie voorheen deur my vir 'n graad aan 'n ander universiteit / fakulteit ingedien is nie. Ek doen voorts afstand van die outeursreg in die verhandeling ten gunste van die Universiteit van die Vrystaat.

_____

CC Joubert

30 Nov 2011